Physics of Solid-State Lasers

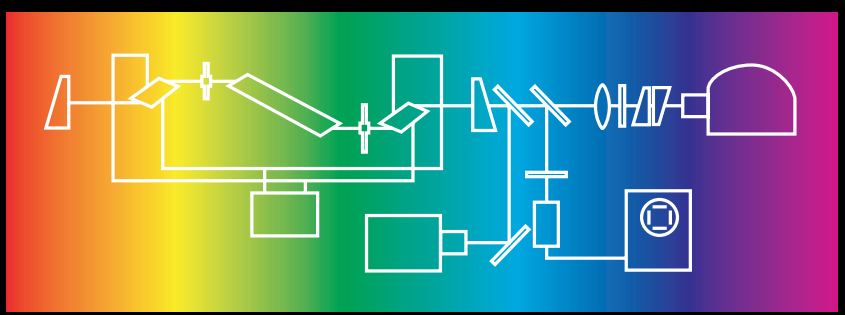

V. V. Antsiferov and G. I. Smirnov

CISP Cambridge International Science Publishing Ltd.

PHYSICS OF SOLID-STATE LASERS

PHYSICS OF SOLID-STATE LASERS

V V ANTSIFEROV and G I SMIRNOV

CAMBRIDGE INTERNATIONAL SCIENCE PUBLISHING

Published by

Cambridge International Science Publishing
7 Meadow Walk, Great Abington, Cambridge CB1 6AZ, UK
http://www.cisp-publishing.com

First published 2005

© V V Antsiferov and G I Smirnov

Conditions of sale
All rights reserved. No part of this publication may be reproduced or transmitted in any form or by any means, electronic or mechanical, including photocopy, recording, or any information storage and retrieval system, without permission in writing from the publisher

British Library Cataloguing in Publication Data
A catalogue record for this book is available from the British Library

ISBN 1-898326-17-7

Printed and bound in Great Britain by Lightning Source UK Ltd

Contents

Preface

In the book, attention is given to the processes of interaction of coherent radiation with solids, the physical relationships governing the generation of laser radiation in dielectric crystals and glasses, activated by luminescent admixtures. Because of their compact form, longevity, and a large number of radiation parameters, solid-state lasers on crystals and glass are used most widely in science and technology in comparison with other types of laser. The most attractive feature of the solid-state lasers as sources of coherent radiation, is the large variety of the lasing conditions, with the typical features including the different conditions of free lasing, passive and active synchronisation of modes, the giant pulse regime. Because of the influence of nonlinear self-effect of radiation, additional nonlinear-optical elements in laser resonators make it possible to control the lasing parameters, including the realisation of new lasing conditions. The expansion of the sphere of application of the solid-state lasers is associated with both the improvement of the technology of formation of new solid-state active media and with the development of new highly efficient methods of controlling laser radiation.

In the monograph, we examine in detail the problem of self-organisation of the radiation of solid-state lasers, describe the theoretical fundamentals of simulation of stochastic processes in the interaction of coherent electromagnetic radiation with the solid, and the principles of statistical nonlinear lasing dynamics. The physical mechanisms of the methods of controlling the radiation of solid-state lasers in the free lasing and giant pulse conditions are described, together with the method of synchronisation of pulses, stabilisation and optimisation of the parameters of solid-state lasers in order to produce powerful monochromatic radiation with adjustable frequency.

The examined general relationships of the physics of solid-state lasers are illustrated by the results of a large number of investigations of the spectral-time, angular and energy characteristics of lasing of lasers on chromium ions in ruby, alexandrite, gadolinium–scandium–

gallium garnet, neodymium ions in silicate and phosphate glass, in crystals of yttrium–aluminium garnet, gadolinium–scandium–gallium garnet with chromium, lanthanum beryllate, potassium–gadolinium tungstate and in a number of other solid-state media. The systematisation and generalisation in this monograph of the very large, often unique experimental material for the physics of solid-state lasers is of fundamental importance for the development of new laser and information technologies.

The book is intended for a wide range of experts working in the area of nonlinear optics, quantum electronics, solid-state physics, surface physics, micro- and nanoelectronics, informatics, for engineers and technologists working in the development and production of appropriate technologies, and for graduates and students of these disciplines.

V.V. Antsiferov and G.I. Smirnov

INTRODUCTION

As regards the most important parameters of coherent radiation, the solid-state lasers occupy the leading positions in quantum electronics. The solid-state lasers on activated crystals and glass are used most widely in practice in different scientific and technical applications, regardless of the strong competition by lasers of other types [1].

The fundamental physical factor, determining the possibility of lasing, is the effect of induced emission of atoms under the effect of the external electromagnetic field, predicted by Einstein [2]. After the discovery of powerful sources of monochromatic electromagnetic fields in the radio-range of the spectrum, Raby examined the central problem of the interaction of laser radiation with the two-level atoms without taking relaxation processes into account and explained the main special features of its dynamic evolution [3,4].

These investigations were continued by Autler and Townes [5] who introduced the concept of the splitting of the levels of the atom, interacting with coherent radiation, i.e. the dynamic Stark effect. The special features of the kinetics of forced transitions, closely associated with the monochromatic nature of the strong external electromagnetic field, consist of the oscillation of the probability of the atom being in the combined states with the frequency proportional to the amplitude of the field. The processes of relaxation disrupt the strict dynamic nature of evolution, but the latter retain its nonlinear-dynamic nature and is controlled by the parameters of radiation [6].

The problems of formation of the inverse population of the levels were of principal importance for the development of lasers. Basov and Prokhorov proposed a method of formation of the inversion of populations in a three-level system using external pumping [7] which was subsequently developed further by Bloembergen [8]. Taking into account the simple variants of relaxation, the nonlinear dynamics of resonance radiation processes in the three-level systems was examined by Kantorovich, Prokhorov and Javan [9,10] who provided a significant contribution to quantum electronics and nonlinear optics.

In particular, the three-level system was used by Maiman in 1960 in the development of the first laser which was of the solid-state type: the active medium was ruby [11]. In 1964, lasing was generated in a laser with Al–Y garnet with Nd, developed on the basis of the four-level system [12].

In solid-state lasers, the high energy lasing parameters are combined with relative wide bands, reliability, compact form and longevity of laser systems of the given type, and also with their capacity to operate in the greatly differing conditions: from the regime of ultrashort pulses of femtosecond duration to the regime of quasi-continuos high power generation. The constant attention of investigators in the physics of solid-state lasers is determined by the constantly increasing range of the application of these systems, the need for modification of the currently available new lasing conditions, the development of methods of controlling the parameters of output radiation [13–22].

The free lasing of longitudinal modes on chromium ions in a ruby crystal, alexandrite, emerald and other media with flat mirrors in the normal conditions always takes place in the regime of non-damping pulsations of radiation intensity. In the case of forced smoothing of longitudinal heterogeneity of the field in ruby using compensating phase regulation, the generation of longitudinal modes in a ruby laser always takes place in a stable quasi-stationary conditions. The change of modes in the lasing process in the conditions of the homogeneous field in the active medium, determined by the thermal drift of the gain line, takes place by the adiabatic mechanism and is not accompanied by pulsations of radiation intensity.

In Nd lasers in different media, the free lasing of longitudinal modes always takes place in the quasi-stationary regime, and this is achieved in the normal conditions without forced smoothing of the longitudinal heterogeneity of the field in the active medium, but with the removal of the effect of technical perturbations of the resonator. In crystals characterised by high homogeneity and heat conductivity, such as Y–Al garnet, beryllium lanthanate, potassium–gadolinium tungstate and a number of others, in the same experimental conditions, it is possible to ensure even more easily the stable quasi-stationary lasing of transverse modes, but only at low values of transverse indexes.

This qualitative difference in the dynamics of free lasing of these lasers is determined by the large differences in the structure of their working levels and, correspondingly, the characteristics of non-linear self-effect of lasing, linked with the dynamic Stark effects.

The role of stochastic factors and the dynamic Stark effect in the self-organisation of radiation of solid-state lasers has attracted special interest of the investigators [23–27]. Analysis of the nonlinear dynamics of the pulsed laser systems and the stability of different lasing regimes makes it possible to solve the problem of reproducibility of the parameters of output radiation and of controlling these parameters, and describe different special features of the self-effect of radiation in nonlinear optical systems [28–31].

Chapter 1

Solid-state chromium lasers in free lasing regime

1.1 SPECTROSCOPIC CHARACTERISTICS OF ACTIVE MEDIA ON CHROMIUM IONS

The electronic configuration of neutral chromium atoms is $(Ar)^3d^5 4s$. Trivalent chromium ions with the electron configuration $(Ar)^3d^3$ lose their screening shell and the spectrum of the ion, determined by 3*d*-electrons, may differ for these ions isomorphously implanted into different matrixes. The interaction of 3*d*-electrons of the chromium ions with the electrical fields surrounding them in the matrixes of the active media determines their energy levels. The energy of the spin-orbital interaction for 3*d*-ions is approximately 100 cm^{-1}, whereas the energy, determined by the electric field of the crystal, is two orders of magnitude higher. This strong field ruptures the bond between the spin **S** and the orbital moment **L** which in this case do not interact which each other. The energy of individual sublevels is determined by the projections of total magnetic moments on the direction of the field and the energy levels are determined by the removal of orbital degeneration with the ratio $(2L + 1)$ under the effect of the crystal field. In the range of the real crystal fields at the trivalent chromium ion the mutual position of the levels ^2E and $^4T_2$ may differ. This makes it possible to produce both narrow-band lasing on *R*-lines ($^2E \rightarrow {}^4A_2$ transition) and the lasing rearranged in a wide band (transition $^4T_2 \rightarrow {}^4A_2$). The ground state of the free ion Cr^{3+}, determined by the Hund rule, is the state $^4F_{3/2}$ with the orbital moment $L = 3$ and the spin $S = 3/2$. As a result of the Stark effect, the intracrystal field partially reduces the degeneration of the levels and leads to the shift and splitting of the therms of the ions. Further degeneration of the levels is removed by the spin-orbital interaction of the electrons.

Table 1.1 Main spectroscopic characteristics of several active media with trivalent chromium ions

Material (notation)	Name	λ_o, nm	$\Delta\lambda$, nm	τ, μs	$\sigma\times10^{-20}$ cm^2	[Ref]
Al_2O_3	Ruby	694.3	0.5	3000	2.5	[32]
Be Al_2O_4	Alexandrite	762	700–800	260	0.7	[33,34]
$Be_3Al_2(SiO_3)_6$	Emerald	768	720–840	65	3.3	[35]
$Gd_3Sc_2Ga_3O_{12}$	GSGG	785	740–840	120	0.9	[36,37]
$Y_3Sc_2Ga_3O_{12}$	YSGG	750	710–790	140	0.6	[36,37]
$KZnF_3$	GSAG	784	760–810	150	0.7	[36,37]
$LaGa_5SiO_{14}$	Perovskite	825	720–900	190	1.3	[38]
$LaGa_5SiO_{14}$	Langasite	960	860–1100	5.3	12	[39]
$LaGa_5NbO_{14}$	Haloharmonate	1060	920–1200	1.3	16	[40]
Mg_2SiO_4	Forsteride	1200	1150–1250	-	-	[41]

λ – the lasing wavelength in the centre of the gain line; $\Delta\lambda$ – the width of the gain line; τ – the lifetime of the upper working level; σ – the cross section of induced transition.

At present, lasing on chromium ions has been achieved in a wide range of wavelengths for greatly different crystal matrixes.

The spectral–time, spatial and energy parameters of lasing of lasers on chromium ions in different active media have been investigated by us in [1–30]. The main spectroscopic characteristics of the examined media are given for comparison in Table 1.

1.2 EXPERIMENTAL METHODS OF EXAMINING FREE LASING PARAMETERS

1.2.1 Experimental equipment

The main parameters of free lasing of solid-state lasers have been investigated on experimental equipment whose diagram is shown in Fig. 1.1. In development of equipment, all measures have been taken to eliminate the effect of technical perturbations of the resonator on the free lasing dynamics. All optical elements of the resonator are placed on very rigid and thick tables with mechanisms for precision angular and linear displacement.

The spurious selection of longitudinal modes in the resonator was completely eliminated: the ends of all elements of the resonator were cut either under the Brewster angle or under a small angle in relation

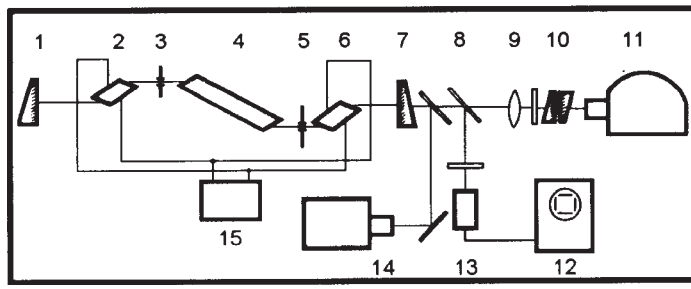

Fig. 1.1. Experimental equipment for examining spectral-time characteristics of radiation of solid state lasers: 1,7) resonator mirrors; 2,6) electrooptical crystals for compensated phase modulation; 3,5) diaphragms for separating TEM_{ooq} modes; 4) active medium; 10) Fabry–Perot interferometer; 11,14) superfast photorecoding devices; 12) oscilloscope; 13) photodiode; 15) generator of sinusoidal voltage.

to the axis of the resonator (in the latter case, the ends of the elements were trans-illuminated); the mirrors of the resonator were sprayed on glass substrates with a wedge; the diaphragms, separating the longitudinal modes, were coated with a lacquer. The active media of the lasers were cooled with distilled water or a liquid filter cutting off the ultraviolet radiation of pumping. The temperature of the cooling liquid was maintained with a thermostat with the accuracy to 0.1°C. The active media were excited with standard xenon pumping lamps in a single-block quartz illuminator, and the shape of the pumping pulse was close to right-angled, with a duration of 0.25–1.0 ms.

The main parameters of free lasing were recorded with a high spatial and time resolution: the intensity was recorded using an avalanche photodiode and an oscilloscope; the spectrum was recorded using a spectrograph or a Fabry–Perot interferometer and high-speed photographic equipment; the distribution of radiation intensity in the near-range (long-range) zone was recorded using a superhigh speed photorecording system or a photochronograph. When recording the radiation spectrum with the Fabry–Perot interferometer, the spurious link between the interferometer and the resonator of the laser was eliminated by means of optical decoupling.

1.2.2 Methods of eliminating technical perturbations of the resonator of a pulse solid-state laser

The main types of technical perturbations of the resonator were detected and examined in detail by the authors of this book in Ref. 9,12,24. Relatively simple methods have been developed for eliminating the

effect of technical perturbations of the resonator on the dynamics of free lasing of pulsed solid-state lasers with lamp pumping. If no special measures are taken to stabilise the intensity of laser radiation, it is almost impossible to determine and examine the individual types of technical perturbations of the laser resonator in the peak regime. Analysis of these perturbations was carried out only in the quasi-continuous regime of lasing of longitudinal (TEM_{ooq}) modes of a ruby laser with flat mirrors obtained by smoothing the longitudinal heterogeneity of the field in the active media using compensated phase modulation (CPM). The oscillographs of radiation intensities (Fig. 1.2) were obtained when pumping energy E_p was three times higher than threshold pumping energy E_t.

1. Mechanical non-axial oscillations of the active rod with a frequency of ~10 kHz form during hydraulic impact through the cooling liquid from pumping lamps at the moment of appearance of the discharge pulse. These oscillations result in periodic displacement of the lasing channel of longitudinal modes, separated by the diaphragms, and the amplitude modulation of the intensity of radiation (Fig. 1.2) on these diaphragms if they are small ($\leq$ 1 mm) and in the case of non-optimum tuning.

The non-axial oscillations of the active rod can be eliminated using a special quantron with mechanical uncoupling and separate cooling of the rod and pumping lamps. However, there are also simple means of eliminating the effect of these oscillations on the lasing dynamics. For this purpose, it is sufficient to increase the diameters of the diaphragms separating the longitudinal modes to 1.4 mm for Cr lasers and to 2.0 mm for Nd lasers, position the diaphragms in the vicinity of the ends of the active rod and adjust them in the optimum manner in relation to the separated lasing channel. The separation of a single Frenel zone is achieved by increasing the length of the resonator to 1.6 m for the Cr lasers and to 2.0 m for the Nd lasers. The dynamic tuning of the diaphragms is carried out on the basis of the shape of the lasing pulse of the screen of the oscilloscope to 0.1 mm after preliminary, static adjustment on the basis of the reference beam of the gas laser and the minimum value of the lasing threshold.

2. The dynamic thermal lens, formed in the active rod as a result of non-uniform heating of the cross-section of the rod, may lead to gradual displacement of the lasing channel and slow modulation of radiation intensity with respect to the amplitude on the diaphragms (Fig. 1.2b) in the case in which the lasing channel does not pass accurately along the axis of this thermal lens. If the lasing channel passes under the maximum possible angle to the axis of the rod, its deviation from the initial direction during the formation of the thermal

lens will be minimum owing to the fact that the effect of one half of the thermal lens in this case is compensated by the effect of the other half. The dynamic setting of the position of the active rod and the diaphragms makes it possible to eliminate the effect of this factor and produce the shape of the lasing pulse close to the shape of the pumping pulse (Fig. 1.2c).

3. The mechanical oscillations of the mirrors of the resonator result in high-frequency modulation of radiation intensity even in the conditions of the uniform field in the active medium (Fig. 1.2c). In the presence of a non-uniform field in the active medium, very small displacements (of the order of $\lambda/4$) of the field of standing waves are sufficient to cause 100% modulation of radiation intensity. The residual modulation of the losses on the mirrors is removed by their dynamic tuning of the oscillogram on the screen of the oscilloscope with the accuracy to 1 angular second (Fig. 1.2d).

4. The thermal drift of the gain line of the active medium, determined by heating of the active medium by the pumping radiation, also causes disruptions in the dynamics of free lasing because it leads to a forced change of the modes during the lasing process. In addition, increase of the length of the active rod as a result of the increase of its temperature leads to the rearrangement of the natural modes of the resonator, with the shift being

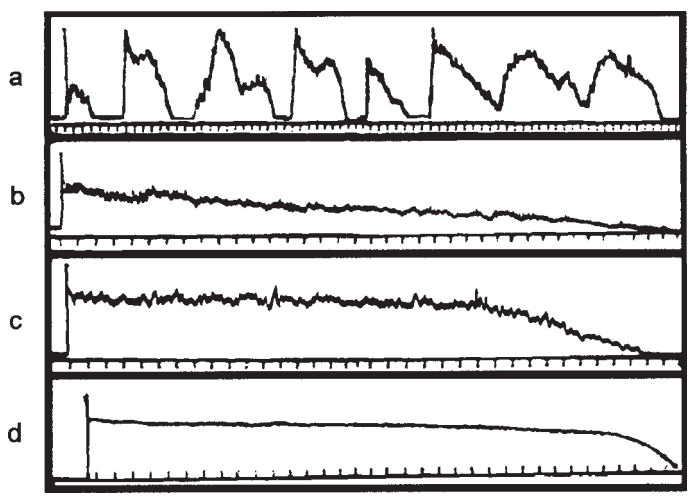

Fig. 1.2. Oscillograms of intensiyies of radiation of TEM_{ooq} modes of a ruby laser with flat mirrors in the conditions of smoothing the longitudinal heterogeneity of the field in the active medium and passive negative feedback, illustrating the effect of technical perturbations of the resonator; $E_p = 3E_t$; markers – 10 (a) and 20 μs (b–d).

$$\Delta\lambda = -\frac{\lambda l \Delta T}{L}\left[(n-1)\alpha_T + \frac{\partial n}{\partial T}\right]. \qquad (1.1)$$

Here l is the length of the active rod; L is the length of the resonator; n is the refractive index of the active medium; α_T is the coefficients of linear expansion of the medium; $\partial n/\partial T$ is the thermooptical coefficient. The rate of rearrangement of the natural modes of the resonator is considerably lower than the speed of thermal drift of the gain line and, as shown by experiments, these two processes do not lead to breaks in quasi-stationary lasing in all examined media. The change of the modes during the lasing process, determined by these factors, is adiabatic in the conditions of the quasi-stationary regime and is not accompanied by radiation pulsations.

5. Other factors, resulting in spurious amplitude modulation of the intensity of laser radiation, which can be relatively easily eliminated, include: the presence of macroheterogeneities in the active medium, the spurious selection of the modes in the resonator, non-active absorption in non-pumped regions of the active medium, and others.

It should be noted that to ensure stable quasi-stationary lasing in solid-state lasers, in addition to the optimisation of the resonator parameters, it is necessary to place the active rod in the centre of the resonator and the diaphragms, separating the longitudinal modes, should be positioned in the vicinity of the ends of the resonator. In this case, the effect of spurious disruptions of the resonator parameters on the lasing dynamics is greatly reduced and the spatial modulation of inversion in the active rod is also reduced.

This method of adjusting the main elements of the resonator makes it possible to eliminate by simple means the effect of external technical disruptions and instability of the resonator parameters on the nature of free lasing and examine in explicit form its dynamics in the pulsed regime.

1.2.3 Methods of producing quasi-stationary lasing

The solid-state lasers with lasing in the quasi-stationary regime with a narrow radiation spectrum stable with time, are used widely in science and technology. The efficient control of the spectral–time characteristics of radiation is possible only in the quasi-stationary regime and only in lasers with flat mirrors.

1. The method of producing quasi-stationary lasing in lasers in different media with optical resonators of critical configuration (confocal

or concentric) characterised by strong degeneration of the modes, is well known. In these lasers, the spatial non-uniformity of the field in the active medium is eliminated as a result of the excitation of a large number of degenerate modes with a high transverse index, high angular divergence and a wide radiation spectrum which is almost impossible to control.

2. The smoothing of the pulsations of radiation intensity is achieved using a negative feedback between laser radiation and losses in the resonator: active [42], in which an electro-optic shutter is placed in the resonator, or passive [43], using darkening filters. However, the application of the negative feedback in the laser with flat mirrors in the conditions of the non-uniform field in the active medium does not make it possible to ensure stable lasing on a single longitudinal mode because this regime is always unstable [44].

3. The forced smoothing of the spatial heterogeneity of the field in the active medium in the lasers with flat mirrors is carried out using the movement of the active medium (running medium) [45,46] or the resonator mirror [47]. However, it is not possible to ensure stable quasi-stationary lasing because the movement of the reflecting surface along the axis of the resonator results in periodic modulation of the *Q*-factor of the resonator and in the kinetic modulation of radiation intensity [48]. In addition, the movement of elements of the resonators is often accompanied by the formation of purely mechanical perturbations in the resonator.

4. Attempts have been made to produce quasi-stationary lasing of the longitudinal waves in a pulsed solid-state laser using a ring-shaped resonator in which the spatial heterogeneity of the field was removed in the running wave regime. One of the waves in the ring-shaped resonator was suppressed using a nonmutual element (Faraday cell) [49]. In the pulsed regime, it is almost impossible to adjust optimally the ring-shaped resonator in the case of lasing of longitudinal modes taking into account the changes with time of the focus of the thermal lens formed in the active rod.

5. In order to generate the quasistationary regime in the laser with flat mirrors, experiments were also carried out using the method of non-resonant feedback in which one of the mirrors of the resonator is replaced by a diffusion reflector [50]. This method is not used widely owing to the fact that the laser of this type is characterised by a high lasing threshold, high losses and low radiation energy.

6. The homogeneous field in the active medium can be produced using circulation-polarised waves generated by two quarter-wave phase sheets [51]. However, this method can be used to realise the quasistationary lasing of solid-state lasers in the pulsed regime.

7. The most efficient method of smoothing the spatial heterogeneity of the field in the active medium of the solid-state laser with flat mirrors is the method of compensated phase modulation (CPM) [1,31]. The CPM method and its advantages are based on the fact that with nonstationary elements of the resonator and the constant length of the resonator, the pattern of the field of standing waves is displaced in relation to the active medium by means of two phase modulators (2 and 6 in Fig. 1.1) positioned on both sides of the active rod; the modulators receive the sinusoidal voltage in the opposite phase from the generator 15. The modulation frequency should satisfy the relationship $\omega_m \geq 2\pi/t_s$, t_s is the duration of the lasing spike. The phase modulators have the form of electro-optic crystals (KDP, $LiNbO_3$, etc.), whose mutual orientation is regulated by means of two crossed polarisers and the linearly polarised radiation of the tuning laser.

To develop the homogeneous field in the active medium between the phase modulators, the intensity of the standing waves

$$I(x, t) = I_0 \sin^2 \left(kx + \beta \sin \omega_m t\right) \tag{1.2}$$

must be equal to $I_0/2$ at any point x. The following condition must be satisfied in this case:

$$\frac{1}{2\pi}\int_{-\pi}^{\pi}\Big[\sin 2kx\left(\sin 2\beta\,\omega_m t\right) - \cos 2kx\left(\sin 2\beta \sin \omega_m t\right)\Big] d\left(\omega_m t\right) = 0 \tag{1.3}$$

The first integral is equal to 0 because it is antisymmetric with respect to t, and the second integral is expressed by means of Bessel's function. Consequently, the criterion (1.3) is reduced to the condition $J_0(2\beta) = 0$, where J_0 is the Bessel function of the zero order. The first zero of this function is situated at the point $\beta = 0.38\pi$. If the phase modulators are represented by the KDP crystals, to develop a homogeneous field between them, the strength of the modulated electric field on the crystals must be $E_z = \beta\lambda/\pi l n_0 r_{63}$. At the length of the crystals l = 5 cm, n_0 = 1.5, $r_{63} = 8.5 \times 10^{-10}$ cm/V, the strength of the electric field is E_z = 1.8 kV/cm, which is in good agreement with the experimental results.

1.2.4 The methods of selection wavelength tuning of the radiation wave

Extensive investigations carried out using single-frequency lasers have stimulated the development of effective methods of controlling the spectral characteristics of laser radiation. The operating principle of the mechanism of selection of longitudinal modes is based on the addition into the laser resonator of the selective dependence of the losses on the frequency of radiation using dispersion elements: prisms, diffraction gratings, interference–polarisation filters, interferometers, resonance reflectors etc. The effect of all dispersion resonators is based on the two mechanisms of selection of the longitudinal modes: angular and amplitude.

In the resonators with the angular mechanism of selection, the bundles of radiation of different longitudinal modes propagate under different angles in relation to the axis of the resonator and the losses differ. The losses will be minimum in the mode for which the resonator was tuned. In the case of amplitude selection, the resonator is tuned for longitudinal modes and the difference in the losses is caused by the spectral dependence of effective transparency, reflectance or polarisation characteristics of the dispersion element.

In the dispersion resonator, the half width of the curve of the dependence of the losses on frequency $\gamma(\omega_i)$ is considerably smaller than the half width of the gain line. The threshold value of amplification is obtained at the point of contact of these two curves, and the wavelength of laser radiation is changed by displacing the curve of the selective losses in relation to the gain line. In practice, this is carried out in most cases using combined dispersion resonators, containing several dispersion elements, one of which ensures a narrow lasing spectrum and the other ones a wide range of radiation wavelength tuning.

The intensity of laser radiation $I(\omega_i)$ at the frequency ω_i for a single beat of the resonator changes in the following manner: $I_{k+1}(\omega_i)/I_k(\omega_i) = \exp \delta(\omega_i)$, where $\delta(\omega_i) = \alpha(\omega_i) - \gamma(\omega_i)$, $\alpha(\omega_i)$ is the amplification coefficient at frequency ω_i. At the increment $\delta > 0$, the intensity of radiation increases, and at $\delta < 0$ it decreases. The difference in the coefficient of the losses, required for suppressing weaker modes, is inversely proportional to the number of passages k of the photons through the resonator during which the intensity reaches the maximum level from the level of spontaneous noise

$$\frac{I_1}{I_2} = \left[\frac{1-\gamma_1}{1-\gamma_2}\right]^k. \qquad (1.4)$$

In the free lasing regime $k \sim 10^3$ and the required difference of the losses for the two modes at which the intensities differ by an order of magnitude at the end of the linear development of lasing is very small: $(\gamma_2 - \gamma_1) \sim 10^{-3}$. In the quasistationary regime, relatively weak mode discrimination is sufficient to ensure lasing on a single longitudinal mode by means of conventional dispersion elements.

1.3 RUBY LASERS

The lasing of forced radiation in the optical region of the spectrum was obtained for the first time in a ruby laser (Cr^{3+}:Al_2O_3). Ruby crystals are characterised by high strength, homogeneity and heat conductivity. The optimum concentration of the impurity ions of Cr is approximately 0.05%, which corresponds to the density of the active centres of 1.6×10^{19} cm^{-3}, and at this concentration the ruby is rose-coloured. Ruby is an anisotropic single crystal with a trigonal symmetry in which the trigonal axis coincides with the optical axis of the crystal. The refractive index of ruby at the lasing wavelength is: $n_o = 1.763$, $n_e = 1.755$. The melting point of the ruby crystal is 2040°C, the hardness according to Moose is 9, density 3.98 g/

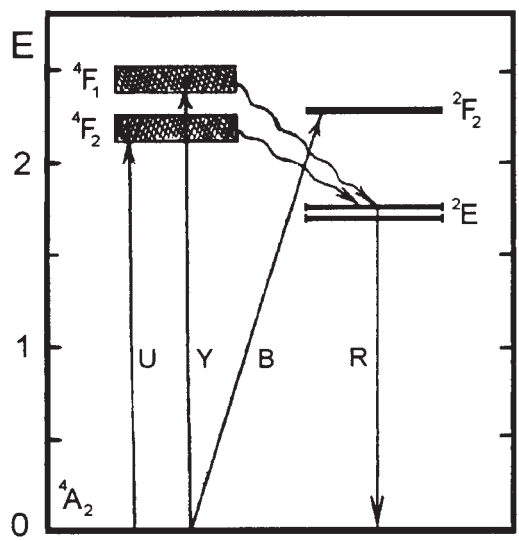

Fig. 1.3. Energy levels E (eV) of chromium ions Cr^{3+} in sapphire (ruby).

cm^3, the thermal expansion coefficient 5.31 (4.78)×10^{-6} deg^{-1}, the thermal optical constant dn/dT = 1.0×10^{-6} deg^{-1}. The ruby crystal is characterised by the highest heat conductivity (42 W/m·grad) of all other active media.

The diagram of the levels of the Cr^{3+} ion in the corundum crystal is shown in Fig. 1.3 in the most widely used symbols. The gain line of ruby is uniformly broadened, and the half width of the R_1-line at room temperature is 0.53 nm and at the liquid nitrogen temperature it decreases to 0.014 nm. During heating of ruby, the centre of the gain line is displaced to the wavelength range of the spectrum with a speed of 6.3 × 10^{-3} nm/deg. The excitation of the metastable level ^2E is carried out through wide bands of pumping absorption $4F_1$ and $^4F_2$ with centres at wavelengths of 410 and 550 nm, respectively, and the width of each band of 100 nm. These absorption bands are connected by rapid (~100 ns) radiationless transitions with the metastable level ^2E. Thus, the ruby laser operates by the three-level mechanism.

1.3.1 Spectral–time characteristics of free lasing TEM_{ooq} in a laser with flat mirrors

The spectral–time and energy parameters of a ruby laser in the free lasing regime have been investigated and analysed by the authors of this book in a number of investigations.

The free lasing of longitudinal (TEM_{ooq}) modes in a ruby laser with flat mirrors always took place in the regime of non-attenuating pulsations of radiation intensity, Fig.1.4. In the case of the non-optimum parameters of the flat resonator there were periodic jumps of the radiation wavelength to the short wave length region of the spectrum, and the radiation pulsations were completely irregular as regards the amplitude and repetition frequency, Fig 1.4c. After optimisation of the resonator parameters (length 1.6 m, the diameter of the diaphragms d = 1.4 mm) and the dynamic tuning of the elements of the resonator using the method described previously, the pulsations of the intensity of radiation became regular as regards the repetition frequency and there was an unidirectional displacement of the wavelength of lasing throughout the entire pumping pulse, Fig. 1.4d.

The residual non-regularity of the radiation pulsations with respect to intensity is associated with the effect of oscillations of the resonator mirrors. In the first lasing peak it was possible to excite a large number of longitudinal modes in the band of the spectrum with a width of approximately 25 pm. During 3–4 peaks of lasing, the number of excited modes was greatly reduced to a single longitudinal mode. This was caused by the effect of a strong dispersion

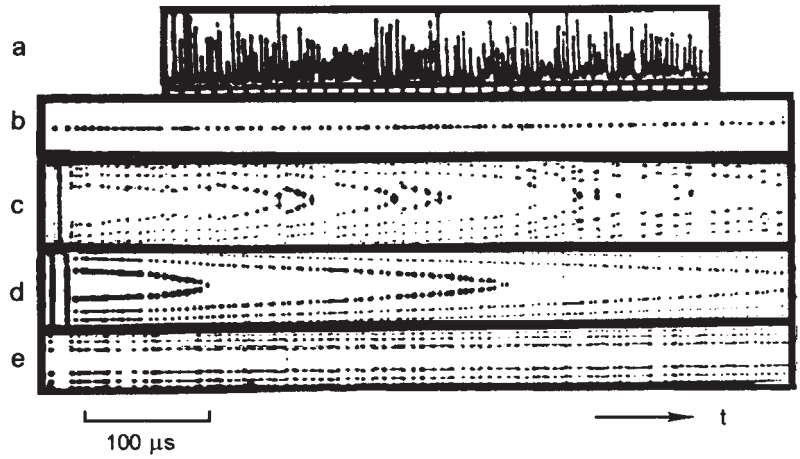

Fig. 1.4. Parameters of lasing of TEM_{ooq} modes of a ruby laser (RL2B 8×120/180 mm) with flat mirrors in normal conditions (c) and with the effect of technical perturbations of the resonator removed (d,e): a) oscillation of radiation intensity, 20 μs markers; b) time evolvement of the distribution of radiation intensity in the long-range zone; c–e) time evolvement of the lasing spectrum without selection of longitudinal modes (c,d) and with selection (e), regions of dispersion of interferometers 24 pm (c,d) and 8 pm (e). $E_p = 3E_l$, length of the resonator L 1 m (c) and 1.6 m (d,e), diameters of diaphragms 1.0 mm (c) and 1.4 mm (a,b,d,e).

of the amplification coefficients of different modes determined by the formation of a longitudinal heterogeneity of inversion in the active medium. In subsequent stages, a single longitudinal mode was excited in every successive peak, and the change of the modes from peak to peak took place in the jumps whose spectral value depended on the ratio of the length of the resonator (L) and ruby (l). The direction of displacement of the wavelength of lasing to the long wave range was determined by the thermal drift of the gain line, and the change of the mode from peak to peak was determined by the longitudinal heterogeneity of inversion.

After lasing of a single longitudinal mode in one of the peaks, the longitudinal distribution of inversion in the active rod has the following form:

$$n_k(x) = n_o - DI_o \sin^2(k\pi / L)x, \tag{1.5}$$

where n_o is the initial level of inversion taking pumping into account; D is a constant coefficient. Under these conditions, the effective amplification factor $\alpha(m)$ as a function of the number of the mode m is proportional to the integral:

$$\alpha(m) \sim \int_{x_o+l}^{x_o+l} I_m(x) B N_k(x) dx. \tag{1.6}$$

Here B is the Einstein coefficient. Integration on the condition that the mode of the standing waves is situated at the point x_o gives:

$$\alpha(m) \sim \frac{A}{l}\left[1 - \frac{\sin 2\pi(k-m)l/L}{2\pi(k-m)l/L}\right]. \tag{1.7}$$

The magnitude of the spectral jump between the longitudinal modes depends both on the ratio L/l and on the position of the active rod in the resonator. In the case in which the ruby crystal is situated in the centre of the resonator and L/l = 8, the magnitude of the spectral jump between the modes was 8 inter-mode intervals [8].

It should be noted that throughout the entire lasing pulse there was unidirectional autosweeping of the wavelength of single-frequency radiation, i.e. displacement of the wavelength without the application of standing dispersion elements which induce large losses in the radiation energy. The rate of sweeping of the lasing wavelength depended on the amount by which pumping exceeded its threshold value and if this value was exceeded three times, the rate was ~0.12 nm/ms, which is four times higher than the speed of the thermal drift of the gain line. During 0.5 ms, the lasing wavelength was displaced by 60 pm and outstripped the centre of the gain line by 45 pm. The ruby laser with these spectral–time radiation characteristics is used as a high-speed spectrometer for the rapid analysis of different optical media [8].

In the regime of non-attenuating radiation pulsations it was not possible to obtain a stable (with respect to time) spectrum of the lasing of longitudinal modes even when using a high-quality selector represented by a Fabry–Perot resonator with the transmission factors of the mirrors of 13%. One to two longitudinal modes were excited in every lasing peak, but the lasing process was accompanied by a random change of the modes from peak to peak within the limits of the pass band of the selector, and the width of the integral radiation spectrum was approximately 5 pm (Fig 1.4e).

The appearance of non-attenuating pulsations of radiation intensity and the absence of stabilisation of the radiation spectrum are associated, as shown by the experiments, with the change of the longitudinal modes during the lasing process and not with the effect of technical perturbations

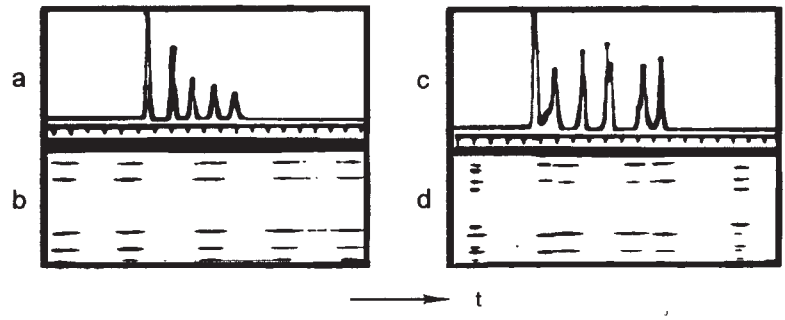

Fig. 1.5 Parameters of lasing of TEM_{ooq} modes of a ruby laser with flat mirrors in normal conditions with rigid selection of the longitudinal modes in the vicinity of the lasing threshhold (a,b) and with increase of the pumping energy by 0.1% (c,d): a,c) oscillograms of radiation intensity, 20 μs markers; b,d) time evolvement of the radiation spectrum, the range of dispersion of the interferrometer 8 pm.

of the resonator. In the vicinity of the lasing threshold in the conditions with even more rigid selection of the longitudinal modes at a pass band of the selector-reference of 2 pm, where the threshold conditions were fulfilled for a single longitudinal mode, the pulsations of radiation intensity always attenuated (Fig. 1.5a, b). With increase of the pumping energy by only 0.1% (i.e. at the unchanged level of technical perturbations), after reaching the lasing of the second mode, attenuation ceased as a result of the alternation of these two modes during the lasing process (Fig 1.5c, d) [11].

The forced smoothing of the longitudinal heterogeneity of the field in the ruby crystal using compensated phase modulation (CPM) always results in stable quasistationary lasing at any excess of pumping above its threshold value (Fig. 1.6). In the first lasing peak, as under conventional conditions, a large number of longitudinal modes were excited in a wide band of the spectrum. This band was determined by the shape of the gain line and by the excess of pumping above the threshold value. However, the decrease of the width of the lasing spectrum to a single longitudinal mode in the conditions of the homogeneous field and, correspondingly, of uniform inversion in the active medium took place during a period an order of magnitude longer (Fig. 1.6c) than in the conditions of non-uniform inversion. In this case, the decrease of the width of the lasing spectrum takes place only as a result of the dispersion generated by the shape of the gain line, in accordance with the law characterised by the relationship:

$$\Delta\lambda_g = \Delta\lambda_o \left(\tau_c / t\right)^{1/2}, \tag{1.8}$$

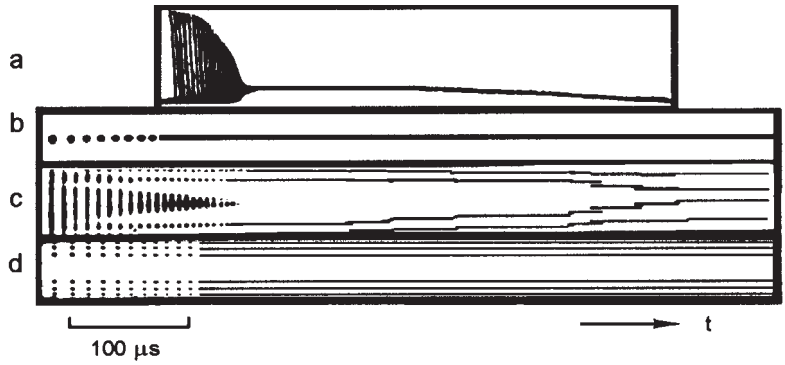

Fig. 1.6 Parameters of the lasing of TEM_{ooq} modes of a ruby laser (PL2B 8×120/180 mm) with flat mirrors (L = 1.6 m, diameter 1.4 mm) with smoothing of the longitudinal heterogeneity of the field in ruby using condensated phase modulation in the conditions of absence of large technical interferences in the resonator (E_p = $3E_t$; a) oscillogram of radiation intensity; b) evolvement of the distribution of radiation intensity in the long range zone; c,d) the time evolvement of the lasing spectrum without selection of longitudinal modes (c) and with selection (d), range of dispersion of the interferrometers 24 pm (c) and 8 pm (d).

where $\Delta\lambda_o$ is the width of the spectrum at the start of lasing, τ_c is the lifetime of the photon in the resonator. After a transition process and reaching the quasistationary lasing regime, the spectral line showed inertia in relation to the thermal drift of the gain line in which stable single-frequency lasing (in the spectrum) was detected periodically over 50–100 μs. Regardless of the thermal drift of the gain line and the rearrangement of the natural modes of the resonator, the change of the longitudinal modes during the process of lasing in the conditions of the homogeneous field and inversion in the active medium took place always adiabatically and was not accompanied by the pulsations of radiation intensity.

The controlling effect of longitudinal heterogeneity of the field in the ruby crystal on the nature of lasing of TEM_{ooq} modes is clearly indicated by the following experiment. When the CPM was started with a certain delay after the start of the pumping pulse, there was always a transition in the lasing process from the regime of non-attenuating pulsations of radiation intensity to quasistationary regime (Fig. 1.7a). If the smoothing process of the heterogeneity of the field was interrupted after establishing single-frequency quasistationary lasing, this was followed immediately by a reversed transition to the regime of non-attenuating pulsations of radiation frequency (Fig. 1.7b) [8].

Fig. 1.7 Oscillograms of intensity of radiation of TEM_{ooq} modes of a ruby laser with flat mirrors (L = 1.6 m, diameter1.4 mm) with application of CPM (a) in the lasing process and without CPM (b), the voltage of the modulating field on the CPM is supplied to the second beam of the oscilloscope; $E_p = 2E_t$.

1.3.2 Single-frequency adjustable quasistationary lasing in a laser with flat mirrors

The efficiency of selection of longitudinal modes rapidly increases in the conditions of the quasistationary regime. At the same parameters of the selector as those shown in Fig. 1.4e, the application of the CPM after the transition process and establishment of the quasistationary regime resulted in the narrowing of the lasing spectrum to a single longitudinal mode and in stabilisation within the limits of the single inter-mode range (Fig. 1.6d).

The efficiency of selection of the longitudinal modes increased even further in smoothing of the longitudinal heterogeneity of the field in the active medium and the conditions of the passive negative feedback in which a KS-14 dimming filter (Fig 1.8d) was placed in the laser resonator under the Brewster angle. The time evolvement of the lasing spectrum (fig 1.8E), obtained at a high spectral resolution of the recording Fabry–Perot interferometer showed that in this case there was a periodic change of modes (with a period of ~40 μs), determined by retuning of the natural modes of the resonator as a result of the decrease of the length of the active rod due to its heating. The number of these transitions during the lasing pulse time can be evaluated using equation (1.1) from the following equation

$$N = 2l\Delta T\left[(n-1)\alpha_T + \partial n/\partial T\right]/\lambda. \qquad (1.9)$$

A single longitudinal mode was generated in the period between the change of the modes, and its displacement in the spectrum during the lasing pulse time was of the order of one inter-mode interval [12],

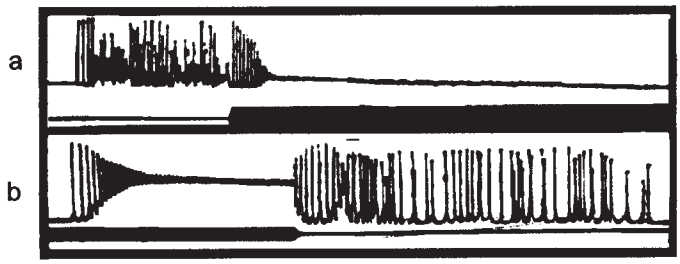

Fig. 1.8 Parameters of the lasing of TEM_{ooq} modes of a ruby laser (PL2B 8×120/180 mm) with flat mirrors (L = 1.6 m, diameter 1.4 mm) with smoothing of the longitudinal heterogeneity of the field in ruby using CPM in the conditions of passive negative feedback, $E_p = 3E_t$: a) oscillogram of radiation intensity, 20 μs markers; b) evolvement of the distribution of the radiation intensity in the long range zone; c-e) the time evolvement of the lasing spectrum without selection of longitudinal modes (c) and with selection (d,e), range of dispersion of the interferometers 12 pm (c), 8 pm (d) and 1.4 pm (e).

as clearly indicated by the interferogram of the integral spectrum of radiation (Fig. 1.9a). The rearrangement of the wavelength of the single-frequency radiation of a laser continuous ruby laser was obtained within the limits of the half width of the R_1-line of amplification of the ruby (~ 0.5 nm) (Fig. 1.9b). The reproducibility of the wavelength of radiation from pulse to pulse was approximately 0.5 pm with stabilisation of the temperature of the ruby and the selector-standard in the range 1°C. Divergence of laser radiation was of the diffraction type (1.5 mrad), and radiation energy was 0.1 J.

Forced sweep of the wavelength in the process of ruby laser lasing was ensured using a Fabry–Perot scanning interferometer with the dispersion range 0.24 nm in the speed range 0.01–0.4 nm/ms. Radiation intensity was stabilised using the CPM and a passive negative feedback. At low speeds (≤ 15 pm/ms) the sweep of the wavelength took place in the quasistationary regime with the size of the spectral transition between the modes equal to 1 inter-mode interval (Fig. 1.10a).

With increasing sweep speed, the change of the modes during the lasing process was accompanied by peaks of radiation intensity whose amplitude depended on the band of the dispersion resonator. As the selectivity of the dispersion resonator increased, the sweep rate at which pulsations of radiation intensity formed during mode change decrease. In the case of high sweep speeds (≥ 0.2 nm/ms) the nature of lasing was determined mainly by the sweep process and the change of the modes during the lasing process was accompanied by 100% pulsations of radiation intensity (Fig. 1.10b, c); the spectral interval between the adjacent peaks increased to $\Delta\lambda_q L/l$, where $\Delta\lambda = \lambda^2/2L$ is the spectral interval between the adjacent longitudinal modes.

1.3.3 Energy parameters of lasing

The energy characteristics of ruby laser radiation were investigated using a ruby crystal with a diameter of 5 mm, 75 mm long, with the ends bevelled under an angle of 1º, with the ends illuminated in a resonator with flat mirrors. Pumping was carried out using an ISP-250 lamp in a quartz single-unit illuminator with a pumping pulse time of 250 μs. The volume of the active medium V_g, excited by the pumping lamp and providing a contribution to the lasing energy, was 0.78 cm^3. Cooling of the crystal and the pumping lamp was carried out using distilled water whose temperature was maintained with a thermostat with an accuracy of 0.1°C.

For correct comparison of the energy characteristics of the radiation of Cr lasers in the examined solid-state media, all graphs of the dependences of the lasing energy on the parameters of the resonator and the active media are presented in Fig. 1.31. The main adequate parameter of comparison is the density of lasing energy E_g/V_g (J/cm^3).

The density of the lasing energy of the ruby laser is halved with increase of the resonator length from 0.4 to 1.6 m (Fig. 1.33a) (1). It should be noted that the resonator length L = 1.6 m is optimum for chromium lasers with flat mirrors for obtaining quasistationary lasing during the removal of the spatial heterogeneity of the field in the active medium. During heating of a ruby crystal from 20 to 60°C, the density of the lasing energy of the ruby laser decreased six times (Fig. 1.33b) (1), and at a constant pumping energy of 0.5 kJ the lasing threshold increased so much that lasing was interrupted.

At a pumping energy of 0.5 kJ, the optimum transmission factor

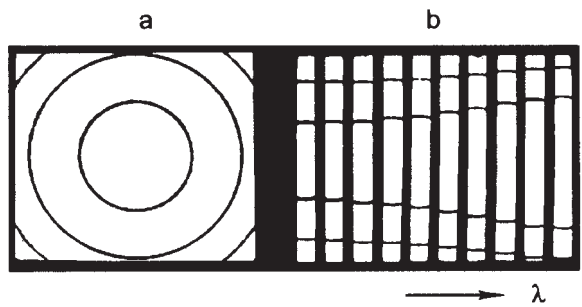

Fig. 1.9 a) interferrogram of the integral lasing spectrum of TEM_{ooq} modes of a ruby laser with smoothing of the longitudinal heterogeneity of the field in ruby using CPM in the conditions of passive negative feedback and selection of longitudinal modes, the range of dispersion of the interferrometer 8 pm; b) sequence of interferrogramsof the radiation spectra of a ruby laser with change of the radiation wavelength, the range of dispersion of the interferrometer 770 pm.

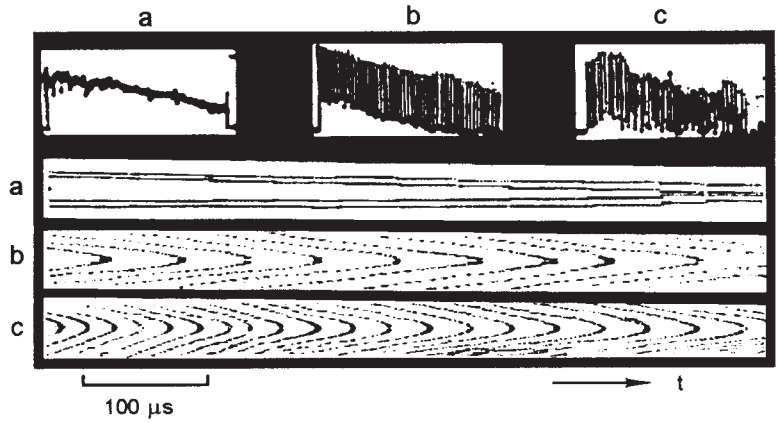

Fig. 1.10 Parameters of lasing of TEM_{ooq} modes of a ruby laser in sweeping the wavelength in the lasing process in the conditions of smoothing the longitudinal heterogeneity of the field using CPM and passive negative feedback, $E_p = 3E_t$; sweep right 15 (a), 150 (b) and 380 pm/ms (c).

of the output m of the resonator at which the maximum density of lasing energy was obtained (0.4 E/cm^3) for a ruby laser was 40% (Fig. 1.33c) (1). In the examined range of the pumping energy, the density of the lasing energy of the ruby laser depended in a linear manner on pumping energy (Fig. 1.33d) (1).

1.3.4 Lasing parameters of TEMmnq modes in a laser with spherical mirrors

The nature of free lasing TEM_{mnq} in a ruby laser with spherical mirrors with a non-critical configuration of the resonators (Fig. 1.11) differed only slightly from that of the lasing of a laser with flat mirrors: in both cases, there were nonregular non-attenuating pulsations of radiation intensity. Several transverse modes were excited in every lasing peak and the index of these modes was higher than in the laser with flat mirrors; these modes alternated during the lasing process (Fig. 1.11b). Lasing started with modes with a low transverse index which may have a higher attenuation coefficient as a result of the focusing of pumping energy on the axis of the rod. The first peak was characterised by the excitation of a large number of longitudinal modes with the width of the lasing spectrum of approximately 50 pm which decreased to 2.5 pm within several peaks (Fig. 1.11c); this is associated with the formation of a spatial heterogeneity of inversion in the active medium leading to the appearance of a large dispersion of the gain coefficient for different modes.

During smoothing of of the spatial heterogeneity in the ruby crystal using compensated phase modulation and the same experimental conditions, the lasing always took place in the quasistationary regime with a wide and uncontrollable spectrum (Fig. 1.12) [5]. Lasing with identical parameters was also detected in lasers with spherical resonators of critical configuration ($L = R$, $2R$) with the spatial heterogeneity of the field in the resonator self-smoothed, as a result of the excitation of a large number of degenerate modes with a high transverse index.

Modes with low transverse indices were excited at the beginning of the pulse. The threshold lasing conditions were at least one rapidly for these modes (Fig. 1.12b). When the conditions of excitation for the modes was high transverse indices were fulfilled the, the cross-section of the lasing region gradually increased, and at the end of the pumping pulse it slightly decrease with decrease in pulse. This time dependence of the transverse distribution of radiation intensity also resulted in the corresponding development of the lasing spectrum with time (Fig. 1.12c).

In the first half of lasing the maximum of the radiation spectrum drifted into the short-wave range, whereas in the second half it drifted into the long-wave range of the spectrum. The short-wave drift of the maximum of the radiation spectrum during the lasing process is possible because of two reasons. Firstly, because of the presence of the temperature gradient between the centre and edges of the active rod, the modes with a high transverse index are excited later than the modes with a low index, and their lasing starts at a lower mean temperature of the active medium. Consequently, the maximum of the effective gain curve and, the correspondingly, the maximum of the lasing spectrum were displaced to the short-wave range during lasing. Secondly, during lasing, the focus f_T of the induced thermal positive lens in the ruby crystal decreases. Assuming that the crystal is situated in the centre of a confocal resonator and the lens is ideally thin, we obtained the following equation for the rate of variation of the lasing wavelength [10]:

$$\frac{d\lambda}{dt} = \frac{3\lambda^2(m+n+1)\partial f_T}{8\pi f_T^2}. \qquad (1.10)$$

For the modes with the indices $m = n \sim 100$, $f_T \sim 1$ m, $\partial f_T/\partial t \sim 1$ m/ms, we have $\partial\lambda/\partial t \sim -0.6$ nm/ms, which greatly exceeds the thermal drift of the gain line to the long-wave region of the spectrum. It should

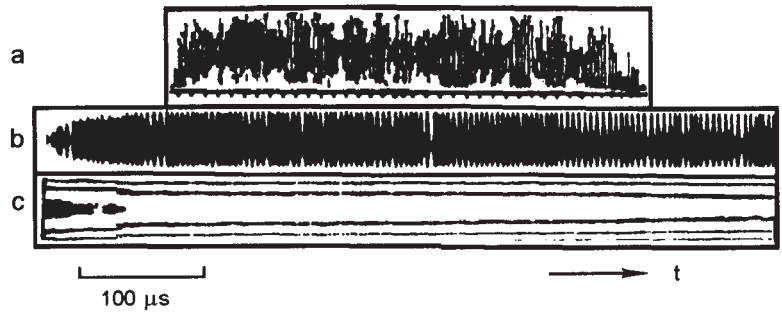

Fig. 1.11 Parameters of lasing of TEM_{mnq} modes of a ruby laser (diameter 12 mm, length 120 mm) with spherical mirrors ???($R_1 = R_2 = 1$ m, $L = 0.6$ m) in normal conditions and in the absence of mode selection, $E_p = 3E_t$; a) oscillogram of radiation intensity, 20 μs markers; b) evolvement of the distribution of the intensity in the near-zone; c) time evolvement of lasing spectrum, the range of dispersion of the interferometer 24 pm.

be noted that in the case of quasistationary lasing of TEM_{mnq} modes in a laser with spherical mirrors, the narrowing of the lasing spectrum did not take place to a single longitudinal mode as in the case of the quasistationary lasing of TEM_{ooq} modes, but it took place in the value determined by the broadening of the tip of the curve of the gain line determined by thermal gradients in the cross-section of the active rod.

The nature of lasing of the ruby laser with spherical mirrors and the direction of displacement of the maximum of the radiation spectrum depend greatly on the cross-section of the active rod taking part in lasing. At a ruby diameter of ≥ 12 mm, the maximum of the radiation spectrum was displaced to the short-wave range throughout the entire lasing pulse (Fig.1.13a). With a decrease of the cross-section of the excitation range of the ruby to 8 mm using two diaphragms, located in the vicinity of the edges of the ruby crystal, the rate of short-wave displacement of the lasing spectrum decreased (Fig. 1.13b). At a diaphragm diameter of 6 mm, the speed of the thermal drift of the gain line exceeded the influence of the effects leading to the short-wave displacement of the maximum of the lasing spectrum (Fig. 1.13c). With a decrease of the aperture of the resonator to 4 mm quasistationary lasing was not achieved even when using compensated phase modulation (Fig. 1.13d) because in this case only transverse modes with low transverse indices were excited and the transverse heterogeneity of the field in the active medium could not be eliminated even using the CPM [10].

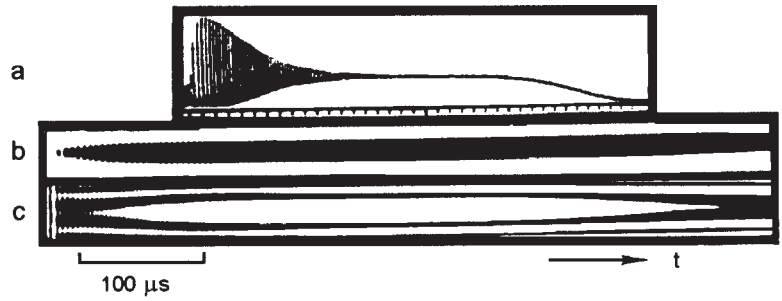

Fig. 1.12 Parameters of the lasing of TEM_{mnq} modes of a ruby laser with spherical mirrors in smoothing of the spatial heterogeneity of the field in ruby using CPM. Laser parameters are the same as those in Fig. 1.11.

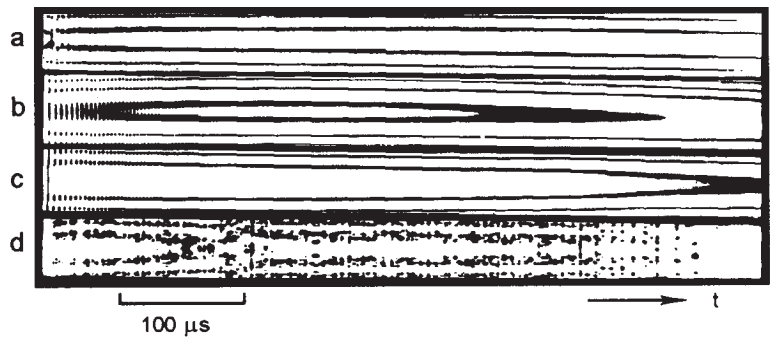

Fig. 1.13 Time evolvement of the lasing spectrum of TEM_{mnq} modes of a ruby laser (diameter 12 mm, length 120 mm) with CPM with spherical mirrors ($R_{12} = R_2 = 1$ m, $L = 0.6$ m) without diaphragm (a) and with two diaphragms in the resonator, diameter 8 mm (b), 6 (c) and 4 mm (d). The range of dispersion of the interferrometer 24 pm; $E_p = 3E_t$.

The inertia of the lasing regime

In contrast to the case of lasing of a laser with flat mirrors where the interaction of the CPM during the lasing process resulted immediately in the transition from the quasistationary regime to the regime of non-attenuating pulsations of radiation intensity (Fig. 1.7b), in the laser with spherical mirrors even short-term smoothing of the spatial heterogeneity of the field at the start of the pulse caused quasistationary lasing after the end of the pulse (Fig. 1.14a) [8]. This switching of the conditions can be carried out at any moment of lasing (Fig. 1.14b).

The reproducibility of this 'inertia of the regime' was 100% in the range of variation of the radius of curvature of the mirrors and the length of the resonator from the minimum possible to 1.5 mm, excluding unstable and critical configurations of the resonator [13]. In this range of variation of the resonator parameters, the quasistationary

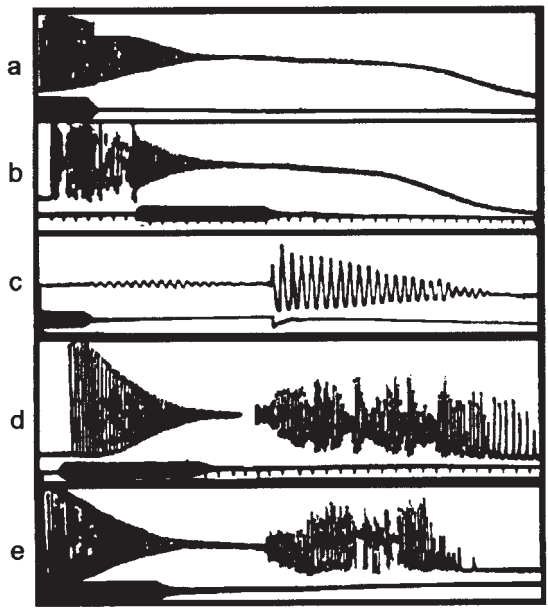

Fig. 1.14 Oscillograms of the intensity of radiation of TEM_{mnq} modes of a ruby laser (diameter 12 mm, length 120 mm) with spherical mirrors (L = 0.7 m, $R_1 = R_2$ = 1 m (a-d) and 1.8 m (e) and without CPM lasing; $E_p = 3E_t$.

lasing regime was resistant to relatively strong external perturbations.

When inversion in the ruby crystal was eliminated using a gigantic pulse with a power of 10 MW from another laser, its effect was followed by the formation of relaxation radiation pulses which rapidly attenuated to the stationary level (Fig. 1.14c). Only in the case in which the lasing was artificially interrupted using an electro-optical gate for a period of ~ 20 μs, sufficient for the attenuation of the fields of the generating modes, there was a reverse transition from the quasistationary regime to the regime of non-attenuating pulsations of radiation (Fig. 1.40d). With an increase of the radius of curvature of the mirrors to $R > 1.5$ m, a similar transition was observed spontaneously at any moment of time after switching off the CPM (Fig. 1.14 e), and in the limiting case of the flat mirrors this switching off the regimes took place simultaneously with the disconnection of the CPM.

The spectrum inertia regime

In lasers with spherical mirrors it is almost impossible to carry out the forced selection of longitudinal modes. However, in a ruby laser with spherical mirrors with strong degeneration of the modes under

specific conditions there may be a spontaneous effect of stabilisation of the radiation wavelength ('inertia of the spectrum') [13]. In this case, in the absence of external and spurious selection of the longitudinal waves a very narrow (~ 0.05 pm) and stable (with respect to spectrum and time) radiation line generates (Fig. 1.15 and 1.16). This effect is achieved in the conditions of the thermal drift of the gain line of the order of 30 pm, the thermal rearrangement of the natural modes of the resonator (~5 pm) and the thermal broadening of the tip of the curve of the gain line (~10 pm). The stable regime of inertia of the spectrum is established when the threshold conditions are fulfilled only for the modes with a high transverse index (m, $n > 100$), and the degree of degeneration of the modes is sufficient for the long-term alternation of the modes in lasing without any change of the radiation wavelength. The reproducibility of the inertia regime of the spectrum increased during an artificial decrease of the Q-factor of the modes with the low transverse index. This is achieved by overlapping the centre of the ruby crystal by a non-transparent screen with a diameter of ~1 mm.

Depending on experimental conditions, spectrum inertia was obtained in both peak (Fig. 1.15) and quasi-continuous (Fig. 1.16) regimes, in the range of radiation of the radius of curvature of the mirrors $20 \leq R \leq 110$ cm and the resonator length $30 \leq L \leq 100$ cm. In the quasistationary regime, spectrum inertia was achieved at considerable de-tuning of the mirrors of the resonator with respect to the angle (~ 30') which resulted in the appearance of a small transverse 'running' of the field, increasing the intensity of the parametrically scattered radiation priming. The latter decreases the time of the linear development of the radiation peaks to such an extent that the pulsations of the radiation intensity overlap in time (Fig. 1.16c).

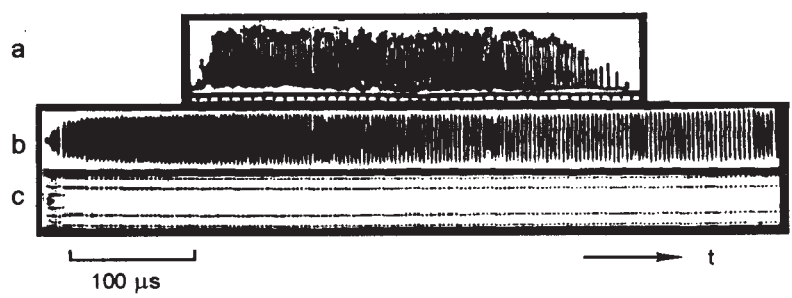

Fig. 1.15 Parameters of the lasing of TEM_{mnq} modes of a ruby laser (diameter 12 mm, length 120 mm) with spherical mirrors ($R_1 = R_2 = 0.5$ m, $L = 0.4$ m) in the regime of 'inertia of the spectrum', $E_p = 3E_t$; a) oscillogram of intensity, 20 μs markers; b) evolvement of the distribution of intensity of radiation in the near-zone; c) time evolvement of lasing spectra, the range of dispersion of the interferometer 24 pm.

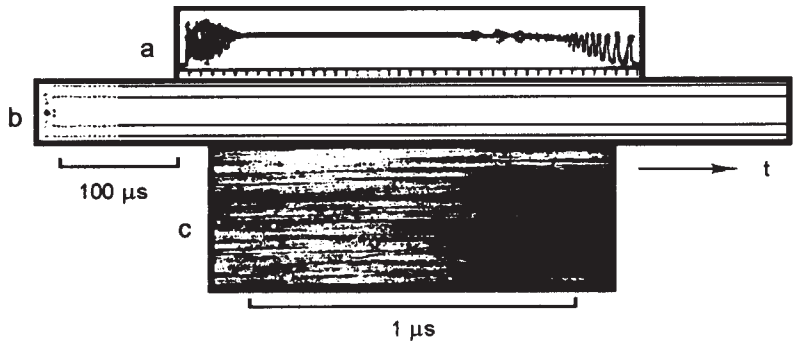

Fig. 1.16 Parameters of the lasing of TEM_{mnq} modes in a ruby laser (diameter 12 mm, length 120 mm) with spherical mirrors (R_1 = R_2 = 1.1 m, L = 0.9 m) in the regime of "inertia of the spectra" with a high constant component of the integral intensity of radiation, $E_p = 3E_t$: a) oscillogram of radiation intensity, 20 μs marker; b) time evolvement of the lasing spectrum, the range of dispersion of the interferrometer 24 pm; c) the fragment of the time evolvement of the distribution of intensity of radiation in the near zone, obtained with high spatial and time resolution.

The simultaneous excitation of the modes with a high transverse index and the establishment of quasistationary lasing are prevented by the spatial heterogeneity of the inversion developed by the modes with low transverse indices at the beginning of lasing (Fig. 1.15b). After establishment of the spectrum inertia regime a single transfer mode with a high index was generated in every peak, as clearly indicated by the time evolvement of the spatial distribution of the radiation intensity in the near zone (Fig. 1.15b and Fig. 1.16c) on the basis of the presence of the distinctive structure of the field. Numerical estimates indicates that after lasing of some mode, the effective gain coefficient with the spatial heterogeneity of inversion taken into account will be maximum for the mode whose frequency is close to or identical with the frequency of the generated mode. The lasing in the subsequent peak starts to develop not from the level of spontaneous noise but from the intensity of priming radiation, formed by the generated mode with its parametric scattering on the spatial heterogeneity of inversion. According to the estimates, the intensity of the priming is several orders of magnitude higher than the intensity of spontaneous noise.

In cases in which the spatial heterogeneity of inversion was smoothed out using compensated phase modulation with some delay from the start of lasing, there was always a transition in the lasing process from the regime of spectrum inertia to the quasistationary lasing with a wide spectrum drifting in time. With complete removal of the selection of the longitudinal modes in which the ends of the ruby crystal were

cut under the Brewster angle, the moment of establishment of the regime of spectrum inertia was extended by approximately ~100 μs in relation to the start of lasing. The decrease of the indices of the transverse modes by means of a diaphragm resulted in jumps of the radiation wavelength during the lasing process as a result of a decrease of the number of generated transverse waves with the same radiation frequency.

The rearrangement of the wavelength of single-frequency radiation within the limits of the maximum of the curve of the gain line in the regime of spectrum inertia was carried out by angular rotation of one of the mirrors of the resonator. In the case of a ruby crystal with a diameter of 12 mm and 120 mm long, when the pumping was three times higher than the laser threshold value, the energy of single-frequency radiation was 5 J.

1.4 ALEXANDRITE LASERS

The lasing of trivalent chromium ions in a chryzoberyll crystal (alexandrite, Cr^{3+}:$BeAl_2O_4$) was reported for the first time on *R*-lines ($^2E \rightarrow {}^4A_2$) in Ref. 33, and for $^4T_2 \rightarrow {}^4A_2$ electron–vibrational transitions $^4T_2 \rightarrow {}^4A_2$ in the investigations carried out in Ref. 34. In the alexandrite crystal, part of the Al^{3+} ions is isomorphously substituted by Cr^{3+} ions. Alexandrite is characterised by high heat conductivity (23 W/m·deg) which is still only half the heat conductivity of the ruby crystal, and the optical resistance to radiation of alexandrite is not inferior to that of the ruby crystal. Alexandrite is a biaxial crystal with a rhombic structure and its refractive index in the individual axes is: n_a = 1.796, n_b = 1.738 and n_c = 1.746. The Moose hardness is 8.5, density 3.7 g/cm^4. The coefficients of thermal expansion of alexandrite are 7.0 (7.9; 9.5)×10^{-6} deg^{-1}, and the thermo-optical constant is dn/dT = 9.4 (8.3)×10^{-6} deg^{-1}. The melting point of alexandrite is 1870°C, and the crystal is characterised by isotropic expansion with increasing temperature. A wider application of the alexandrite crystal is prevented by both the toxicity of beryllium (i.e. the component of alexandrite) and by the relatively complicated technology of crystal growth.

The excited state of alexandrite is represented by a superposition of two states of the chromium ions ^2E and $^4T_2$ (Fig. 1.17), with the relaxation time between them being 10^{-11} s. The energy range between these states is $\Delta E \sim 800$ cm^{-1}, which is almost four times higher than the value of kT at room temperature (208 cm^{-1}), resulting in the thermal instability of the energy characteristics of radiation. The transition cross-section increases from 0.7×10^{-20} at 300 K to 2×10^{-20} cm^{-2} at T = 470 K. The transition from the level ^2E to the ground state $^4A_2$ is forbidden in respect of spin and consequently, the lifetime is long,

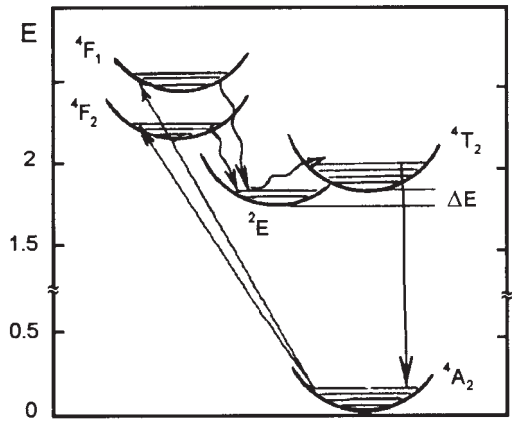

Fig. 1.17 Diagram of energy levels E (eV) of chromium ions Cr^{3+} in chryzoberyll (aleksandrite).

1.54 ms. The relatively short-lived state $^4T_2$, with the transition from the state being forbidden as intra-configuration, but permitted with respect to spin, has a lifetime of 6.6 μs. Therefore, the effective lifetime of the total upper laser level (^2E, $^4T_2$), determined by the relationship

$$\tau = \frac{1+\exp(-\Delta E/kT)}{W_1+W_2\exp(-\Delta E/kT)}, \qquad (1.11)$$

is 300 μs. Here W_1 and W_2 are the rates of deactivation of the states ^2E and $^4T_2$, respectively. In optical pumping, the excited ions build-up on the metastable level ^2E and are transferred, as a result of thermal excitation, through the energy gap ΔE to the level $^4T_2$, and the population of the state $^4T_2$ is only ~5% of the population of the level ^2E. A relatively high gain factor on the upper laser level in the alexandrite crystal is obtained as a result of the high probability of the transition $^4T_2 \rightarrow {}^4A_2$ determined by the low local symmetry of the impurity centres taking part in the lasing.

Alexandrite lasers operate in all possible lasing conditions: free lasing, Q-factor modulation and mode synchronization, in pulsed, pulsed-periodic and continuous regimes.

1.4.1 Spectral–time lasing parameters

The spectral–time, spatial and energy characteristics of free lasing of alexandrite lasers have been investigated by the authors of the book

in [15,16,18–29]. Free lasing of TEM_{ooq} (Fig. 1.18) and TEM_{mnq} (Fig. 1.19) modes in an alexandrite laser with flat mirrors under normal conditions and with the elimination of the effect of technical perturbations of the resonator, as in the case of the ruby laser, took place in the regime of non-attenuating pulsations of radiation intensity.

The nature of development of the lasing spectrum with time depends on the physical state of alexandrite crystals, on the temperature and the existence of discrimination of modes in the resonator. In the case of separation of TEM_{ooq} modes the width of the instantaneous lasing spectrum decreased in individual peaks to ~1 nm (Fig. 1.18c) [50], but the width of the integral radiation spectrum did not differ from the lasing spectrum of TEM_{mnq} modes.

In long-term operation of alexandrite in the conditions of incomplete cut-off of ultraviolet radiation the lasing threshold at a radiation wavelength of 734 nm increased and with time the lasing on this wavelength completely disappeared even at low temperatures (~10°C) of the crystals and high pumping levels (Fig. 1.19a). The lasing on this wavelength did not appear also in the case of non-irradiated crystal at a crystal temperature of ≥70°C (Fig. 1.19e). In the case of the low discrimination of the longitudinal waves, introduced by the illuminated ends of the crystals, the radiation spectrum contained a fine discrete structure (Fig. 1.19b), which disappeared after complete removal of the spurious selection of longitudinal waves when the ends of the crystals were cut under the Brewster angle (Fig. 1.19c-e). Only in this case the lasing spectrum showed clearly the vibrational structure (Fig. 1.22). In this case, the duration of the peaks of free lasing increased

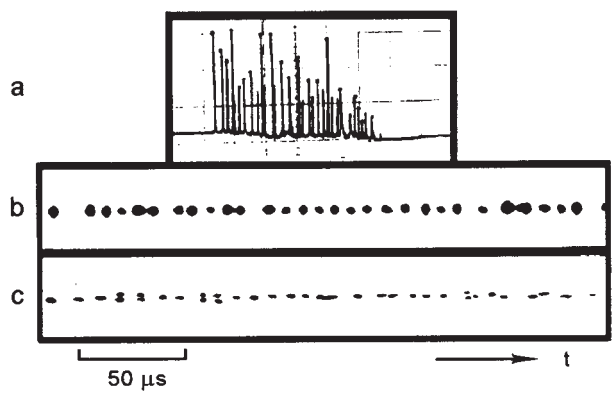

Fig. 1.18 Parameters of lasing of TEM_{ooq} of a Aleksandrite laser (5 mm diameter, 80 mm long) with flat mirrors in the absence of longitudinal mode selection, $E_{pI} = 5E_p$; a) oscillogram of the intensity, 50 μs/div; b) evolvement of the distribution of radation in the near-zone; c) time evolvement of the spectrum.

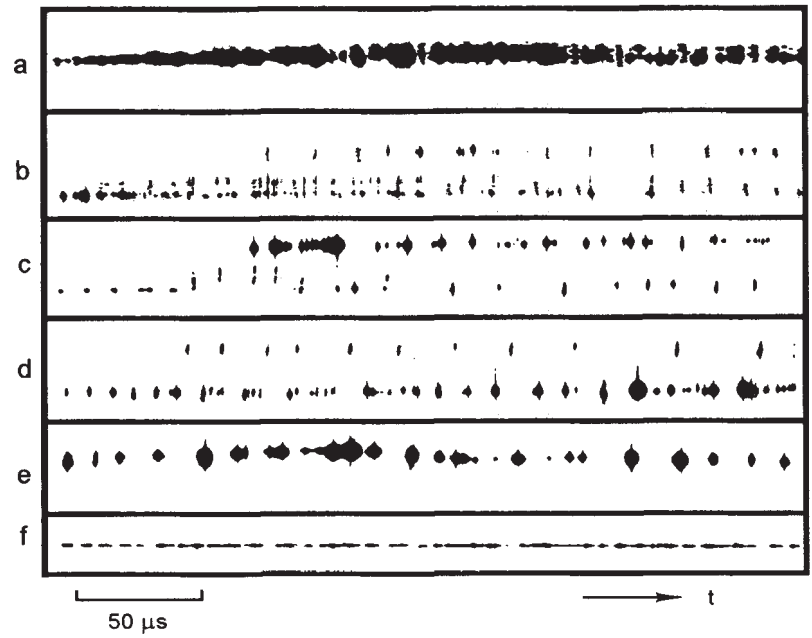

Fig. 1.19 Time evolvement of the lasing spectrum of TEM_{mnq} modes of an aleksandrite laser with different crystals with flat mirrors in the absence of longitudinal mode selection (c-e) and with longitudinal mode selection (f), in the conditions of weak spurious selection of modes (b). The temperature of aleksandrite crystals T = 10 (a-d) and 70 °C (e,f), L = 1.5 m, $E_p = 8E_t$.

(Fig. 1.19c-e). The distance between the components of the vibrational structure of the spectrum was 1.5 nm and did not depend on the temperature of the alexandrite crystal [18,20].

The application of a prism dispersion resonator with an angular dispersion of ~3 angular min/nm made it possible to stabilise the lasing spectrum, reduced its width to ~1 nm (Fig. 1.19f) and rearrange the radiation wavelength in the range 700–800 nm (Fig. 1.20).

In the conditions with a low spurious selection of the longitudinal modes, the integral radiation spectrum contained a fine discrete structure of the radiation spectrum (Fig. 1.21). With the completely spurious selection of the modes where the ends of the alexandrite crystals were cut under the Brewster angle, the fine structure of the spectrum disappeared and the integral radiation spectrum showed clearly the vibrational structure of the spectrum, Fig. 1.22. With increase of the pumping energy, the width of the integral radiation spectrum increased and when the pumping energy was eight times higher than the threshold value, its width was ~40 nm (Fig. 1.21a). During heating of the alexandrite crystal the short-wave components in the radiation spectrum

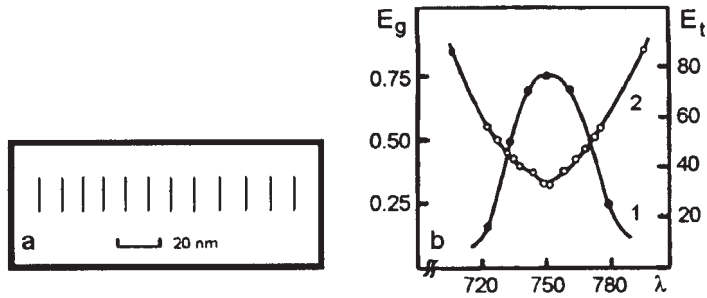

Fig. 1.20 a) sequence of spectrograms of the integral spectrum of lasing of TEM_{mnq} modes of an aleksandrite laser (diameter 4 mm, length 70 mm) with flat mirrors (L = 1.6 m) illustrating the diagram of tuning the radiation wavelength, $E_p = 8E_t$; b) dependence of the lasing energy E_g (J) (1) and threshhold pumping energy E_t (J) (2) of an aleksandrite laser in a dispersion resonator on the wavelength of radiation λ (nm).

gradually disappeared and at a temperature of approximately 70°C lasing took place only in the vicinity of the wavelength of 750 nm (Fig. 1.21b). In the absence of spurious selection of the longitudinal waves, the maximum of the concentration of radiation energy after this wavelength was displaced to the short-wave region of the spectrum with increasing pumping energy, Fig. 1.22b.

In the temperature range of the alexandrite crystal of 10–50°C, the mean speed of the thermal drift of the gain line was 0.01 nm/deg. The speed rapidly increased to 0.13 nm/deg at temperatures higher than 50°C (Fig. 1.23) [18, 20]. This displacement of the lasing spectrum of the laser on electronic–vibrational transitions is associated with the dependence of the gain factor α(ω) of the active media on temperature:

$$\alpha(\omega) = \sigma\left\{n^* - n_o \exp\left[\frac{\hbar(\omega - \omega_o)}{kT}\right]\right\}, \qquad (1.12)$$

where σ is the radiation cross-section of the induced transition; n^* is the number of excited chromium ions of the level $^4T_2$; n_o is the number of chromium ions in the ground state $^4A_2$; ω_o is the frequency of the effective phonon-less transition.

1.4.2 Energy parameters of lasing

Figure 1.33 shows the dependences for the lasing energy density of the alexandrite laser with a diameter of 5.5 mm × 80 mm, with the ends under the Brewster angle and V_g = 1.42 cm^3. Pumping of the crystal was carried out using IPF-800 lamp with a pumping pulse

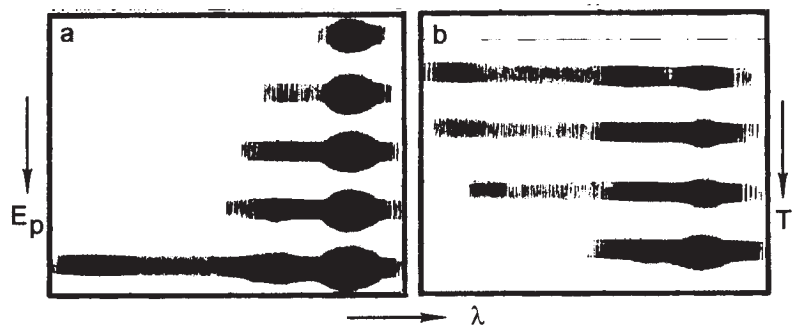

Fig. 1.21 Spectrograms of radiation of TEM_{mnq} modes of an aleksandrite laser (5 mm diameter, length 70 mm) with flat mirrors (L = 0.4 m) with slight spurious selection of the longitudinal mode: a) at a constant temperature of the crystal (T = 10 °C) and different pumping energies E_p = 2, 4, 5, 6 and $8E_t$; b) at a constant pumping energy ($E_p = 8E_t$) and different temperatures of the crystal T = 15, 25, 35 and 45 °C.

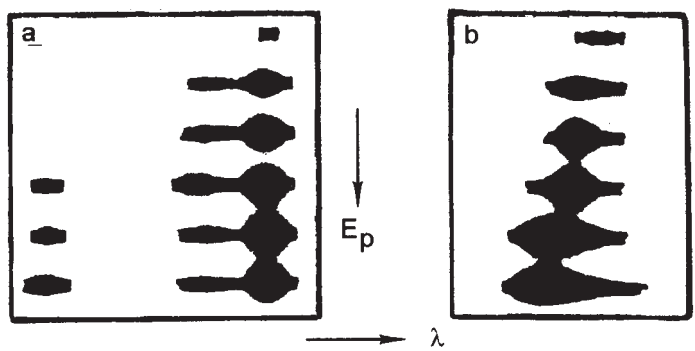

Fig. 1.22 Spectrograms of radiation of TEM_{mnq} modes of an aleksandrite laser (diameter 5.5 mm, length 80 mm) with flat mirrors (L = 1.5 m) with complete exclusion of spurious selection of longitudinal modes: a) at a constant temperature of the crystal (T = 10 °C) and different pumping energies E_p = 2, 4, 5, 6 and $8E_t$; b) at a crystal temperature of T = 70 °C and pumping energies of E_p = 3, 4, 5, 6, 7, and $8E_t$.

time of 250 μs in the experimental equipment described previously. The short-wave pumping radiation (≤ 300 nm) was cut-off by a liquid filter.

Increase of the resonator length from 0.4 to 1.6 m with other resonator and pumping parameters constant resulted in a decrease of the density of lasing energy of the alexandrite laser by a factor of 4 (Fig. 1.33a) (2) [18,20]. At a constant pumping energy and with heating of the crystal from 10 to 90°C, the density of the lasing energy of the alexandrite laser increased three times (Fig. 1.33b) (2) [18]. At a pumping energy of 0.5 kJ, the optimum transmission factor of the output mirror of the alexandrite laser resonator was 25% (Fig. 1.33c) (2) and the density

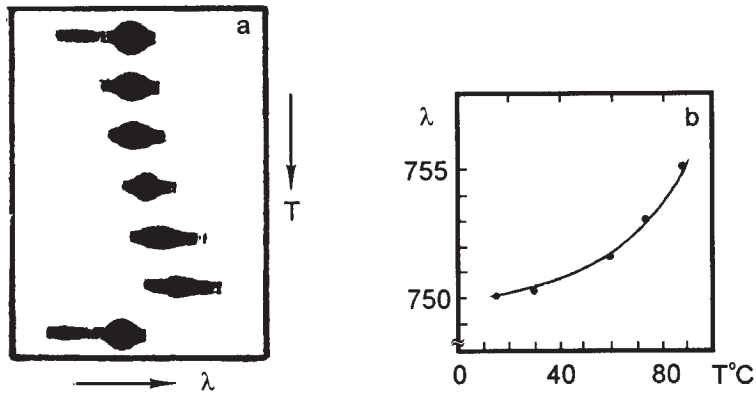

Fig. 1.23 a) spectrograms of the integral spectrum of the lasing of TEM_{mnq} modes of an aleksandrite laser (diameter 5.5 mm, length 80 mm) with flat mirrors (L = 1.6 m) without spurious selection of longitudinal modes, with constant pumping energy (E_p–3E_t) and different crystal temperatures T = 15, 30, 45, 75, 85 and 15 °C; b) dependence of the position of the maximum of the lasing spectrum of TEM_{mnq} modes of an aleksandrite laser at wavelength λ = 750 nm on crystal temperature T.

of lasing energy was E_g/V_g = 1.5 J/cm^3. The density of lasing energy of the alexandrite laser depended in a linear manner on the pumping energy at low values of this energy (Fig. 1.33d) (2). Increasing pumping energy (≥ 0.4 kJ) resulted in a deviation from the linear dependence associated with the increase of the fraction of the energy of the pumping pulse, radiating in the ultraviolet region of the spectrum, which was cut-off by the liquid filter [18].

1.5 EMERALD LASERS

The lasing of trivalent chromium ions in an emerald crystal at the electronic–vibrational transitions $^4T_2 \rightarrow {}^4A_2$ was examined for the first time in Ref. 35. The adjustable lasing of the laser on an emerald crystal at the transition $^4T_2 \rightarrow {}^4A_2$ during laser pumping was investigated in Ref. 52–54, and of R-lines of chromium ions in Ref. 54, 55. The energy characteristics of lasing of an emerald laser, with the crystal grown by the flux method, with valve pumping, was investigated in Ref. 56.

The emerald crystal (Cr^{3+}:$Be_3Al_2(SiO_3)_6$) is a chromium beryll, uniaxial, negative, has refractive indices n_o = 1.58 and n_e = 1.575. With a chromium ions concentration of 0.01–1%, the crystal is green. Its melting point is 1470 °C which is 400 degrees lower than the melting point of the alexandrite crystal. The heat conductivity of the emerald crystal is almost six times lower than that of alexandrite and equals 4 W/m·grad, and the thermal expansion coefficient is 2.6(2.9)×

10^{-6} deg^{-1}. The Moose hardness of the emerald crystal is 8.0, density 2.68 g/cm^3. The emerald crystals are grown by two methods: hydrothermal and flux. The emerald crystals grown by the flux method have better optical quality and contain a smaller content of secondary impurities. Non-selective losses of the emerald crystals, grown by the hydrothermal methods, are of the order of 0.1 cm^{-1}.

Lasing of the electronic–vibrational transitions $^4T_2 \rightarrow {}^4A_2$ in the emerald crystal takes place in the wavelength range 700–850 nm. The energy gap in the levels $^4T_2$ and ^2E of the chromium ions in the crystal is 400 cm^{-1}, which is half the value in the alexandrite crystal. At room temperature, the lifetime of the excited state of the chromium ion in the beryll crystal is 65 μs, and the transition cross-section is $\sigma = 3.3 \times 10^{-20}$ cm^2. The optical absorption spectra of the emerald crystal (Fig. 1.24) are typical of the matrixes containing the Cr^{3+} ions in the octahedral environment of the oxygen ions. The wide bands in the blue and red regions (Y,U) of the spectrum belong to the permitted transitions $^4A_2 \rightarrow {}^4T_1$, $^4T_2$ respectively. The triplet levels in the emerald crystal are split by the trigonal component of the crystal field leading to differences of the π and σ components in absorption. The narrow absorption lines at 681 and 684 nm are associated with the transitions $^4A_2 \rightarrow {}^2E$ (R_1 and R_2-lines) forbidden with respect to spin. The fine structure of the U line is determined by the electron-phonon interaction. The emerald crystal is characterised by a more complicated structure and, as indicated by the position of the U band, by a weaker crystal field D_q = 1600 cm^{-1} (for alexandrite D_q = 7040 cm^{-1}).

In the emerald crystals, strong ultraviolet absorption starts at shorter wavelengths than in the case of the alexandrite, in the range 300 nm for the crystals prepared by the flux method and 360 nm in the crystals prepared by the hydrothermal method; in the latter case, additional bands exist in the range 380–450 nm. The short-wave absorption of emerald is determined mainly by secondary impurities, especially iron, whose concentration reaches 0.001 wt% in the flux specimens and 0.1 wt% in the hydrothermal specimens.

The luminescence spectra of the chromium ions in the emerald crystal (Fig. 1.25) are characterised by the dominance of a wide band with the maximum at a wavelength of 770 nm, corresponding to the $^4T_2 \rightarrow {}^4A_2$ transition.

The intensity of the R_1 and R_2 lines in the emerald crystal is lower. This associated with the lower energy gap ΔE between the levels ^2E and $^4T_2$. In the emerald crystal, these levels are close to the thermal equilibrium (kT = 208 cm^{-1}) already at room temperature, and the metastable level ^2E is sufficiently clear through the short-life level

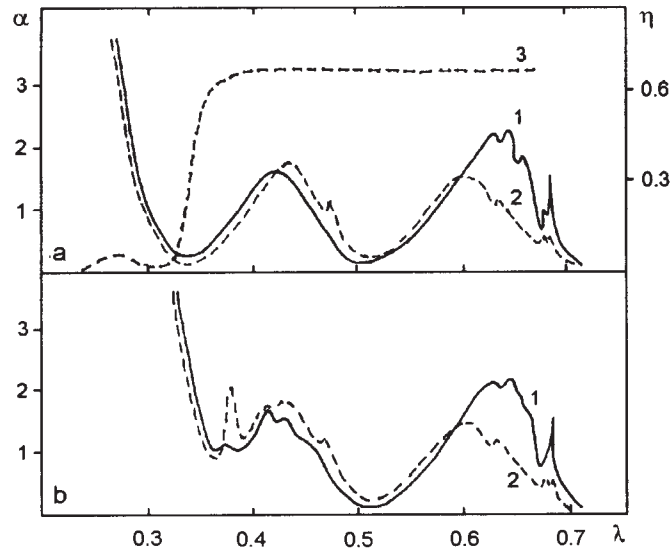

Fig. 1.24 Dependence of the absorption coefficients α (cm^{-1}) (1,2) and the quantum yield of luminesence η on the wavelength λ(μm) for flux (a) and hydrothermal (b) emerald at T = 300 K, 1) E || C, 2) E ⊥ C.

$^4T_2$. In alexandrite as a result of a higher value of ΔE = 800 cm^{-1}, this takes place at higher temperatures.

The absolute quantum yield of the luminescence of the chromium ions in the emerald crystal is 0.7 for the crystal produced by the flux method, and approximately 0.01 for the crystal produced by the hydrothermal methods. The constant quantum yield in the range of absorption of chromium ions and its decrease in the range smaller than 380 nm indicated that the short-wave absorption, observed in the crystals, is associated with the chromium ions.

Difficulties in producing the emerald crystals with the dimensions standard for the lasers are associated with the very low growth rate of the crystals which is an order of magnitude lower than the growth rate of the alexandrite crystals, and the toxicity of the component, i.e. beryllium, prevents the extensive application of the emerald lasers

1.5.1 Spectral–time parameters of lasing

The spectral and energy parameters of lasing of the emerald laser were investigated by the authors of this book in Ref. 30. The lasing spectrum TEM_{mnq} of the emerald laser (Fig. 1.26) is almost identical with the similar lasing spectra of the alexandrite laser. In the presence of even weak spurious selection of the longitudinal modes, introduced by the ends of the crystal, the lasing spectra of the emerald laser,

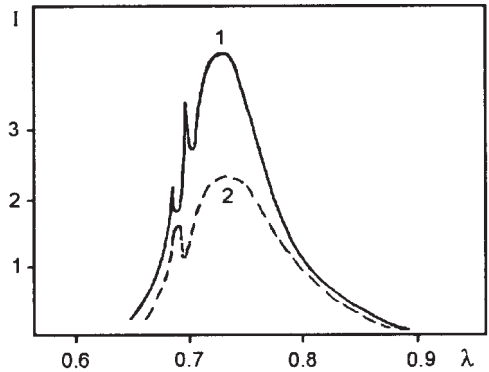

Fig. 1.25 Dependence of the intentsity of luminesence I (rel.units) of the emerald crystal on the wavelength λ (μm) at T = 300 K, 1) E || C, 2) E ⊥ C.

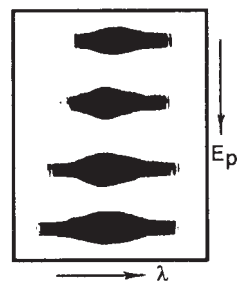

Fig. 1.26 Spectrograms of radiation of TEM_{mnq} modes of an emerald laser at T = 20 °C in relation to pumping energy E_p = 3, 4, 6, $8E_t$.

like the lasing spectra of the alexandrite laser, are characterised by a fine discrete structure. At room temperature and low pumping levels, the lasing of the emerald laser takes place in a wide spectrum range with the maximum wavelength of 770 nm. With increase of the pumping energy the lasing spectrum was broadened into the short-wave range, and when the pumping energy was eight times higher than the threshold energy, the width of the lasing spectrum of the emerald laser was approximately 30 nm. The width of the lasing spectrum depended in a linear manner on the pumping energy.

The rearrangement of the wavelength of lasing of the emerald laser was carried out in a dispersion resonator using three dispersion prisms produced from TF-5 glass with a general angular dispersion of the order of 3 ang.min/nm. The wavelength of lasing was rearranged in the range 710–830 nm, with the stabilisation of the wavelength of radiation in the range ~1 nm.

Experiments shows that the lasing of the TEM_{ooq} and TEM_{mmq} modes in the emerald laser, like the all other active media with the chromium

ions, always took place in the energy of non-attenuating pulsations of the radiation intensity. The nature of development of the lasing spectrum with time for the emerald laser depended, as in the case of the alexandrite laser, on the physical state of the emerald crystals and the presence of spurious discrimination of the longitudinal modes in the laser resonator. In the conditions with incomplete cut-off of ultraviolet pumping radiation, the nature of development of the lasing spectrum of the emerald laser with time changed greatly.

1.5.2 Energy parameters of lasing

The investigations were carried out on an emerald crystal with a diameter of 3 mm, 35 mm long, the volume V_g = 0.21 cm^3, groaned by the flux method with the concentration of chromium ions of the 0.7 wt%. The ends of the crystal are cut under an angle of 1°. Pumping was carried out with an ISP-250 lamp in a quartz single-unit illuminator with the pumping pulse time of 250 μs. Ultraviolet radiation was cut-off with a liquid filter.

Figure 1.33 shows the dependence of the density of lasing energy E_g/V_g (J/cm^3) of an emerald crystal laser (5) on the parameters of the resonator and crystal temperature. The heat conductivity of the emerald crystal is considerably lower than the heat conductivity of the alexandrite crystal and this resulted in a stronger dependence of the energy of lasing of the emerald laser on the length of the resonator (Fig. 1.33a) (5). In contrast to the alexandrite laser, the emerald laser did not show any distinctive dependence of the lasing energy on the temperature of the active medium (Fig. 1.33b) (5). This was caused by the fact that the energy gap between the metastable level ^2E and the upper working level $^4T_2$ of the chromium ions in the emerald laser is considerably smaller and its effective population already takes place at room temperature. At a pumping energy of 0.5 J, the maximum lasing energy in the emerald laser is obtained at the maximum transmission factor of the output mirror of the resonator being 40% (Fig. 1.33c) (5). The threshold energy of pumping in the emerald laser was considerably lower than in the alexandrite laser in the entire range of radiation coefficients T_2. At the optimum transmission factor of the output power, the lasing energy of the emerald laser increased in a linear manner in the range of low pumping energies (Fig. 1.33d) (5), and at higher pumping energies the linear dependence was disrupted.

1.6 CHROMIUM LASERS IN RARE-EARTH–GALLIUM GARNETS

Depending on the strength of the crystal field of the active medium, the energy position of the level $^4T_2$ of the chromium ion Cr^{3+} changes

greatly, whereas the position of the level ^2E remains almost constant. To obtain a small difference in the energy ΔE between the levels $^4T_2$ and ^2E, the strength of the crystal field should be ~1500 cm^{-1}. Decrease of the energy ΔE increases the population of the level $^4T_2$ and the lasing efficiency. This condition in satisfied by the crystals of rare earth–gallium garnets (REGG) [36, 37] in which the ions Cr^{3+} are in a weaker crystal field in comparison with the alexandrite and aluminium garnets. This is associated with the higher value of the lattice constant in the case of the REGG.

The REGG crystals are characterised by higher isomorphous capacity, have higher technological properties, the lower melting point, and do not contain toxic components, like alexandrite or emerald. The general formula of the gallium garnets $A_3B_2B_3O_{12}$ makes it possible to change in a wide range the chemical composition and produce a laser matrix with the required spectral characteristics. The similarity of the ion radii of Ga^{3+} and Cr^{3+} makes it possible to add large numbers of the chromium ions to the gallium garnets. The lasing of the chromium ions in the REGG crystals, like in the chryzoberyll, takes place at the electronic–vibrational transitions $^4T_2 \rightarrow {}^4A_2$, so that it is possible to carry out rearrangement of the lasing wavelength of these crystals in the range 700–900 nm.

Important shortcomings of the gallium garments, which inhibit their extensive applications, are: 1. low heat conductivity which in the case of R4 valve pumping resulted in high deformation of the resonator and the losses of radiation energy; 2. susceptibility to the formation of stable dye centres even in pumping with the radiation of the visible range with absorption on the lasing wavelength. This also results in large losses of radiation energy and in instability of this energy during operation. In contrast to dynamic dye centres, the stable dye centres the breakdown only after a high temperature of the crystals. This requires regular annealing of the crystals in a high-temperature furnace.

1.6.1 Spectral–time parameters of lasing

The spectral–time and energy characteristics of the free lasing of chromium lasers on the crystals of REGG have been investigated by the authors of this book in Ref. 17, 19, 20, 21–29.

The free lasing of the chromium ions in REGG crystals in lasers with flat mirrors under normal conditions was also observed in the regime of non-attenuating pulsations of radiation intensity, as in lasers based on ruby and alexandrite. Figure 1.27 shows the typical parameters of the free lasing of a Cr laser in a crystal of the gadolinium-scandium–gallium garnet (Cr^{3+}:GSGG). In the absence of the selection of longitudinal modes, the vibrational structure of the spectrum was

detected in every lasing peak (Fig. 1.27c). However, as a result of a large red displacement of the spectrum during the lasing process, determined by the heating of the crystal as a result of its low heat conductivity, this structure is completely masked in the integral spectrum (Fig. 1.28a and 1.29a), in contrast to lasing in the alexandrite laser. The displacement of the maximum of the lasing spectrum at 200 μs was approximately 5 nm (Fig. 1.27c). This corresponds to heating of the GSGG crystal by 40°C. In a prism dispersion resonator with an angular dispersion of 3 angular min/nm, the lasing spectrum narrowed down and stabilised in the range 1.09 nm (Fig. 1.27d). Lasing with similar parameters was also detected in other REGG crystals. The resultant ranges of rearrangement of the radiation wavelength of REGG lasers were: 740–840 nm (GSGG), 710–790 m (YSGG) and 760–810 nm (GSAG). In the absence of the selection of the longitudinal modes, the width of the integral spectrum of lasing of REGG laser and the position of its maximum depended both on pumping energy and crystal temperature. With doubling of pumping energy, the width of the integral radiation spectrum of the Cr:YSGG increased three times, and its maximum was displaced to the short-wave region of the spectrum (Fig. 1.28). When heating the Cr:YSGG crystal, the maximum of the integral spectrum of lasing and, correspondingly, the maximum of the gain line were displaced to the long-wave region with a mean rate of ~0.13 nm/deg, and its width slightly increased (Fig. 1.29).

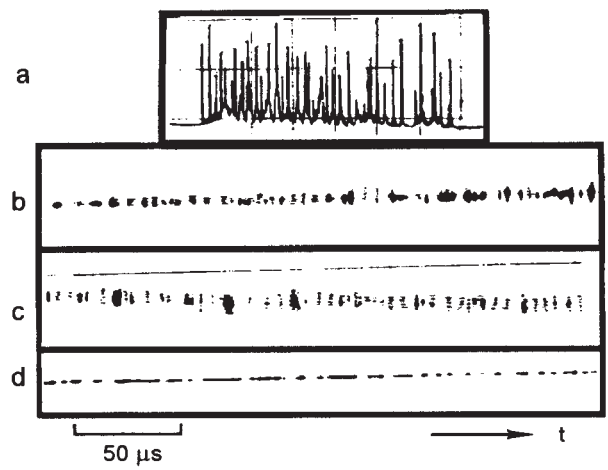

Fig. 1.27 Parameters of lasing of TEM_{mnq} modes of a Cr:GSGG laser (diameter 4 mm, length 90 mm) with flat mirrors (L = 1.3 m), $E_p = 2E_t$; a) oscillogram of intensity of radiation, scale 40 μs/div; b) time evolvement of the distribution of radiation intensity in the near-zone; c,d) time evolvement of the lasing spectrum without (c) and with longitudinal mode selection (d).

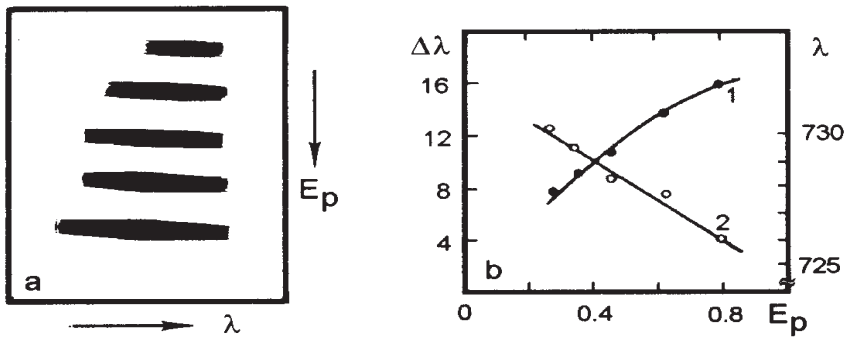

Fig. 1.28 a) spectrograms of the integral spectrum of lasing of TEM_{mnq} modes of Cr:YSGG laser (diameter 4 mm, length 90 mm) with flat mirrors (L = 1.6 m) at constant temperature of the crystal (T = 20 °C) and different pumping energies of E_p = 1.2, 1.4, 1.7, 2.0 and 2.3 E_t, E_t = 160 J; b) dependence of the width of the integral lasing spectrum Δλ (nm) and position of its maximum along λ_0 (nm) (2) of the Cr:YSGG laser on pumping energy E_p (kJ).

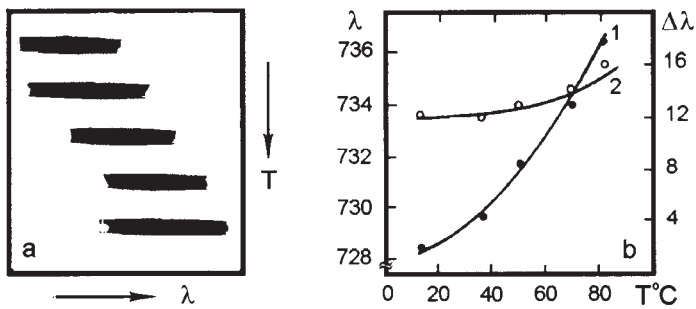

Fig. 1.29 a) spectrograms of the integral spectrum of lasing of TEM_{mnq} modes of Cr:YSGG laser (diameter 4 mm, length 90 mm) with flat mirrors (L = 1.6 m) at constant pumping energy ($E_p = 2E_t$) and different crystal temperatures (T = 15, 35, 50, 70 and 85 °C); b) dependence of the width of the integral lasing spectrum Δλ (nm) and position of its maximum along λ_0 (nm) (2) on crystal temperature T.

1.6.2 Energy parameters of lasing

The energy characteristics of the radiation of chromium lasers in the REGG crystals: gadolinium–scandium–gallium garnet (GSGG), yttrium–scandium–gallium garnet (YSGG) and gadolinium–scandium-aluminium garnet (GSAG) with a diameter of 4 mm, the length 50 mm, and with V_g = 0.5 cm^3, were investigated in a resonator with flat mirrors in the absence of spurious selection of the modes in the experimental equipment discussed previously. The ultraviolet radiation of pumping was cut-off by a liquid filter.

The energy dependences of the examined lasers are presented in Fig. 1.33: Cr:YSGG (3), Cr:GSGG (4) and Cr:GSAG (6). In con-

trast to the ruby, alexandrite and emerald lasers, the REGG did not show such a large decrease of lasing energy with increasing resonator length (Fig. 1.33a) (3,4,6) in the range of low pumping levels. The heating of the crystals to 90°C did not cause any large losses of radiation energy (Fig. 1.33b) (3,4,6). At a pumping energy of 0.5 kJ, the values of the optimum coefficients of transmission of the output mirrors of the resonators of the lasers on REGG crystals, at which in the maximum lasing energy was obtained, were in the range 30–40% (Fig. 1.33c) (3,4,6). In the examined range of pumping, the lasing energy of the REGG lasers depended in a linear manner on the pumping energy (Fig. 1.33d) (3,4,6).

1.7 LASER ON CHROMIUM IONS IN A CRYSTAL OF POTASSIUM-SCANDIUM TUNGSTATE

In order to widen the spectral range of lasing of solid-state lasers, it is interesting to examine a large number of crystals with the impurity of chromium ions, generated on the electronic–vibrational transitions.

The lasing of trivalent chromium ions on the electronic–vibrational transitions in tungstate crystals was observed in $Zn(WO)_4$ [57] and $Sc_2(WO_4)_3$ [58]. The growth of crystals of binary tungstates with trivalent chromium ions is associated with certain difficulties, due to the formation of a sheelite structure of the crystal in the phase the transitions with a decrease of the temperature of the crystal from the melt to room temperature, in which the trivalent chromium ions are implanted only with difficulties. The authors of Ref. 59 observed for the first time the lasing of Cr^{3+} ions on a crystal of binary potassium tungstate-scandium and investigated some energy characteristics of radiation. The results show that these crystals are almost free from the concentration decay of luminescence to the values of the concentration of the activator of 10 wt%.

The absorption spectrum of the Cr^{3+}:$KSc(WO_4)_2$ crystal with the content of the chromium ions of 5 wt% is presented in Fig. 1.30. In comparison with the ruby crystal, the maximum of the absorption spectrum of the chromium ions in the crystal of the potassium-scandium tungstate is displaced to the long-wave range of the spectrum. The wide absorption bands in the blue and red regions of the spectrum (V & U-bands) correspond to the permitted transitions ${}^4A_2 \rightarrow {}^4T_1$ and ${}^4T_2$, respectively.

The half width of the luminescence spectrum of the chromium ions in the crystal of the potassium–scandium tungstate in lamp pumping is 78–59 μm with a maximum at a wavelength of 870 nm (Fig. 1.31). In the case of laser pumping by the second harmonics of a Nd laser, the half width of the luminescence spectrum slightly decreases

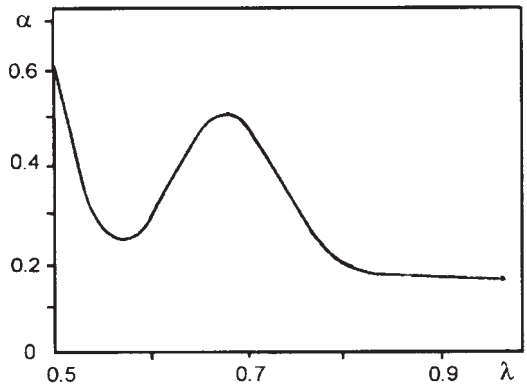

Fig. 1.30 Dependence of absorption coefficient α (cm^{-1}) on the wavelength λ (μm) of Cr^{3+} ions in a crystal of potassium-scandium tungstate at T = 300 K.

and amounts to 810–940 nm with the centre at a wavelength of 875 nm.

1.7.1 Spectral and energy parameters of lasing

The spectral and energy parameters of the lasing of a Cr laser nn the potassium–scandium tungstate crystal were investigated by the authors of this book in Ref. 30. Investigations were carried out on a crystal of binary potassium–scandium tungstate with an impurity of chromium ions (Cr^{3+}:$KSc(WO_4)_2$, Cr: KSW) with a size of 4 × 4 × 5 mm, grown by the method of spontaneous crystallisation, with the concentration of chromium ions of 5 wt%. The measured lifetime of the upper working level at room temperature was 15 μs. Pumping of the active element Cr:KSW was carried out with a ruby laser in the free lasing regime with the pulse time of approximately 1 ms and the radiation energy in the pulse of 2 J.

At room temperature, the lasing of chromium ions was detected on the electronic–vibrational transitions $^4A_2 \rightarrow {}^4T_1$ in the Cr:KSW laser with a centre at a wavelength of 870 nm and the width of the lasing spectrum of the order of 20 nm with the pumping energy 5 times higher than the threshold energy. The threshold energy of pumping was approximately 25 mJ. With increasing pumping energy the width of the lasing spectrum increased almost linearly in some pumping range, excluding the region of saturation. In a dispersion resonator, the rearrangement of the wavelength of lasing was observed in the range 820–930 nm. The lasing energy of the Cr:KSW laser was characterised by an almost linear dependence (Fig. 1.32) on the pumping energy of the ruby laser.

The lasing of longitudinal and transverse modes in the Cr:KSW

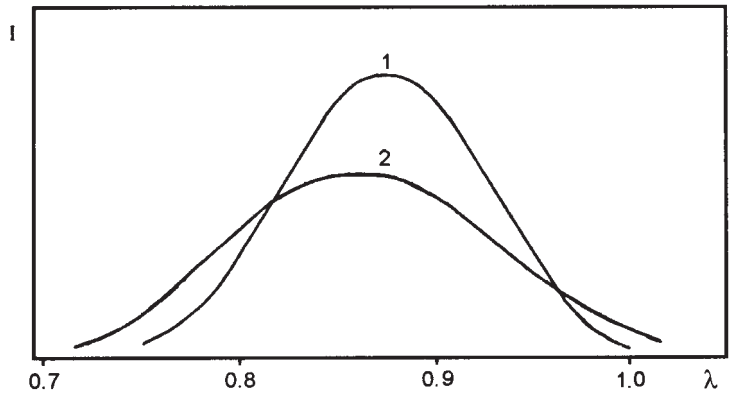

Fig. 1.31 Dependence of the intensity of luminescence I (rel.units) of Cr^{3+} ions in a crystal of potassium–scandium tungstate on wavelength α (μm) in laser (1) and lamp (2) excitation at T = 300 K.

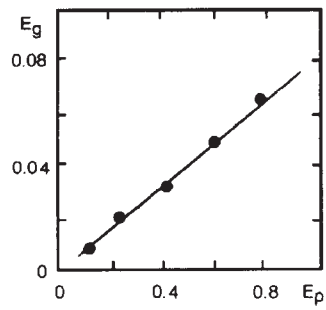

Fig. 1.32 Dependence of the lasing energy E_g (J) of a Cr:KSW laser on pumping energy E_p (J) of a ruby laser.

laser with flat mirrors under normal conditions with the effect of technical perturbations of the resonator eliminated always took place in the regime of non-attenuating pulsations of radiation intensity, as in other active media with chromium ions.

1.8 OPTIMISATION OF THE ENERGY CHARACTERISTICS OF RADIATION OF CHROMIUM LASERS

The energy parameters of the lasing of chromium lasers in the media examined by the authors were measured in almost all investigations [6–30], and they were compared in Ref. 19, 21, 22–24, 26, 28. The maximum values of the energy characteristics of the radiation of lasers were obtained as a result of optimisation of their parameters: the temperature of the active medium, the length of the resonator and the transmission coefficient of its output mirror.

With increase of the length of the flat resonator from the mini-

mum possible to 1.5 m, the radiation energy of a ruby laser was halved, and in the case of alexandrite and emerald lasers it decreased 4–5 times (Fig. 1.33a). This difference is caused by the formation of a thermal lens with a shorter focusing distance in the alexandrite and emerald lasers. This lens transforms the flat resonator to a spherical one with equivalent parameters:

$$L_s = L\left(1 - L/4f_T\right), \quad R_s = 2f_T\left(1 - L/4f_t\right). \tag{1.13}$$

The minimum losses of radiation in the resonator and the highest lasing energy of the lasers were obtained only if the condition of stability of the equivalent spherical resonator was fulfilled:

$$0 \le \left(1 - L/2f_T\right)^2 \le 1. \tag{1.14}$$

With increase of the pumping energy the optimum coefficients of trans-

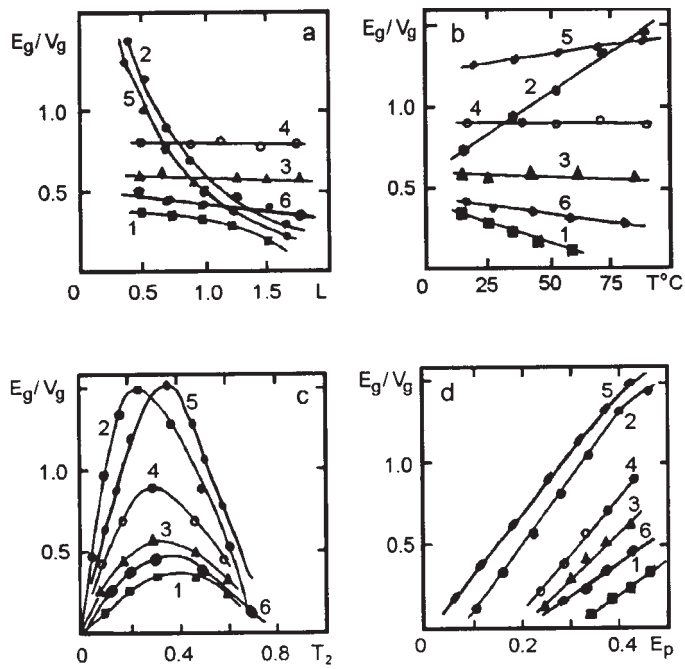

Fig. 1.33 Dependence of the density of lasing energy E_g/V_g (J/cm^3) on resonator length L (m) (a); temperature of active medium T (b); the coefficients of transmission of the output mirror at resonance T_2 (c) at a constant pumping energy of E_p = 0.5 kJ (a,b,c) and pumping energy E_p (kJ) (d) for ruby lasers (1), aleksandrite lasers (2), Cr:YSGG (3), Cr:GSGG (4), emerald (5) and Cr:GSAG (6) lasers. The generated volumes of the active media V_g = 0.78 (ruby), 1.42 (alexandrite), 0.21 (emerald) and 0.5 cm^3 (Cr:YSGG, Cr:GSGG, Cr:GSAG).

mission of the output mirror of the resonator, at which the lasing energy was maximum, increase. At a pumping energy of ~0.5 kJ the values of the optimum transmission factors for the measured active media reached saturation (Fig. 1.33b). When heating the crystals from 20 to 60 °C, the radiation energy of the alexandrite laser was doubled, and the radiation energy of the ruby laser decreased 6 times, whereas the radiation energy of the emerald crystals of the rare-earth–gallium garnets changed only slightly (Fig. 1.33c). The increase of the radiation energy of the alexandrite laser with increasing crystal temperature is determined by the increase of the population of the upper working level $^4T_2$ as a result of its thermal excitation from the metastable level ^2E.

In the pumping range to 0.5 kJ, the radiation energy of the chromium lasers in all active media depended linearly on pumping energy (Fig. 1.33d). At higher pumping levels there was a deviation from the linear dependence. This is caused by the fact that increasing pumping energy increases the diffraction of pumping radiation in the ultraviolet region of the spectrum. In the case in which the ultraviolet radiation of pumping was converted by dissolution of the KH-20 dye to the green range of the spectrum, which contains one of the wide bands of absorption of the chromium ions, the dependence of radiation energy on pumping energy remained linear even at high pumping levels.

Chapter 2

Solid-state neodymium lasers in free lasing regime

2.1 SPECTROSCOPIC CHARACTERISTICS OF ACTIVE MEDIA ON NEODYMIUM IONS

Lasing on the Nd ions was produced in a very wide range of active media (crystals and glass) where the majority of these media operates in the four-level system. The absorption and luminescence spectra of the neodymium ions Nd^{3+} are determined by three electrons of the 4*f*-shell which is sufficiently screened by 5*s* and 5*p*-shells. The energy of interaction with 4*f*-electrons is only 100 cm^{-1}. This energy is lower in comparison with the energy of spin-orbital interaction. The weak crystalline field does not fracture the bond between the orbital and spin moments of the electrons and the Stark splitting of the energy levels of the ions is smaller in comparison with the splitting of its fine structure. The total angular moment **J** is retained; $(2J + 1)$ of energy sublevels correspond to different projections of the moment on the direction of the electric field.

The position of the energy levels of the Nd ions is determined by the Coulomb interaction of the electrons with the nucleus of with each other (Fig. 2.1). As a result of the spin-orbital interaction of the electrons, the energy levels of the ions are split into sublevels (multiplets) with a spectral range ~10^3 cm^{-1}, having the same moments *L* and *S*, but differing in the mutual orientation of the moments, i.e. in the total moment **J**. In the electric field of the matrix of the active media, every multiplet is split into Stark sublevels with the spectral range of approximately 10^2 cm^{-1}. The Stark splitting of the sublevels changes from matrix to matrix and the position of the levels does not change greatly.

Pumping transfers the Nd ions from the ground state $^4I_{9/2}$ to several relatively narrow (in comparison with chromium ions) absorption bands. The two main bands $^4F_{5/2}$ and $^4F_{7/2}$ are located on wavelengths of 0.8 and 0.73 μm, respectively, which are linked by a rapid (~10 ns) emissionless relaxation with the metastable level $^4F_{3/2}$ being the upper working level.

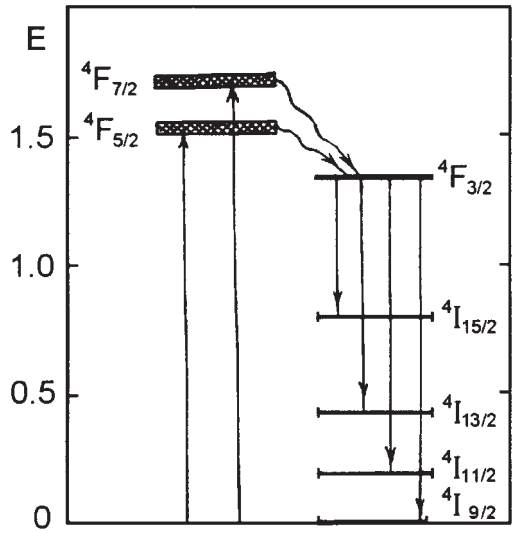

Fig.2.1 Diagram of energy levels E (eV) of neodymium ions at Nd^{3+}.

Four radiation lines correspond to the transitions from the level $^4F_{3/2}$ to the levels ^4I: 1.83 μm ($^4I_{15/2}$), 1.33 μm ($^4I_{13/2}$), 1.06 μm ($^4I_{11/2}$) and 0.9 μm ($^4I_{9/2}$). The highest probability is recorded for the laser transition $^4F_{3/2} \rightarrow {}^4I_{11/2}$ in which approximately 60% of the energy stored on the upper level is $^4I_{11/2}$. The energy range between the $^4I_{11/2}$ state and the ground state $^4I_{9/2}$ is approximately 2000 cm^{-1} which is an order of magnitude higher than the value kT, and this results in the four-level nature of lasing on this transition.

The spectral–time, spatial, angular and energy parameters of lasing of Nd lasers in different media were investigated by the authors of this book in [1–29]. The main spectroscopic characteristics of the examined active media with the Nd^{3+} ions in the transition $^4F_{3/2} \rightarrow {}^4I_{11/2}$ are presented in Table 2.1.

2.2 NEODYMIUM GLASS LASERS

Lasing on Nd ions in glass was obtained for the first time in Ref. 38. Glass differs from the crystal by the absence of the ordered structure; the frequencies of the Stark components of the different ions do not coincide with each other and the gain line is characterised by the non-uniform broadening. Consequently, the cross-section of the induced transition of the Nd ions in glasses is smaller than in the crystals, and the lasing spectrum of the Nd ions shows fork splitting [39]. The value of the uniform broadening of the individual active centres is approximately 3 nm [40].

Table 2.1

Material	Name	λ_0, nm	$\Delta\lambda$, nm	τ, μs	$\sigma \cdot 10^{-20}$, cm^2	[Ref]
Silicon glass	GLS-7	1055	22	410	1.1	[30]
Phosphate glass	GLS-22	1054	19	300	3.5	[30]
Li–Nd–La phosphate glass	KNFS	1054	16	200	3.8	[31]
$Y_3Al_5O_{12}$	YAG	1064	0.62	255	33	[32, 33]
$Gd_3Sc_2Ga_3O_{12}:Cr^{3+}$	GSGS:Cr	1061	1.4	280	15	[31]
$La_2Be_2O_5$	BLN	1070	3.4	120	15	[35]
La Mg $Al_{11}O_{19}$	LNA	1055	2.9	320	3.2	[36]
$KGd(WO_4)_2$	KGW	1067	2.0	120	38	[37]
$KY(WO_4)_2$	KYW	1069	2.1	110	38	[37]

Here λ_0 is the wavelength of lasing in the centre of the gain line; $\Delta\lambda$ is the width of the gain line; τ is the lifetime of the upper working level; σ is the cross-section of the induced transition.

Irradiation of Nd glass with pumping radiation with a wavelength shorter than 400 nm results in the formation of dynamic dye centres in these crystals associated with the matrix of the glass and showing absorption at the lasing wavelength. This results in the losses and modulation of radiation intensity [41]. The line structure of the lasing spectrum, observed in Nd glass lasers is determined by the presence of the spurious selection of longitudinal modes in the resonator [42].

The parameters, optical homogeneity and transparency (the absorption losses are of the order of 10^{-3} cm^{-1}) of the Nd glass laser are considerably superior to those of the artificial crystals with Nd. The dimensions of the active elements made of glass are restricted by the obtainable pumping parameters and not by technology, as in the case of crystals. Nd glass does not contain metallic impurities and is characterised by the highest beam resistance to radiation. The failure threshold of glass is $10^3 \div 10^4$ J/cm^2 in the free lasing regime, $10^2 \div 10^3$ J/cm^2 in the regime of the giant pulse, and $1 \div 10$ J/cm^2 in the regime of supershort radiation pulses.

Both silicate and phosphate glasses are used in practice. The silicate glasses have higher technological properties and high mechanical strength and chemical resistance but they are characterised by a smaller cross-section of the induced transition and a higher non-linear refractive

index. This limits the applicability of these materials in powerful amplifiers. The phosphate glasses are characterised by higher efficiency, lower lasing threshold, a narrower radiation spectrum, a higher threshold of non-linear effects and better thermo-optical characteristics. A significant disadvantage of the phosphate glasses is their low mechanical strength and high hygroscopicity. Consequently, the ends of active elements require special protection.

The main physical and spectral characteristics of the investigated phosphate glasses GLS-22 were as follows: the concentration of Nd ions 1.6% (2.0×10^{20} cm^{-3}); density 3.5 cm g/cm^3; refractive index 1.58; heat conductivity 0.4 W/m · deg; absorption factor 2×10^{-3} cm^{-1}; the coefficient of linear expansion 10.6×10^{-6} deg^{-1}; the thermo-optical coefficient -5.7×10^{-6} deg^{-1}; quantum yield 0.6–0.8. The maxima of the wavelengths (absorption factors) of the most intensive absorption bands were 512 nm (0.45 cm^{-1}), 525 nm (0.77 cm^{-1}), 585 nm (2.67 cm^{-1}), 746 nm (1.47 cm^{-1}), 804 nm (1.85 cm^{-1}) and 804 n (0.47 cm^{-1})**.** The maximum of the wavelength of luminescence was 1055 nm, the maximum of the lasing wavelength 1054 nm, the lifetime of the upper working level 300 μs, the transitions section $^4F_{3/2} \rightarrow {}^4I_{11/2}$ 3.5×10 cm^2, the width of the gain line 19 nm (effective width 28 nm).

The efficiency of lasing of glass lasers can be increased by increasing the concentration of active ions. However, at a Nd ions concentration of ≥ 3% (2×10^{20} cm^{-3}), the majority of active media are characterised by a decrease of the quantum yield and the efficiency of lasing as a result of the concentrational decay of luminescence (CDL). CDL greatly intensifies in cases in which the distance between the adjacent Nd ions decreases to 0.3 nm.

In the dipole–dipole interaction, the probability of decay is proportional to R^{-6}, where R is the distance between the interacting particles. Therefore, the increase of the distance between the adjacent ions by a factor 1.5 results in a large decrease of the CDL with the concentration of the active ions increasing by almost an order of magnitude. For example, for Li–Nd–La phosphate glass (KNFS) with the minimum distance between the adjacent Nd ions of 0.47 nm, the concentration of the active ions may increase to 3×10^{21} cm^{-3} without any large decrease of the quantum yield [31]. The application of KNFS glass in practice is restricted by the extremely high hygroscopicity of this material, low hardness and heat conductivity.

The main and spectroscopic characteristics of the examined KNFS glasses: the concentration of Nd ions 4 and 8×10^{20} cm^{-3}; density 2.85g/cm^3; refractive index 1.55; the coefficient of linear expansion 0.8×10^{-6} deg^{-1}; the thermo-optical coefficient 1.3×10^{-6} deg^{-1}; the maximum of the lasing wavelength 1054 nm; the section of the $^4F_{3/2} \rightarrow {}^4I_{11/2}$ transition

3.8×10^{-20} cm^2; the lifetime of the upper level is changed from 330 to 80 μs with the change of the concentration of the Nd ions from 4 to 30×10^{20} cm^{-3}.

2.2.1 Spectral–time lasing parameters

The spectral–time, angular and energy characteristics of the free lasing of Nd lasers in different glasses were investigated by the authors of this book in Ref. 1,3,4,9,11,18,19,22–28.

In the Nd glass lasers with spherical mirrors, the lasing of TEM_{mnq} modes takes place in the regime of non-attenuating and non-regular pulsations of radiation intensity in all cases, with the exception of the case in which the configuration of the resonator is confocal or concentric (critical). When smoothing the spatial heterogeneity of the field in the active medium by compensated phase modulation (CPM) in a wide range of the radiation of the parameters of the spherical resonator or in the case of excitation of a large number of degenerate waves in resonators with critical configuration, it is always possible to achieve quasistationary lasing.

In a laser with a flat resonator with optimum length ($L \sim 2$ m) and a low value of the indices of the transverse modes (m, $n \leq 5$), the lasing of TEM_{mnq} modes takes place in the quasistationary regime. The spatial competition of these modes increases with increasing values of the indices of the transverse waves. This competition leads to the alternation of the transverse (Fig. 2.2b) and longitudinal modes (Fig. 2.2c) during the lasing process and the formation of non-attenuating pulsations of radiation intensity. In this case it is not possible to stabilise the radiation wavelength when using a complex dispersion resonator (Fig. 2.2d) [3,4].

The quasistationary lasing of TEM_{ooq} modes in a Nd glass laser that was stable in a wide pumping range (Fig. 2.3) [3,4] was obtained with the optimum parameters of the flat resonator (length 2 m, diaphragm diameter 2 mm). This was carried out by dynamic tuning of the elements of the resonators. The procedure used in this case was described previously. In contrast to Cr lasers, in the Nd lasers it is not necessary to smooth-out the longitudinal heterogeneity of the field in the active medium. The silicate glass is characterised by fork splitting of the spectrum during the lasing process (Fig. 2.3c), determined by the non-uniform nature of broadening of the gain line. At low Nd ion concentrations (~ 1%) phosphate glass did not show such splitting of the lasing spectrum (Fig. 2.3d) because of the higher rate of transfer of excitation energy inside the non-uniformly broadened line. Increase of the concentration of the Nd ions in the phosphate glass and the KNFS time glass resulted in the splitting of the lasing spectrum with a finer structure (Fig. 2.3e). When using the complex dispersion resonator (with dispersion prisms

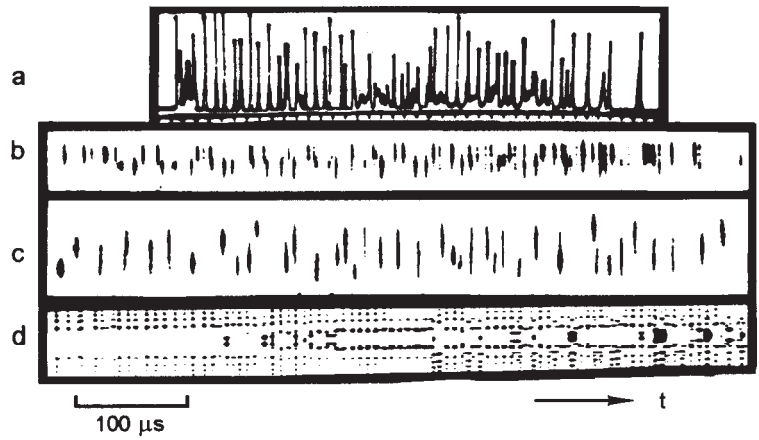

Fig.2.2 Parameters of the lasing of TEM$_{mnq}$ modes of a Nd laser on silicate glass (diameter 8 mm, length 130 mm) with flat mirrors (L = 2 mm) without selection of longitudinal modes (a–c) and with selection (d), $E_p = 2E_t$; a) the oscillogram of the intensity of radiation, 20 μs marks; b) the time evolvement of the distribution of radiation intensity in the near-zone; c,d) time evolvement of the radiation spectrum from DFS-8 spectrograph (c) Fabry–Perot interferometer, dispersion range 20 pm.

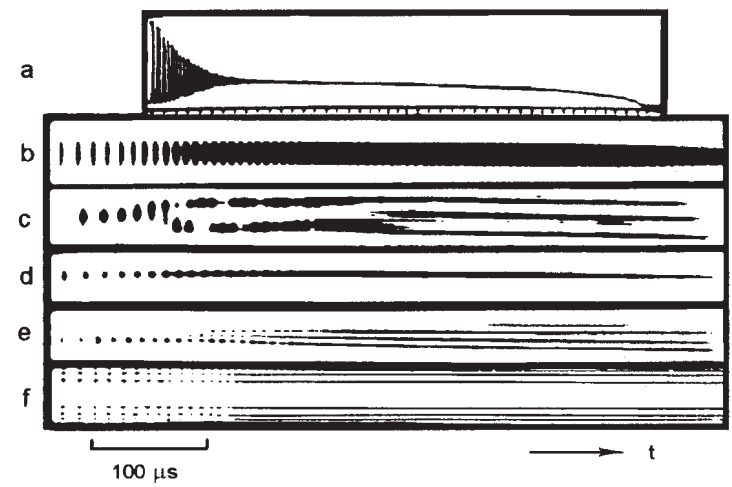

Fig.2.3 Parameters of the lasing of TEM $_{ooq}$ modes of neodymium laser in silicate glass (8 mm diameter, 130 mm length) phosphate (diameter 6.3 mm, length 120 mm) and concentrated phosphate glass (6.3 mm diameter, length 100 mm) with flat mirrors (L = 2 m, diameter 2 m) with elimination of the effect of technical interference of the resonator without selection of the longitudinal modes (a–e) and with selection (f), $E_p = 4E_t$; a) oscillogram of radiation intensity, 20 μs marks; b) time evolvement of the distribution of intensity in the near-range zone; e–f) time evolvement of the lasing spectrum from DFS-8 spectrograph (c–e) Fabry–Perot interferometer (f), the region of dispersion of the interferometer 20 pm.

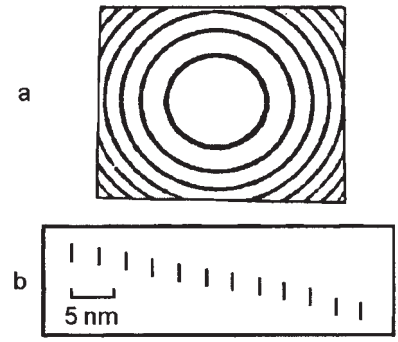

Fig.2.4 Interferogram of the integral spectrum of radiation of TEM_{ooq} modes of the neodymium laser in glass in quasi-stationary regime with selection of longitudinal modes (a), $E_p = 4E_t$; b) sequence of radiation spectrographs, illustrating the range of rearrangement of the wavelength of lasing of the Nd glass laser.

and the Fabry–Perot selector-etalon) it was possible to obtained stable single-frequency quasistationary lasing of the TEM_{ooq} modes in all types of glass (Fig. 2.3f). In a this case, the width of the integral radiation spectrum was approximately 0.3 pm (Fig. 2.4 a), and the width of the rearrangement range was 30 nm (Fig. 2.4b) [11].

2.2.2 Energy parameters of lasing

Experiments were carried out using standard active elements of silicate glass (LGS-250) and phosphate glass (GLS-22) with the ends cut under an angle of 1° and illuminated ends, with the concentration of the Nd ions of 2×10^{20} cm^{-3}, the dimensions: diameter 6.3 × 110 mm. The volumes of the active media, contributing to the lasing energy, were $V_g = 2.5$ cm^3. Li–Nd–La phosphate glass (KNFS) was characterised by the concentration of Nd ions of 4×10^{20} cm^{-3}, diameter 6.3 mm, 75 mm length, with $V_g = 2$ cm^3. Pumping was carried out using an IFP-800 lamp in a quartz single-block illuminator doped with europium, with the pumping pulse time of 250 μs. Liquid filters were used for additional cutting off of ultraviolet pumping radiation.

Of all the active media with the Nd ions, examined in these investigations, the lowest efficiency was recorded in the case of silicate glass characterised by the lowest value of the laser transition cross-section. Therefore, the lowest energy characteristics of radiation were obtained in the case of silicate glasses, the highest for the concentrated phosphate glasses (KNFS). With increase of the length of the flat resonator and a constant energy of pumping, the lasing energy of the lasers on glass decreased (Fig. 2.29a) (4,6), as in the majority of active media. However, if the lasing energy of the silicate and phosphate (6) glasses was halved when the length was increased from 0.3 to 1.6 m, the lasing

energy of the KNFS glass (4) decreased 4 times. When heating the silicate and phosphate glasses from 10 to 90 °C, the lasing energy decreased almost linearly by a factor of 1.2 (Fig. 2.29b) (6). For the KNFS glass, the temperature dependence could not be recorded because when heating this type of glass microcracks appeared as a result of thermal deformation of the glass. At high pumping energy, these microcracks resulted in failure of the active elements.

For every pumping level there is the optimum coefficient of transmission of the output mirror of the resonator at which the energy of lasing is maximum. At a pumping energy of 300 J the optimum transmission factor for the silicate and phosphate glasses was approximately 35%, and for the KNFS glass it was 50% (Fig. 2.29c) (4,6). As indicated by Fig. 2.30a (4,6), with increase of the pumping energy the values of the optimum factors reach saturation approaching 40 and 60%, respectively. At a low pumping energy, the increase of the lasing energy is linear (Fig. 2.29d) (4,6). The linear dependence was already violated at pumping energies of approximately 100 J.

If the ratio of the lasing energies of the lasers on KNFS and GLS-22 at low pumping energy level was 2, then at a pumping energy of 500 J this ratio was almost halved. This was determined by higher thermal-optical deformation of KNFS glass which failed at high pumping energy. At a pumping energy of 500 J, the density of the lasing energy of the lasers was E_g/V_g = 0.8 J/cm^3 for GLS-22 and 1.6 J/cm^3 for KNFS. At low pumping energy levels, the divergence of the radiation of the two lasers was almost identical, and with increase of the pumping energy, the divergence of radiation of the laser on KNFS increased more rapidly (Fig. 2.30b).

2.3 Nd:YAG LASERS

Of the entire range of the crystals, the crystals of yttrium–aluminium garnet with neodymium, Nd^{3+}:$Y_3Al_5O_{12}$(Nd:YAG), are used most widely. These crystals are characterised by a large number of unique properties and are capable of operating in all possible lasing regimes. The Nd:YAG crystals have the cubic symmetry and are characterised by relatively high values of heat conductivity (14 W/m·deg) and Moose hardness (8.5). The density of the garnet crystals is 5.04 g/cm^3, melting point 1930 °C, the thermal expansion coefficient 6.96 × 10^{-6} deg^{-1}, and the thermo-optical constant dn/dT = 9.86 × 10^{-6} deg^{-1} [32]. The transparency region of the garnet crystal is 0.24–6.0 μm. The Nd:YAG crystals are characterised by high resistance to optical radiation, a low excitation threshold and their service life is almost unlimited. Mean powers of continuous lasing of up to several kW have been obtained in the case of Nd:YAG lasers.

The optimum concentration of the Nd ions in the Nd:YAG crystal is approximately 1%, which corresponds to the concentration of Nd ions of 1.38×10^{20} cm^{-3}. The cross-section of the transition $^4F_{3/2} \rightarrow {}^4I_{11/2}$ (λ = 1064 nm) is 3.3×10^{-19} cm^2, the width of the gain line is 0.62 nm, and the lifetime of the upper working level is 250 μs [33]. The main absorption bands of the Nd ions in the YAG crystal correspond to the transition from the ground to the following levels: $^4F_{3/2}$ (880 nm), ($^4F_{5/2}$ + $^2H_{9/2}$)(810 nm), ($^4F_{7/2}$ + $^4S_{3/4}$)(750 nm), ($^4G_{7/2}$ + $^2G_{5/2}$) (580 nm) and ($^2K_{13/2}$ + $^4G_{7/2}$ + $^4G_{9/2}$) (520 nm). In the absence of dispersion elements in the resonator, the lasing of the Nd:YAG laser takes place only on the transition $^4F_{3/2} \rightarrow {}^4I_{11/2}$(1064 nm), characterised by the maximum value of the cross-section of induced transition. The spectroscopic and time characteristics of radiation of Nd:YAG lasers under different regimes have been examined quite extensively in Ref. 34.

2.3.1 Spectral–time parameters of free lasing in pulsed regime

The spectral–time, angular and energy characteristics of free lasing of Nd:YAG lasers have been investigated by the authors of this book in detail in Ref. 4,5,11,18,19,22–28.

The stable quasistationary lasing of TEM_{ooq} modes (Fig. 2.5) in a Nd:YAG laser with a flat resonator with the optimum parameters (length 2 m, the diameter of the diaphragms 2 mm) was achieved without forced smoothing of the longitudinal heterogeneity of the field in the crystal during the removal of the effect of technical perturbations of the resonator using the method described previously. Under normal conditions in the transition regime the relaxation pulsations of radiation intensity were regular with respect to the repetition frequency and slightly irregular with respect to amplitude (Fig. 2.5a). They became completely irregular (Fig. 2.6a) in forced smoothing of the longitudinal heterogeneity of the field in the garnet crystal by means of compensated phase modulation (CPM). The width of the instantaneous spectrum of the quasistationary lasing of the Nd:YAG laser in the normal conditions and with the pumping level considerably higher than the threshold level was 30 pm (Fig. 2.5c). The width remained almost completely constant during smoothing of the longitudinal heterogeneity of the field at inversion in the active medium (Fig. 2.6c), in contrast to the ruby laser in which the smoothing of the heterogeneity of inversion always leads to single-frequency quasistationary lasing of TEM_{ooq} modes (Fig. 1.6c) [4,5].

The experimental value of the instantaneous width of the lasing spectrum ($\Delta\lambda_g$) is in relatively good agreement with the calculated value, obtained from the rate equations in the case in which the active medium with the length l completely fills the resonator (l/L = 1) [43]:

$$\Delta\lambda_g = \lambda^2\left[\frac{x-1}{x}\delta\lambda_q(\Delta\lambda)^2\right]^{1/3}, \qquad (2.1)$$

where $\Delta\lambda$ is the width of the gain line; $\delta\lambda_q$ is the spectral range between the longitudinal modes; $x = E_p/E_t$ is the amount by which the pumping level exceeds the threshold value. In a general case in which $l/L \ll 1$, accurate analytical calculations of the width of the lasing spectrum are almost impossible because of the additional discrimination of the longitudinal waves which depends not only on the ratio l/L but also on the position of the active rod in the resonator.

In the quasistationary regime, it was relatively easy to obtain the single-frequency lasing of the TEM_{ooq} modes (Fig. 2.5d) using the Fabry–Perot selector-etalon with a transmission band of of 25 pm (the base of the etalon 1 mm, the transmission coefficient of the mirrors 0.15).

In the Nd:YAG laser with flat mirrors in the same experimental conditions it was considerably easier to obtain the quasistationary lasing of the TEM_{mnq} modes (Fig. 2.7) in a wide pumping range [4,5]. In this case, the values of the indices of the transverse modes must be low (m, $n < 10$). Consequently, the transition pulsations of the radiation intensity were irregular not only with respect to the amplitude but also the repetition frequency. This is associated with the alternation of the transverse modes (Fig. 2.7b and 2.8), with a different excitation volumes and, consequently, the gain and the duration of linear development of lasing. The width

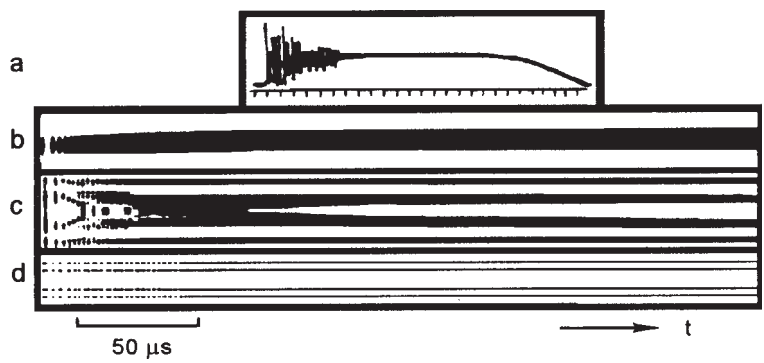

Fig.2.5 Parameters of the lasing of TEM_{ooq} modes of Nd:YAG laser with flat mirrors (L = 2 m, diameter 2 mm) in normal conditions with elimination of the effect of technical interference of the resonator without selection of the longitudinal modes (a–c) and with selection (d), $E_p = 20E_t$; a) oscillograms of radiation intensity, 20 μs marks; b) evolvement of the distribution of radiation intensity in the near-range zone; c) time evolvement of radiation spectrum, the region of dispersion of the interferometers 56 pm (c) and 20 pm (d).

of the instantaneous spectral of quasistationary lasing (Fig. 2.7c) did not differ from the lasing spectrum of the longitudinal modes and reached saturation when the pumping was four times higher than the threshold level. Increase of the indices of the transverse waves, with a decrease of the resonator length, was accompanied by the alternation of the transverse modes during the entire lasing pulse, associated with the increase in the competition of the modes, as a result of the greater overlapping of their excitation volumes. At high pumping, this resulted in the appearance of a low-level of non-attenuating pulsations of radiation intensity with the retention of a high level of the constant component of the integral

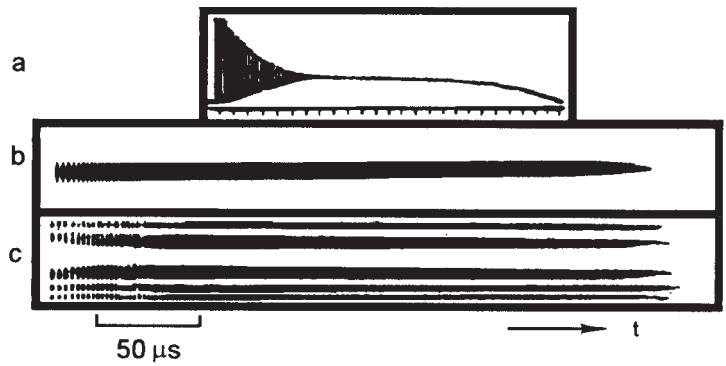

Fig.2.6 Parameters of the lasing of TEM_{ooq} modes of the Nd:YAG laser with flat mirrors in smoothing the longitudinal heterogeneity of the field in the active medium using compensated phase modulation. The laser parameters are the same as those shown in Fig. 2.5.

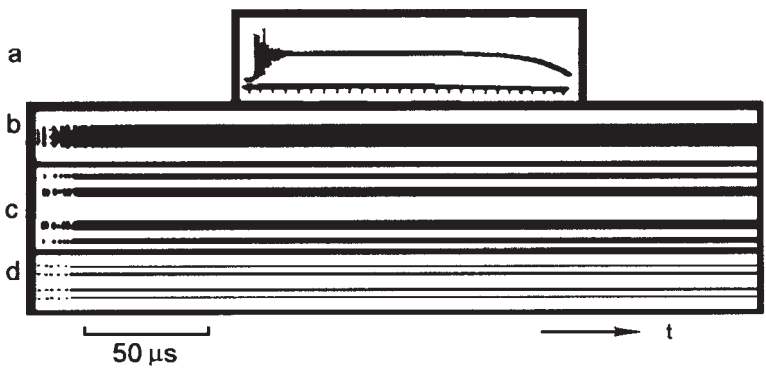

Fig.2.7 Parameters of the lasing of TEM_{mnq} modes of Nd:YAG laser (diameter 5 mm, length 100 mm) with flat mirrors (L = 2 m) in normal conditions with elimination of the effect of technical interference of the resonator without selection of the longitudinal modes (a–c) and with selection (d), $E_p = 40E_t$; a) oscillograms of radiation intensity, 20 μs marks; b) evolvement of the distribution of radiation intensity in the near-range zone; c) time evolvement of radiation spectrum, the region of dispersion of the interferometers 70 pm (c) and 20 pm (d).

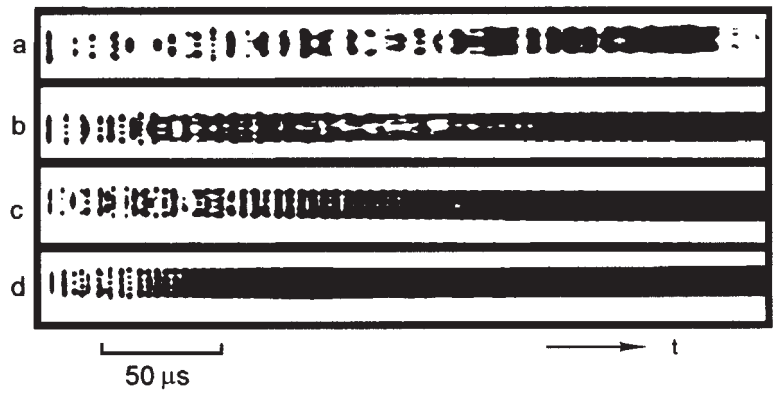

Fig.2.8 Time evolvement of the distribution of radiation intensity of TEM_{mnq} modes of Nd:YAG laser in the near-range zone; E_p/E_t = 1.5 (a), 2 (b), 4 (c) and 20 (d).

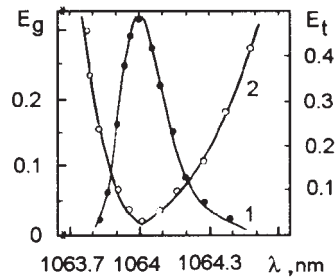

Fig.2.9 Dependence of the energy of one-particle lasing E_g (J) (1) and threshhold pumping E_t (kJ) (2) of Nd:YAG laser (diameter 5 mm, length 50 mm) on the lasing wavelength λ (nm) in the dispersion resonator.

intensity of radiation. In the conditions of stable quasistationary regime of the Nd:YAG laser it was quite easy to ensure single-frequency lasing of the TEM_{mnq} modes (Fig. 2.7d) when using a Fabry–Perot selector-etalon, with a transmission band of 25 pm. This was accompanied by a smooth change of the wavelength of radiation within the limits of the width of the gain line (Fig. 2.9).

In a non-selective resonator with a low level of pumping, lasing at the $^4F_{3/2} \rightarrow {}^4I_{11/2}$ transition took place at a radiation wavelength of 1064 nm (transition between the Stark sublevels $R_2 \rightarrow Y_3$). When the pumping was four times higher than the threshold value, the second radiation line also reached lasing at a wavelength of 1061 nm (transition $R_1 \rightarrow Y_1$), and the threshold of appearance of this lasing was almost completely independent of the temperature of the crystal.

The thermal drift of the gain line of the Nd:YAG crystal was measured from the displacement of the spectrum of quasistationary lasing during heating a crystal with pumping slightly higher than the threshold value

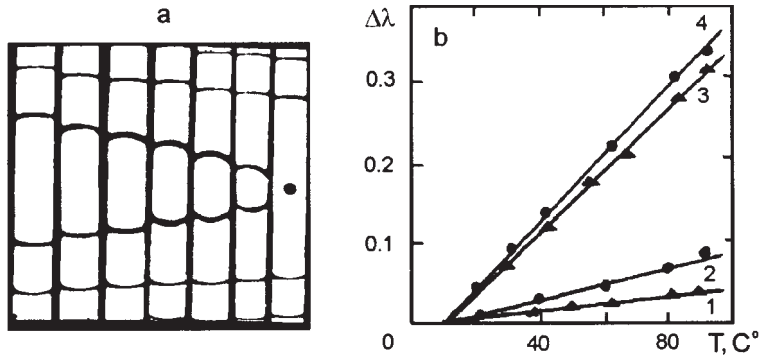

Fig.2.10 a) Sequence of interferograms of the spectrum of quasi-stationary lasing of Nd:YAG laser at different temperatures of the crystal T = 10, 30, 40, 60, 70, 80 and 90 °C. The region of dispersion of the interferometer 570 nm, L = 2 m; b) dependence of the displacement of the lasing wavelength Δλ (nm) on the temperature of active media of Nd lasers on crystals of YAG (4), GSGG:Cr (3) BLN (1), KGW (2).

($E_p \sim 2E_t$), Fig. 2.10. With completely removal of the spurious selection of the longitudinal modes, the centre of gravity of the spectrum of quasistationary lasing coincided, according to the measurements, with high accuracy with the maximum of the gain line. The measured main velocity of the thermal drift of the gain line on the interferograms of the radiation spectrum (Fig. 2.10a) in the examined temperature range reached the value $d\lambda/dT$ = 4.3 pm/deg (Fig. 2.10b) [11], and its value was in excellent agreement with the value obtained in Ref. 44 in the analysis of luminescence spectra.

In a Nd:YAG laser with a spherical resonator of critical configuration, the lasing of TEM_{mnq} modes also took place in the quasistationary regime. The width of the instantaneous spectrum of the quasistationary lasing decreased to 8 pm, as a result of smoothing of the spatial heterogeneity of the inversion, which basically determines the width of the spectrum. The centre of gravity of the radiation spectrum was displaced to the long-wave range with a mean speed of 20 pm/ms, indicating the heating of the garnet crystal by 3°C during the lasing pulse.

In the case of a smaller detuning of the setting of the resonator from the critical configuration there was alternation of both the transverse and longitudinal modes during lasing. When pumping was considerably higher than the threshold level, this process was accompanied by pulsations of integral radiation intensity.

2.3.2 Energy parameters of lasing in pulsed regime

Investigations were carried out on a crystal of yttrium–aluminium garnet with Nd (Nd:YAG) with the ends machined to the same angle, with

illumination, diameter 6.3 mm, length 100 mm. The volume of the active medium, contributing to the lasing energy, was V_g = 2.5 cm^3. The concentration of the Nd ions in the crystal was 1%. The crystal was selected from a large batch of crystals on the basis of optical and the thermo-optical homogeneity and, consequently, was capable of operation with continuous lamp pumping. Pumping in the pulsed regime was carried out using an IFP-800 lamp, with the pumping pulse time of 250 μs. Ultraviolet radiation was cut off with a liquid filter.

With decrease of the resonator length of a flat resonator from 0.3 to 1.6 m at constant pumping, the lasing energy of the Nd:YAG laser decreased by only a factor of 1.1 (Fig. 2.29a) (3). Heating of the garnet crystal in the temperature range from 10 to 90 °C resulted in a very small decrease of the lasing energy by a factor of 1.06 (Fig. 2.29b) (3). The maximum lasing energy of the Nd:YAG laser at a pumping energy of 300 J was obtained in a relatively wide range of the radiation of the transmission factor of the output mirror of the resonator from 30 to 70% (Fig. 2.29c) (3). At a high pumping energy, the values of the optimum transmission factor reached saturation at a factor of approximately 40% (Fig. 2.30a) (3). The lasing energy of the Nd:YAG laser depended in a linear manner on the pumping energy at low levels of this energy, and with increase of the pumping energy this linearity of the dependence was disrupted (Fig. 2.29d) (3). At a pumping energy of 500 J, the density of lasing energy of the Nd:YAG laser was E_g/V_g = 2.8 J/cm^3. The divergence of radiation of the Nd:YAG laser with respect to a level of 0.1 at a pumping energy of 300 J was 1.2×10^{-4} rad (Fig. 2.30b) (3), and the lasing energy was 5 J, radiation luminosity 5.3×10^8 W/cm^2·ster.

2.3.3 Spectral–time and energy characteristics of lasing in continuous regime

From the large number of the active media, activated by the Nd ions, only the Nd:YAG crystals can operate efficiently during continuous lamp pumping. At the same time, the application of laser, especially diode pumping, makes it possible to achieve efficient lasing of the Nd lasers in the majority of active media. The parameters of the Nd:YAG laser in the continuous regime were investigated by the authors of this book in Ref. 6,7,11,14,27.

The presence of even weak spurious selection of the longitudinal modes, induced by the illuminated edges of the crystals, resulted in the formation of non-attenuating pulsations of radiation intensity, especially in the case of lasing of the TEM_{ooq} modes (Fig. 2.11a). In this case, the spectrum of stationary lasing widened to 12 pm (Fig. 2.11b). The complete elimination of the spurious selection of the longitudinal modes resulted in the stable stationary lasing without pulsations of radiation intensity (Fig. 2.11c),

and the width of the radiation spectrum decrease to 5 pm (Fig. 2.11d). The simultaneous stationary lasing on several longitudinal modes was observed in this case.

In the case of lasing of TEM_{mnq} modes and with pumping considerably higher than the threshold level, the radiation intensity depended only a very slightly on the effect of the spurious selection of the longitudinal modes. However, in this case also, the effect of external perturbations of the resonator on the nature of lasing was very strong (Fig. 2.12 a), and the width of the lasing spectrum increased to 30 pm (Fig. 2. 12b). With the elimination of external perturbations, lasing took place with a very low (≤ 1%) level of the residual pulsations of radiation intensity (Fig. 2.12c). The complete elimination of the spurious selection of the longitudinal modes increased the stability of the stationary regime in relation to external perturbations and the use the width of the lasing spectrum to 8 pm (Fig. 2.12d).

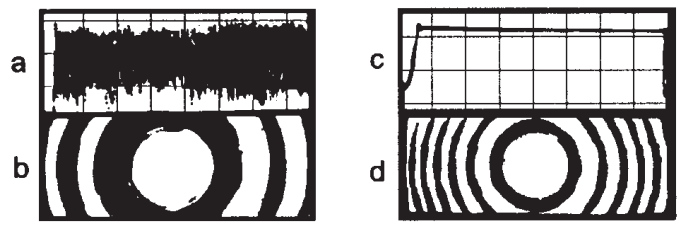

Fig.2.11 Parameters of lasing of TEM_{ooq} modes of a continuous neodymium laser (diameter 6.3 mm, length 100 mm) with flat mirrors (L = 0.3 m) in the presence of spurious selection of longitudinal modes (a,b) and its absence (c,d), $P_p = 4P_t$; a,c) oscillograms of radiation intensity, scale 100 μs/division, for better reading of the zero level of intensity radiation was modulated by an external modulator; b,d) interferograms of the lasing spectrum, the range of dispersion of the interferometer 20 pm.

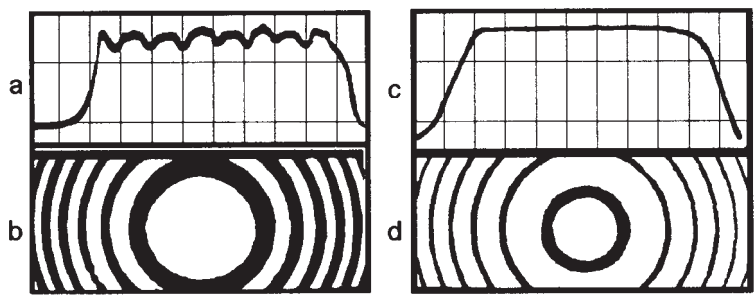

Fig.2.12 Parameters of the lasing of TEM_{mnq} modes of a continuous neodymium laser (diameter 6.3 mm, length 100 mm) with flat mirrors (L = 0.3 m) in the presence of spurious selection of longitudinal modes (a,b) and its absence (c,d), $P_p = 4P_t$; a,c) oscillograms of radiation intensity, scale 500 μs/division, b,d) interferograms of the lasing spectrum, the range of dispersion of the interferometer 56 pm.

In continuous lamp pumping, the active rod shows the formation of strong thermal-optical deformations with the formation of a thermal lens. This resulted in extensive deformation of the optical resonator and the wave front of radiation of TEM_{mnq} modes (Fig. 2.13, b–d). In this case, when using standard spherical optics, it is not possible to carry out correction of the radiation front and efficient focusing of radiation.

The focusing distance of the thermal lens f_T, induced in the crystal, can be approximately calculated [45], knowing the characteristics of the YAG crystal and the pumping power, absorbed in the crystal

$$f_T = \frac{hl}{\kappa\left(\alpha C n^3 + 1/2\partial n/\partial T\right)}, \tag{2.2}$$

where h is the heat transfer coefficient; l is the length of the crystal; κ is the heat conductivity coefficient; α is the coefficient of linear expansion; C is the photoelasticity coefficient; n is the refractive index; $\partial n/\partial T$ is the thermo-optical coefficient. The experimental focusing distance f_T was measured using the Fabry–Yudin method in two planes: the crystal–lamp plane and in the plane orthogonal to this plane, at various points along the radius of the crystal. In a quantron with an elliptical illuminator, spherical aberrations of the thermal lens are more marked (Fig. 2. 14a) than in the case of a cylindrical illuminator (Fig. 2.14b).

The distribution of temperature in the crystal along its radius was determined from the variation of the distribution of the refractive index Δn (r) in the cross-section of the rod which was determined on Mach–Zender interferograms (Fig. 2.15) from the equation

$$\Delta n(r) = n(r) - n(0) = \lambda N(r)/4l, \tag{2.3}$$

here $N(r)$ is the number of the interference ring. The anisotropy of the variation of the refractive index in the cross-section of the rod at dif-

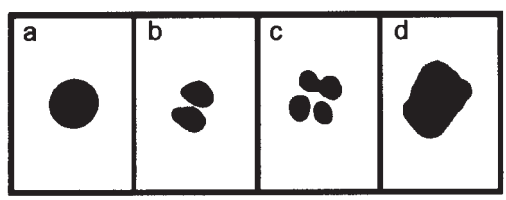

Fig.2.13 Distribution of intensity of radiation of a powerful continuous Nd:YAG laser (diameter 6.3 mm, length 100 mm) in the near-range zone for transverse modes TEM_{ooq} (a), TEM_{o1q} (b), TEM_{11q} (c) and TEM_{mnq} (d); P_p = 6 kW.

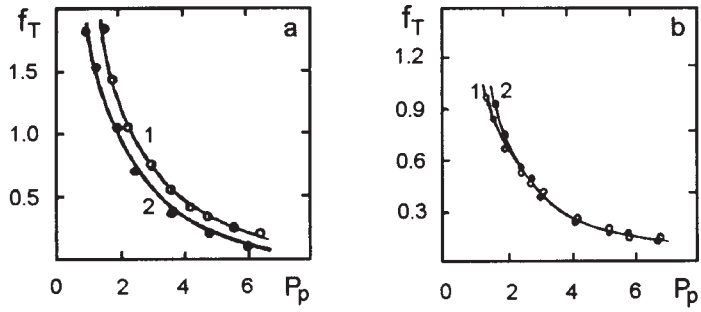

Fig.2.14 Dependences of the Foci of the thermal length f_T (m) on pumping power P_p (kW) in the crystal-lamp plane (2) and in the plane normal to the former (1) for a garnet crystal (6.3 mm diameter, 100 mm length) in an eliptical illuminator at $r/r_0 = 0.2$ (1) and for a crystal (diameter 5 mm, length 100 mm) in a cylindrical illuminator at $r/r_0 = 0.5$ (b).

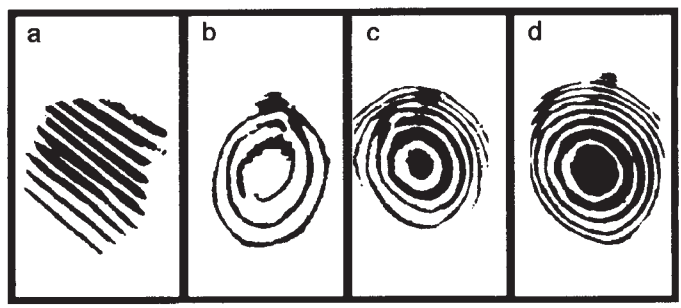

Fig.2.15 Mach–Zender interferograms obtained in a garnet crystal (diameter 6.3 mm, length 100 mm) in an eliptical illuminator. $P_p = 0$ (a), 1.5 (b), 3.0 (c) and 5 kW (d).

ferent pumping powers is associated with both the physical properties of the garnet crystal and with the parameters of the illuminator. The dependence of the distribution of temperature $T(r)$ in the crystal on the radius r, calculated from the equation

$$T(r) = \left[\lambda N(r) / 2l\partial n / \partial T\right], \tag{2.4}$$

is shown in Fig. 2.16. On the graph, the temperature dependence can be approximated with sufficient accuracy by the parabola:

$$T(r) = \Delta T\left(1 - r^2 / r_0^2\right), \tag{2. 5}$$

where r_0 is the radius of the crystal.

The thermal lens, formed in the garnet crystal, transform the flat laser resonator to a spherical one with equivalent parameters (1.13). The maximum power of laser radiation was obtained when fulfilling the coefficient of

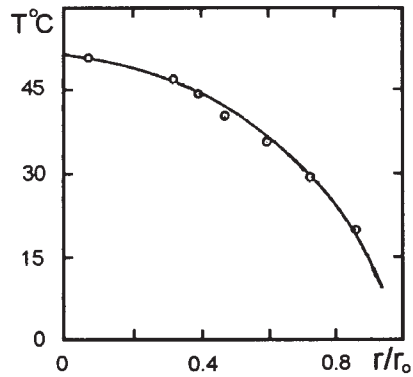

Fig.2.16 Dependence of the radial distribution of temperature T in a garnet crystal (diameter 6.3 mm, length 100 mm) at P_p = 5 kW.

the stability of the equivalent resonator (1.40) at respectively the optimisation of the resonator length L (2.17a) and the transmission factor of the output mirror of the resonator T_2 (Fig. 2.17b). The power P_g (Fig. 2.17c) and divergence θ (Fig. 2.17d) of laser radiation depended in a linear manner on pumping power P_p. For a Nd:YAG crystal with a diameter of 6.3 mm, 100 mm long, at a pumping power of 6 kW, the lasing power was 150 W, with the divergence of radiation of 20 mrad. The increase of the divergence of radiation took place as a result of both the increase of the number and indices of the transverse modes and the increase of the divergence of every individual mode, due to the decrease of the focusing distance of the thermal lens.

2.4 Nd LASERS ON GADOLINIUM–SCANDIUM–GALLIUM GARNET WITH CHROMIUM

Significant advances in the physics and technology of solid-state lasers are associated with the development of crystals of gadolinium-scandium–gallium garnets, activated by Nd ions and sensitised by chromium ions (Nd^{3+}:Cr^{3+}3+:GSGG). The application of chromium ions as a joint activator of the Nd ions has made it possible to decrease greatly the efficiency of the GSGG crystal.

The chromium ions, characterised by wide absorption bands, can absorb more efficiently pumping radiation and transfer excitation to the upper working level of Nd ions $^4F_{3/2}$ without radiation from the excited level $^4T_2$ by the multipole-resonance regime. This rapid transfer of excitation (in comparison with the rate of deactivation of the $^4F_{3/2}$ level) is possible because of the fact that the energy gap between the levels ^2E and $^4T_2$ of the chromium ions is equal to 0 and there is no luminescence of the R-line of the chromium crystals.

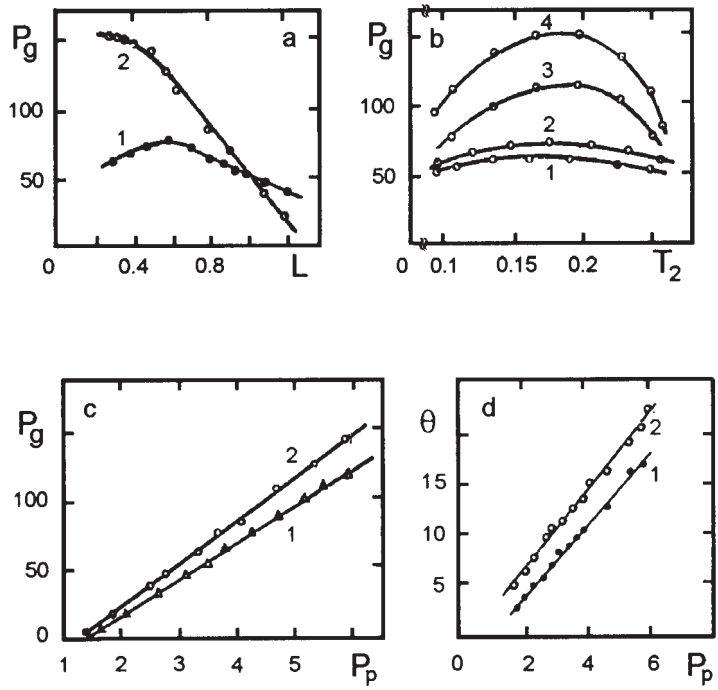

Fig.2.17 Dependence of the lasing power P_g (W) (a,b,c) and the angle of convergence of radiation θ (mrad) (d) on the length of the flat resonator L (m) (a), the coefficient of transmission of the output mirror T_2 (b) and pumping power P_p (kW) (c,d): a) P_p = 3.5 (1) and 6 kW (2), T_2 = 0.2; b) P_p = 3 (1), 4 (2), 5 (3) and 6 kW (4), L = 0.55 (1), 0.53 (2), 0.35 (3) and 0.33 m (4); c) crystal, 5 mm diameter, 100 mm long (1) and 6.3 mm diameter, 100 mm long (2); d) in the crystal–lamp plane (2) and in the plane normal to it (1).

The decay of the excited level of the chromium ions in the GSGG crystal in the absence of Nd ions takes place exponentially with a decay time of 180 μs and does not depend on the concentration of chromium ions up to 6×10^{20} cm^{-3} (without concentrational decay of luminescence). When adding Nd ions to the crystal, the decay time of the $^4T_2$ level rapidly decreases as a result of the transfer of excitation energy by the levels of the Nd ions, and decay becomes non-exponential.

The optimum concentrations of the ions of chromium and Nd in GSGG are approximately 10^{20} cm^{-3}. In the Nd:Cr: GSGG crystal it is possible to ensure the effective lasing of Nd ions at a wavelength of 936 nm (transition $^4F_{3/2} \rightarrow {}^4I_{9/2}$) as a result of the sensitisation effect. The concentration of the Cr and Nd ions was selected to ensure that the resonance losses as a result of absorption on the $^4I_{9/2} - {}^4F_{3/2}$ transition do not exceed the permissible value of ~0.01 cm^{-1}. This is comparable with the losses in the active element.

The efficiency of build-up of energy in the Nd:Cr: GSGG crystal is 1.7 times higher [46], and the efficiency factor is twice the value [47] in the Nd:YAG crystal. However, the widening of the absorption bands of pumping results in a larger increase of heat lasing in the Nd:Cr:GSGG the crystal and, consequently, this crystal is characterised by considerably stronger effects of induced birefringence, the thermal lens and thermoelastic stresses. At the same pumping power, the focusing distance of the thermal lens in the Nd:Cr:GSGG crystal is 4.5 times shorter than in the Nd:YAG crystal [46]. In the Nd:Cr:GSGG crystal, it is possible to obtain a specific power of free lasing in the pulsed regime of 7 kW/cm^2 [48] and in the continuous regime 0.15 kW/cm^2 [49].

The Nd:Cr:GSGG crystal has a cubic structure, and its main spectral and physical characteristics are: melting point 1850 °C, density 6.5 g/cm^3, the refractive index of the crystal at a wavelength of 1060 nm 1.94, heat conductivity 6.02 W/m·deg, the thermo-optical constant $13\cdot10^{-6}$ deg^{-1}, the lifetime of the chromium ions 120 μs, the width of the gain line at the $^4F_{3/2}\rightarrow{}^4I_{11/2}$ transition 1.4 nm, the cross-section of this transition $1.5\cdot10^{-19}$ cm^2.

2.4.1 Spectral–time characteristics of radiation

The spectral–time, angular and energy parameters of lasing of the Nd:Cr:GSGG laser were investigated by the authors of this book in Ref. 11,12,16,18–20,22–28, with the non-optimum length of the flat resonator of 1.6 m for the Nd ions. This is determined by high thermo-optical deformation of the active rod and the laser resonator. A further increase of the resonator length resulted in a large decrease of the radiation energy due to a rapid increase of the losses of the equivalent spherical resonator. The high level of thermo-optical deformation of the crystal did not make it possible to obtain, in the Nd:Cr:GSGG crystal, the quasistationary lasing of TEM_{mnq} modes which was achieved only for the TEM_{ooq} modes (Fig. 2.18). In this case, the quasistationary regime of lasing was highly unstable in relation to the smallest perturbations of the resonator and, consequently, this required careful tuning of all elements of the resonator.

In the absence of the selection of the longitudinal modes, the width of the instantaneous spectrum of quasistationary lasing was 70 pm (Fig. 2.18c). This parameter reached saturation when the pumping was three times higher than the threshold value. The single-frequency tunable quasistationary lasing of the TEM_{ooq} modes (Fig. 2.18d) was obtained using a complex dispersion resonator, consisting of two Fabry–Perot selectors-etalons with the transmission factors of the mirrors of 20% and the dispersion ranges of 1.88 and 0.56 nm. The general range of retuning of the radiation wavelength at the $^4F_{3/2}\rightarrow{}^4I_{11/2}$ transition between the Stark sublevels $R_2\rightarrow Y_3$ (1064 nm) and $R_1\rightarrow Y_1$ (1060 nm) was ap-

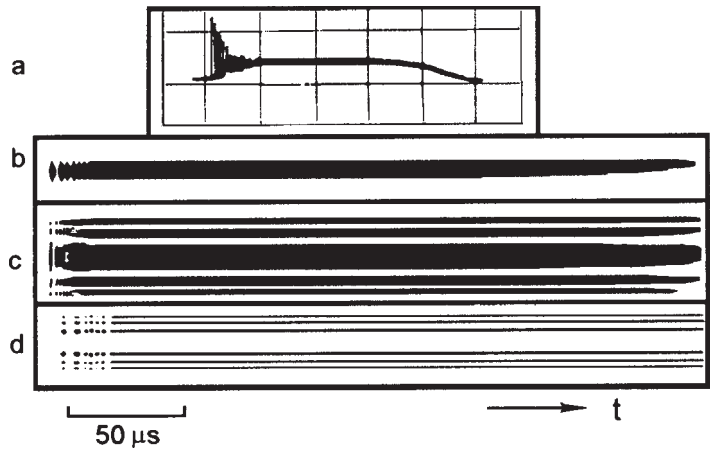

Fig.2.18 Parameters of the lasing of TEM_{ooq} modes of the Nd:CR:GSGG laser (diameter 4 mm, length 90 mm) with flat mirrors (L = 1.6 m, diameter 1.6 mm), $E_p = 5E_t$; a) oscillogram of radiation intensity, scale 50 μs/div; b) evolvement of the distribution of the intensity in the near-range zone; c,d) time evolvements of the lasing spectrum without selection of longitudinal modes (c) and with selection (d), the range of dispersion of the interferometer is 110 pm (c) and 20 pm (d).

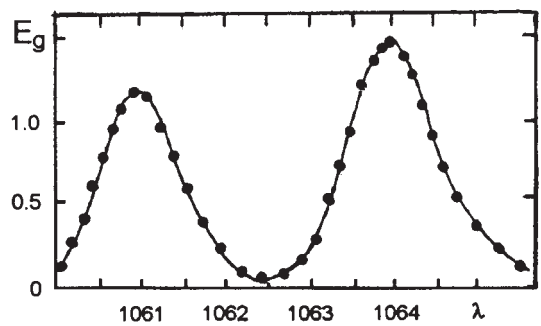

Fig.2.19 Dependence of the energy of one-particle lasing E_g (J) of Nd:Cr:GSGG laser on the lasing wavelength λ (nm) in a dispersion resonator; E_p = 0.3 kJ.

proximately 3 nm (Fig. 2.19).

In a non-selective resonator, the lasing threshold at a wavelength of 1061 nm at room temperature was 6 times higher than the lasing threshold at a wavelength of 1064 nm. At a temperature of 80 °C, the lasing threshold at a wavelength of 1061 nm decreased three times (Fig. 2.20a). The thermal drift of the gain line in the Nd:Cr:GSGG crystal was measured during heating of the crystal from the displacement of the maximum of the spectrum of quasistationary lasing from pulsed pulse on the interferograms of the spectrum (Fig. 2.20a). The mean speed of the thermal drift of the gain line in the examined temperature range was 4.0 pm/deg (Fig. 2.10b).

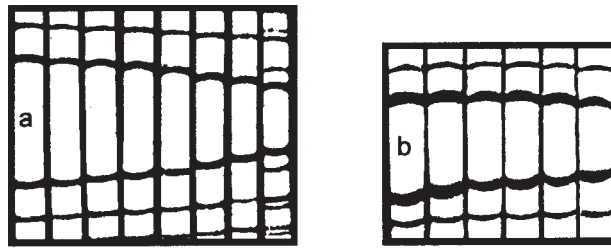

Fig.2.20 Interferograms of the spectra of quasi-stationary lasing of Nd:Cr:GSGG (a) and Nd:BLN (b) lasers at different crystal temperatures: a) T = 10, 30, 40, 50, 60, 70, 80 and 90 °C; b) T = 10, 30, 40, 50, 60, 70, 80 °C. The range of dispersion of the interferometers 560 pm (a) and 280 pm (b); $E_p = 2E_t$ (a) and $4E_t$ (b).

2.4.2 Energy parameters of lasing

The energy characteristics of the radiation of a Nd:Cr:GSGG laser with flat mirrors was investigated using a crystal 4 mm × 90 mm long, with bevelled and illuminated ends. The concentration of the Nd ions in the crystal was $2 \cdot 10^{20}$ cm^{-3}, and the concentration of the chromium ions was $3 \cdot 10^{20}$ cm^{-3}. Pumping of the crystal was carried out with an ISP-250 lamp, pumping pulse time was 250 μs. The volume of the active medium, contributing to lasing energy, was V_g = 0.5 cm^3. The ultraviolet radiation of pumping was cut off with a liquid filter.

The lasing energy of the Nd:Cr:GSGG laser decreased 1.75 times when the resonator length was increased from 0.3 to 1.6 m (Fig. 2.29a) (1). Heating the crystal from 10 to 90°C resulted in a linear decrease of the lasing energy of the examined laser by a factor of 1.2 (Fig. 2.29b) (1). The maximum density of the lasing energy of the Nd:Cr:GSGG laser of 4.5 J/cm^3 at a pumping energy of 300 J was obtained at a transmission factor of the output mirror of T_2 = 96%, i.e. when the output mirror of the resonator was represented by a non-sprayed wedge-shaped substrate made of K-8 glass (Fig. 2.29c) (1). The transmission factor of the output mirror T_2 was saturated to its maximum value of 96% already at a pumping energy of 100 J (Fig. 2.30a) (1). The dependence of the lasing energy of the Nd:Cr:GSGG laser on pumping energy was non-linear almost in the entire examined pumping energy range (Fig. 2.29d) (1). At a pumping energy of 500 J the density of the lasing energy of the Nd:Cr:GSGG laser was E_g/V_g = 4.8 J/cm^3. At a constant resonator length and with the pumping energy changing from 100 to 500 J, the divergence of radiation of the Nd:Cr:GSGG laser was doubled (Fig. 2.30b) (1). Thus, the radiation luminosity of $6 \cdot 10^7$ W/cm^2·ster was obtained in the examined laser.

2.5 Nd-DOPED LANTHANUM BERYLLATE LASERS

The single crystals of lanthanum beryllate ($La_2Be_2O_5$) are characterised by monoclinic symmetry. This results in a considerable anisotropy of the thermophysical and spectral–luminescence characteristics of these crystals. The heat conductivity coefficients of the Nd:BLN crystal at room temperature in the main axes are 4.6 (4.7 and 4.7) W/m·deg. The refractive index of the BLN the crystal in the axes is: n_a = 1.96, n_b = 1.99, n_c = 2.03. Its coefficients of thermal expansion in the axes are 7.0 (7.9 and 9.5)· 10^{-6} deg^{-1}. The density of the Nd:BLN crystal is 6.06 g/cm^3, the melting point of the Nd:BLN crystals is 1361°C.

The Nd ions in the La beryllate crystal (Nd:BLN) are characterised by a wide uniformly broadened gain line (3.4 nm) so that it is possible to change the wavelength of radiation in a relatively wide region of the spectrum.

The cross-section of the transition $^4F_{3/2} \rightarrow {}^4I_{11/2}$ at room temperature is 1.5 × 10^{-19} cm^2. The optimum concentration of the Nd ions in the BLN crystal, resulting in the maximum intensity of luminescence, is 1.8%. At this concentration, the lifetime of the upper working level of the Nd ions is 110 μs. The technology of growth of these crystals has been sufficiently developed and active elements of standard dimensions are being grown.

Some integral parameters of free lasing have been investigated in lamp [50] and laser [51] pumping.

2.5.1 Spectral–time parameters of lasing

The spectral–time, spatial, angular and energy characteristics of radiation of lasers on Nd ions in crystals of La beryllate ($La_2Be_2O_5$) were examined in detail by the authors of this work in [8, 10, 11, 13, 18, 19, 22–28].

With the optimum parameters of the flat resonator after eliminating the effect of technical perturbations of the resonator in the Nd: BLN laser it is possible to obtain stable quasistationary lasing of the TEM_{ooq} (Fig. 2.21b, c) and TEM_{mnq} modes (Fig. 2.21d,e). The Nd: BLN crystals are inferior in their heat conductivity and homogeneity to the Nd: YAG crystals and, consequently, the quasistationary lasing of the TEM_{ooq} modes of the Nd:BLN laser is more sensitive to weak perturbations of the resonator and requires more careful adjustment of the elements of the resonator. In the absence of the selection of the longitudinal modes, a radiation spectrum 250 pm is excited in the first peak, and within several peaks its width decreases to the stationary value determined by the pumping level (Fig. 2.21c) [8]. When the pumping level is 10 times higher than its threshold volume, the stationary instantaneous with of the spectrum of lasing was 120 pm. The process of lasing was accompanied by the

displacement of the emission spectrum to the long-wave length region at a speed of 0.2 nm/ms as a result of the thermal drift of the gain line, determined by heating of the crystal. Thus, during the pumping pulse of 0.25ms, the Nd:BLN crystal was heated to approximately 60 °C [8].

The speed of the thermal drift of the gain line was measured from the displacement of the spectrum of quasistationary lasing (Fig. 2.20b) with the pumping slightly higher than the threshold level and with controlled heating of the crystal with an accuracy to 0.1 °C. In the examined range of radiation of the temperature of the Nd:BLN crystal, the speed of the thermal drift of the gain line was characterised by a linear dependence and was 0.84 pm/deg (Fig. 2.10b) [10].

The quasistationary lasing of TEM_{mnq} modes was achieved only for the modes with a low transverse index (m, $n \leq 5$) when only a small number of the modes was excited and the spatial competition of the modes was greatly weakened. This regime is more sensitive to the external perturbations and the regime of lasing of the longitudinal waves. The width of the instantaneous spectrum of lasing of TEM_{mnq} modes (Fig. 2.21e) corresponded to the lasing spectrum of TEM_{ooq} modes. In the

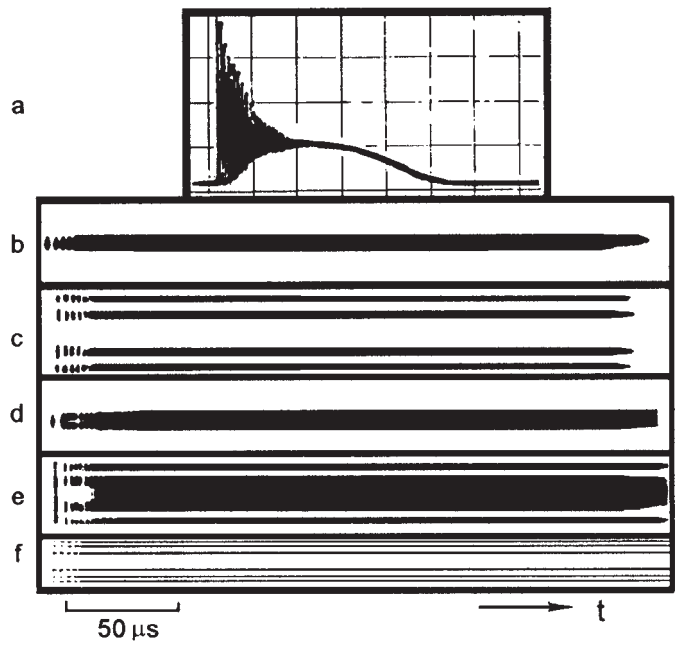

Fig.2.21 Parameters of the lasing of TEM_{00q} (b,c) and TEM_{mnq} modes (d,e) of Nd:BLN laser (4 mm in diameter, 70 mm long) with flat mirrors (L = 2 m, T_2 = 0.7) without (c,e) and with selection of the longitudinal modes (f), $E_p = 10E_t$: b,d) evolvement of the distribution of radiation intensity in the near-range zonel; c,e,f) time evolvement of the lasing spectrum, the range of dispersion of the interferometers 280 pm (c,e) and 20 pm (f).

complex dispersion resonator, consisting of two Fabry–Perot selectors-etalons, we achieved the single-frequency quasistationary lasing of TEM_{ooq} and TEM_{mnq} modes (Fig. 2.21f). The change of the wavelength of the single-frequency radiation at the transition $^4F_{3/2} \rightarrow {}^4I_{11/2}$ approximately 6 nm (Fig. 2.22) and the width of the integral radiation spectrum was 3 pm [10].

2.5.2 Energy parameters of lasing

Investigations were carried out on the crystals of La beryllate with Nd (Nd:BLN), 4 mm in diameter, 70 mm long, with the bevelled and clarified ends in a flat mirror laser. The concentration of the Nd ions in the crystals was 2%. The pumping of active elements was conducted using an INP 5/45 lamp, in a quartz single-block illuminator, with the cutting off of the ultraviolet radiation of pumping. The lasing volume in this case was V_g = 0.56 cm^3.

The lasing energy of the Nd:BLN laser decreased by a factor of 2.2 when the length of the resonator was increased from 0.3 to 1.6 m (Fig. 2.29a) (2). Heating of the La beryllate crystal in the range from 10 to 90 °C decreased the lasing energy of the Nd:BLN laser by a factor of 1.5 (Fig. 2.29b) (2). At a pumping energy of 300 J, the maximum energy of lasing of the laser was obtained at a transmission factor of the output mirror of the resonator of 70% (Fig. 2.29c) (2).

With increase of the pumping energy, the value of the optimum transmission factor T_2 at which the maximum energy is obtained, tended to its limiting value of 85% (Fig. 2.30a) (2). If at a low pumping energy

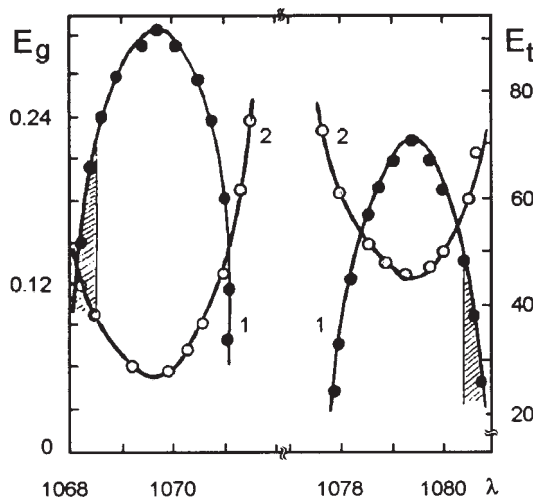

Fig.2.22 Dependence of the energy of one-particle lasing E_g (J) (1) and threshhold energy E_t (J) (2) of Nd:BLN laser on the wavelength λ (nm) in a dispersion resonator (L = 2 m); E_p = 200 J.

level the efficiency of lasing of the Nd:BLN laser was comparable with the efficiency the lasing of the Nd:YAG laser, then with increasing energy of the pumping, the efficiency of lasing of the Nd:BLN laser was higher than the efficiency of lasing of the Nd:YAG laser, and at a pumping energy of 500 J the density of energy of the Nd:BLN laser was 2.8 J/cm^3, and for the Nd:YAG laser it was 2.6 J/cm^3 (Fig. 2.29d) (2). The heat conductivity of the La beryllate crystal is considerably lower than that of the crystal of the yttrium–aluminium garnet. In the experiments, this was reflected in an increase of the angular divergence of radiation of the Nd:BLN laser and in a decrease of the luminosity of radiation in comparison with the Nd:YAG laser (Fig. 2.30b) (2).

2.6 Nd LASERS IN HEXA-ALUMINATES OF LANTHANUM-MAGNESIUM AND LANTHANUM–BERYLLIUM

Recently, special attention has been given to the application of crystals of hexa-aluminates of La–Mg and La–Be in which the Nd ion concentration may reach tens of percent at a slight concentration decay of luminescence. Therefore, it may be expected that the efficiency of lasing on these crystals will be relatively high.

The single crystals of the hexa-aluminate of La–Mg with Nd (Nd^{3+}:$LaMgAl_{11}O_{19}$, Nd:LNA) are characterised by a hexagonal structure and a relatively low anisotropy of properties in different crystallographic directions. Optically, these are anisotropic uniaxial crystals. They melt congruently at a temperature of 1870°C. The density of the crystals of LNA is 4.04 g/cm^3, hardness (Moose) is 7.5. The heat conductivity of the LNA crystals is relatively high and equals 14 W/m·deg($\perp$c) and 10 W/m·deg(||c).

The Nd:LNA crystals may have a relatively high concentration of Nd ions (to 7×10^{20} cm^{-3}) with slight concentration decay of luminescence. The cross-section of the laser transition $^4F_{3/2} \rightarrow {}^4I_{11/2}$ in the crystal is 3.2×10^{-19} cm^{-3}, the lifetime of the upper level is 320 μs, the half-width of the gain line is 3 nm. The lasing of Nd ions in the crystal of the hexa-aluminate of La–Mg was recorded for the first time in Ref. 52 and 53. The integral characteristics of radiation of the Nd:LNA laser were investigated in lamp [53] and laser [56] pumping.

The lasing of Nd ions in the crystal hexa-aluminate of La–Be (Nd^{3+}:$LaBeAl_{11}O_{19}$, Nd:GALB) was investigated in Ref. 54 and 55. The Moose hardness of the Nd:GALB crystals was ~7, density 4.15 g/cm^3. The lifetime of the upper level of the laser transition $^4F_{3/2} \rightarrow {}^4I_{11/2}$ is 150 μs at room temperature. The absorption spectra of the examined Nd:GALB crystal (Fig. 2.23) contained a large number of lines determined by transitions from the ground state $^4I_{9/2}$ to the excited levels ^4F, ^2H, ^4S, ^2G, ^4G and other multiplets of the Nd ions. The luminescence spectra

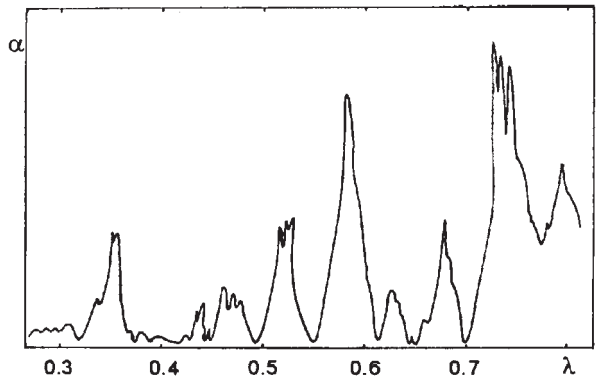

Fig.2.23 Dependence of the coefficient of absorption α (cm^{-1}) of neodymium ions (Nd^{3+}) on the wavelength λ (μm) on the crystal of lanthanum–beryllium hexa-aluminate at room temperature.

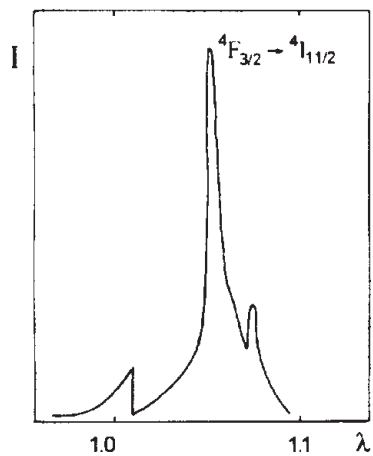

Fig.2.24 Dependence of the intensity of luminescence I (rel.units) of neodymium ions in the crystal of lanthanum–beryllium hexa-aluminate on wavelength λ (μm) in transition $^4F_{3/2} \rightarrow {}^4I_{11/2}$ at room temperature.

of the crystal on the transition $^4F_{3/2} \rightarrow {}^4I_{11/2}$ (Fig. 2.24) are considerably wider indicating the disordered structure of the crystal.

2.6.1 Spectral and time parameters of lasing

Of all the examined Nd lasers, the quasistationary lasing with lamp pumping could not be obtained only in the Nd:LNA flat mirror laser because of high thermal strains of the crystal. In this case, it was not possible to obtain the optimum parameters of the resonator which make it possible to eliminate the effect of technical perturbations in the Nd lasers and obtain quasistationary lasing. The regime of non-attenuating pulsations of the radiation intensity was characterised by the random alternation

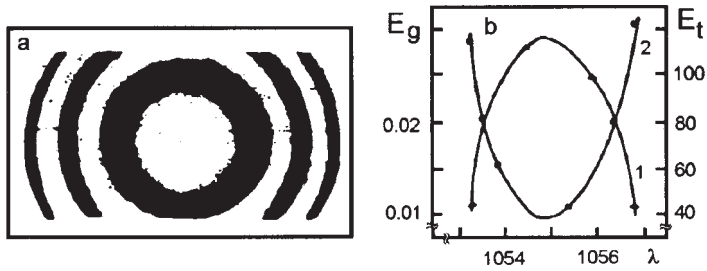

Fig.2.25 a) Interferogram of the integral spectrum of lasing of TEM_{mnq} modes of Nd:LNA laser (diameter 3 mm, length 50 mm) with flat mirrors (L = 0.4 m) in the absence of selection of longitudinal modes, range of dispersion of the interferometer 560 pm, $E_p = 2E_t$; b) dependence of lasing energy E_q (J) (1) and the threshhold energy of pumping E_t (J) (2) on wavelength λ (nm) in a dispersion resonator with a selector-etalon with a temperature range of 5.5 nm, $E_p = 2E_t$.

of the spectral components of the spectrum, and when the a pumping level was twice as high as the threshold level and there was no selection of the longitudinal modes, the width of the integral radiation spectrum was 1 nm (Fig. 2.25a). This indicates the non-uniform nature of broadening of the gain line. When using a Fabry–Perot selector-etalon with a dispersion range of 5.6 nm, the width of the lasing spectrum decreased to 5.6 nm, and this was accompanied by the rearrangement of the radiation wavelength in the range 3.5 nm (Fig. 2.25b).

In free lasing regime with pumping slightly higher than the threshold value, the width of the integral spectrum of lasing of the Nd:GALB laser was approximately 0.3 nm, as in the Nd:LNA laser. In the absence of spurious selection of the longitudinal modes, the width of the integral spectrum of the Nd:GALB laser increased with increasing pumping energy and when the pumping value was twice the threshold level, it was approximately 1 nm and reached saturation. This large increase of the width of the lasing spectrum was evidently determined by the non-uniform nature of broadening of the gain line of the Nd:GALB crystal as in the case of the Nd:LNA crystal. The nature of lasing of the Nd:GALB laser was almost identical with the nature of lasing of the Nd:LNA laser.

The addition of the Fabry–Perot selector-etalon with a dispersion range of 5 nm into the resonator of the Nd:GALB laser reduced the width of the lasing spectrum to 0.03 nm and made it possible to change the lasing wavelength lasing in the range of the order of 3 nm in the vicinity of the centre of the maximum of the gain line.

2.6.2 Energy parameters of lasing

Investigations were carried out on lasers with flat mirrors on crystals Nd:LNA and Nd:GALB, 3 mm in diameter, 50 mm long, with bevel-

led and clarified ends. The volumes of the active media, contributing to lasing energy, were V_g = 0.28 cm^3. The concentration of the Nd ions in the crystals was 5 wt%. Pumping was carried out with an ISP-250 lamp with a pumping pulse time of 250 μs in a quartz single-unit illuminator. The ultraviolet radiation of pumping was cut-off with a liquid filter.

The nature of the dependences of the lasing energies of the Nd:LNA and Nd:GALB lasers was almost identical and, consequently, Figs. 2.29 and 2.30 show these relationships only for the laser on the Nd:LNA crystal which is a better known active medium, and the efficiency of lasing of the Nd:GALB laser was slightly higher than that of the Nd:LNA laser. With an increase of the length of the resonator from 0.2 to 1.6 m at a constant pumping energy, the lasing energy of the lasers decreased by a factor of 3 (Fig. 2.29a) (5).

The large decrease of lasing energy with increasing resonator length is caused mainly by high thermo-optical deformation of the crystals which transformed the flat resonator of the laser to an unstable equivalent spherical resonator with high losses. At a constant length of the resonator, heating of the crystals from 10 to 90 °C resulted in a decrease of lasing energy by a factor of 1.5 (Fig. 2.29b) (5).

At a pumping energy of 300 J, the maximum lasing energy of the lasers was obtained at the transmission factor of the output mirror of the resonator T_2 of approximately 70% (Fig. 2.29c). With increase of the pumping energy, the optimum transmission factor T_2 tended to its maximum value of 90% (Fig. 2.30a) (5). In the range of low pumping energies, the lasing energy of the lasers depended in a linear manner on the pumping energy, and with increase of pumping energy the linear form of the dependence was disrupted, and at a pumping energy of 500 J the density of the lasing energy was approximately E_g/V_g = 1.2 J cm^3 (Fig. 2.29d). This is associated with both the thermal deformation of the laser resonator and with the energy losses of pumping where the short-wave part of pumping radiation was cut-off by a liquid filter.

2.7 Nd LASERS ON POTASSIUM–GADOLINIUM AND POTASSIUM–YTTRIUM TUNGSTATES

The single crystals of the binary potassium–gadolinium tungstate ($KGd(WO_4)_2$, KGW) belong to monoclinic crystals, and this results in the anisotropy of the thermophysical and spectral–luminescence characteristics of these crystals. The heat conductivity coefficient of KGW crystals is several times lower than that of YAG crystals, and the coefficients of heat conductivity of the KGW crystals are characterised by anisotropy in the three main crystallographic axes: [100] k = 2.8 W/m·deg, [010] k = 2.2 W/m·deg, [001] k = 3.5 W/m·deg. This greatly restricts the area

of application of these crystals in the lasing regime with continuous lamp pumping.

The thermal expansion coefficients are also characterised by the corresponding anisotropy in the direction of the axes: 4 (1.4; 8.5) × 10^{-6} deg^{-1}. The refractive index of the KGW crystal at a wavelength of 1067 nm is: n_a = 2.03, n_b = 1.94 and n_c = 1.98. The thermo-optical constants of these crystals are characterised by even greater anisotropy along the axes: dn_a/dT = + 8×10^{-7} deg^{-1}, dn_b/dT = -5.5×10^{-6} deg^{-6}, dn_c / dT = $+1.7\times10^{-6}$ deg^{-1}, with the orientation of the heating region parallel to the *c* axis. Since the temperature coefficient has positive and negative values, at a specific orientation of the KGW crystal the thermal lens may not form in the resonator. The density of the KGW crystals is 7.27 g/cm^3, hardness (Moose) 5, melting point 1075 °C, which is 900 degrees lower than in the YAG crystals. Consequently, it is possible to grow larger active specimens of KGW crystals and, as indicated by experiments, with higher optical quality.

The absorption bands of the Nd ions in the KGW almost coincide with the corresponding absorption bands in the YAG, but the absorption bands of the Nd: KGW crystal are considerably wider and less truncated resulting in more efficient absorption of radiation of the pumping lamps. The cross-section of the $^4F_{3/2}\rightarrow{}^4I_{11/2}$ transition of the Nd:KGW crystal at a wavelength of 1067 nm is 3.8×10^{-19} which, according to the latest spectroscopic measurements [32], is larger than the cross-section of these transitions in the Nd:YAG crystal. The width of the gain line of the Nd:KGW crystal is 7 times greater than that of the gain line of the Nd:YAG crystal and is 4.3 nm, so that Nd:KGW crystals can be used in tunable lasers. The lifetime of the upper working level of the Nd:KGW crystal depends only slightly on the concentration of the Nd ions, and with increase of the concentration of these ions from 1 to 10 at.% the lifetime is only halved from 142 to 70 μs. This high concentration of the activator results in a high efficiency factor of the Nd:KGW crystal, but only at low pumping levels and the small dimensions of the active element.

The lasing on Nd ions in the crystals of potassium–yttrium (Nd:KYW) and potassium–gadolinium (Nd: KGW) tungstates was reported for the first time in Ref. 37.

2.7.1 Spectral–time parameters of lasing

The spectral–time, spatial and angular parameters of lasing of Nd: KGW and Nd:KYW lasers were investigated in Ref. 4,11,17–19,22–28.

At the optimum parameters of the flat resonator and as a result of eliminating the effect of technical perturbations of the resonator in the Nd:KGW laser, it was possible to obtain quite easily the stable

quasistationary lasing of TEM_{ooq} (Fig. 2.26b, d) and TEM_{mnq} modes (Fig. 2.26c, d). The quasistationary lasing of the TEM_{mnq} modes was realised only at low values of the indices of the transverse modes (m, $n \leq 5$). The short duration of the transition process is determined by the short lifetime of the upper working level. The instantaneous width of the structureless spectrum in the quasistationary regime was 15 pm (Fig. 2.26d), and reached saturation when the pumping value was 5 times higher than the threshold value. It is evident that this wide spectrum of lasing in the lasers with the uniformly broadened gain line without selection of the longitudinal modes is caused by their self-synchronization. This should be accompanied by the appearance of a continuous spectrum with the period ($c/2L$), where c is the velocity of light, L is the length of the resonator. The recording of the lasing spectrum with a time resolution of approximately 1 ns has confirmed this.

In a dispersion resonator with a Fabry–Perot selector-etalon, with a dispersion range of 5.7 nm, it was possible to obtain single-frequency quasistationary lasing of TEM_{ooq} and TEM_{mnq} modes (Fig. 2.26e), with smooth tuning of the radiation wavelength in the range 4 nm.

The speed of the thermal drift of the gain line into the long-wave region of the spectrum in the Nd:KGW and Nd:KYW crystals during

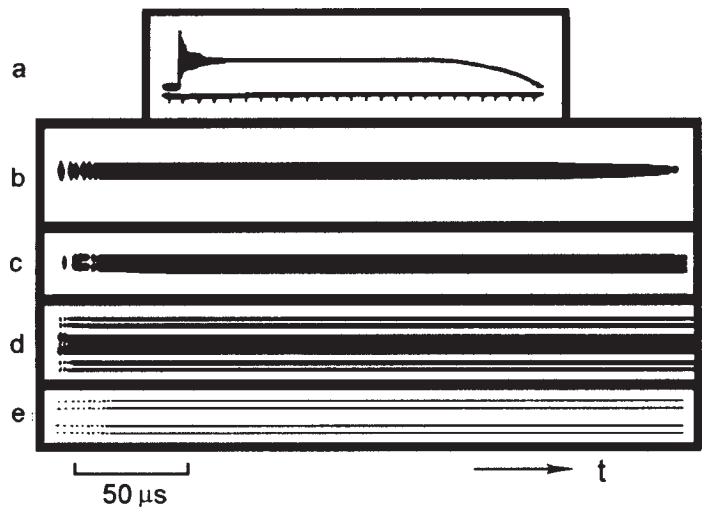

Fig.2.26 Parameters of the lasing of TEM_{ooq} (b,d) and TEM_{mnq} (c,d) modes of Nd:KGW laser (diameter 6 mm, length 90 mm) with flat mirrors (L = 2 m, T_2 = 0.5), E_p = $10E_t$; a) oscillogram of radiation intensity, 20 μs marks; b,c) time evolvement of the distribution of radiation intensity of TEM_{ooq} (b) and TEM_{mnq} (c) modes in the near-range zone; d,e) time evolvement of the lasing spectrum of TEM_{mnq} modes (c) in the near-range zone; d,e) time evolvement of the lasing spectrum of TEM_{ooq} and TEM_{mnq} modes without (d) and with selection of the longitudinal modes (e), the range of dispersion of the interferometer 190 pm (d) and 20 pm (e).

heating, recorded on the basis of the interferograms of the lasing spectrum, was approximately 0.9 pm/deg (Fig. 2.10b).

The spectral–time parameters of lasing of Nd:KYW laser under normal conditions were almost identical with the lasing parameters of the Nd:KGW laser. An original regime was realised in the Nd:KYW laser in which the dispersion element in the resonator with flat mirrors was represented by an active rod whose ends were cut under an angle of approximately 10° in relation to each other and in relation to the axis of the rod. In this case, it is possible to ensure the self-sweep of the radiation wavelength to the short-wave range of the spectrum with a high constant of the component of the integral intensity of radiation (Fig. 2.25). The laser resonator did not contain any additional selecting elements and the maximum of the gain line was displaced to the long-wave region of the spectrum.

The displacement of the lasing wavelength (self-sweep) took place in the case in which the lasing channel, determined by the diaphragms, did not pass accurately along the axis of the rod and the induced thermal lens. The variation of the focus of the thermal lens in the process of lasing resulted in a smooth deflection of the beam in the angle and in the sweep of the radiation wavelength as a result of the dispersion of the active rod. The sweep rate of the lasing wavelength depended on the pumping energy and the dispersion of the active element. For the parameters of the Nd:KYW laser, shown in Fig. 2.27, this rate was approximately 0.4 nm/ms.

After the transition process, a single longitudinal mode was excited in every peak. The change of the modes in the lasing process was adiabatic and was not accompanied by the pulsations of the integral intensity of radiation as a result of the low sweep rate of the wavelength. The absence of the selecting elements in the resonator, which leads to significant losses of radiation intensity, has made it possible to obtain satisfactory radiation

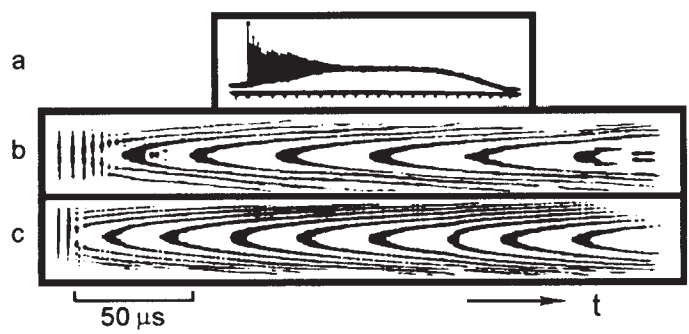

Fig.2.27 Parameters of lasing of TEM_{ooq} modes of Nd:KYW laser (diameter 5 mm, length 80 mm) with flat mirrors (L = 2 m): a) oscillogram of radiation intensity, 20 μs marks; b,c) time evolvement of the lasing spectrum at different pumping levels $E_p = 3E_t$ (b) and $I4E_t$ (c), the range of dispersion of the interferometer 20 pm.

energy characteristics in such a sweep-laser.

2.7.2 Energy parameters of lasing

Investigations were carried out on a laser with flat mirrors on a crystal of binary potassium–gadolinium tungstate with Nd (Nd:KGW), 5 mm diameter, 100 mm long, with bevelled and illuminated ends. The concentration of the Nd ions was 3%. The volume of the active medium, providing a contribution to the lasing energy, was V_g = 1.57 cm^3. Pumping was carried out using a IPF-800 pulsed lamp, the pumping pulse time was 250 μs. The ultraviolet radiation of pumping was cut-off with the liquid filter.

The efficiency of lasing of the examined Nd:KGW crystal was slightly higher than that of Russian standard active elements produced from the Nd:YAG crystals. In the Nd:KGW laser, all energy characteristics were identical to the characteristics obtained for the majority of Nd media (Fig. 2.29 and 2.30). With increase of the length of the resonator, the lasing energy of the Nd:KGW laser decreased by a factor of 1.3 (Fig. 2.29 a, b) (7). When heating the crystal from 10 to 90 °C, the lasing energy of the Nd:KGW laser decreased only by a factor of 1.2 (Fig. 2.29b) (7).

At a pumping energy of 300 J, the maximum lasing energy was obtained at the optical coefficient of transmission of the mirror of the resonator of 50% (Fig. 2.29c) (7). The divergence of the radiation of the Nd:KGW laser was similar to the diffraction divergence (Fig. 2.30b) because of the examined active media, the Nd:KGW crystals are characterised by higher optical homogeneity.

2.8 Nd LASERS ON SELF-ACTIVATED CRYSTALS

In widely used crystal laser media, active ions represent an impurity and substitute a specific type of atoms of the matrix lattice. In the majority of cases, the ion of the activator differs from the substituted ion of the matrix by a whole number of parameters: ion radius, mass, etc. This imposes certain restrictions of the possibility of activation of the matrix with respect to concentration, and the increase of concentration results in thermal stresses causing failure of the crystal.

The self-activated crystals include the $RbNd(WO_4)_2$ crystal, whose structure and lattice parameters were determined in Ref. 72. The concentration of Nd ions in the crystal was 6×10^{21} cm^{-3}, the lifetime of the upper working level was 10 μs, the cross-section of the $^4F_{3/2} \rightarrow {}^4I_{11/2}$ transition at room temperature was 2.5×10^{-19} cm^2, the wavelength at the maximum of the luminescence line was 1065 nm, the width of the gain line was ~2 nm. As regards the parameters, the crystal of the Rb–Nd tungstate

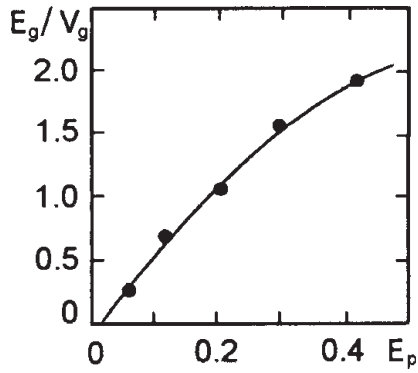

Fig.2.28 Dependence of the specific energy of lasing E_g/V_g (J/cm^3) of the laser on a self-activated crystal of rubydium–neodymium tungstate on pumping energy E_p (kJ) at room temperature and the resonator length L = 0.2 m.

is very similar to the parameters of the crystals of potassium–gadolinium tungstate (Nd:KGW). Some characteristics of radiation of the laser on the crystal of Rb–Nd tungstate were investigated in Ref. 73.

The authors of this book investigated a laser on a crystal of Rb–Nd tungstate with the crystal size of 3 mm diameter, 30 mm^2 long, in experimental equipment described previously [29].

Figure 2.28 shows the graph of the dependence of the specific lasing energy of the laser on the pumping energy, which shows that the differential efficiency of the laser on the self-activated crystal of the Rb–Nd tungstate corresponds almost completely to the differential efficiency of the Nd:YAG laser, irrespective of the considerably shorter lifetime of the working upper level and the cross-section of the forced transition. It is likely that these losses are compensated by a considerably higher concentration of the Nd ions in the self-activated crystal. At low pumping energies, the dependence of the lasing energy of the laser was almost linear, and with increasing pumping energy, it deviated from the linear dependence. This is associated with the fact that increase of the radiation energy of the pumping lamp increases the fraction of ultraviolet radiation of pumping which does not agree with the absorption spectrum of the Nd ions in the self-activated crystal.

When technical perturbations of the resonator were eliminated, it was possible to obtain stable quasistationary lasing of the TEM_{mnq} and TEM_{ooq} modes of the laser on the crystal of Rb–Nd tungstate, as in other widely used Nd media. The decay time of the transition pulsations of the radiation intensity of the laser on the self-activated crystal rapidly decreased in comparison with the Nd:YAG laser in accordance with the lifetime of the upper working level.

The shorter lifetime of the upper working level of the laser on the

self-activated crystal of Rb–Nd tungstate results in a considerably lower sensitivity of this laser to technical perturbations in the laser resonator. Consequently, it is far easier to obtain the quasistationary lasing of the laser on the self-activated crystal in comparison with other Nd media.

2.9 OPTIMISATION OF THE ENERGY CHARACTERISTICS OF RADIATION OF PULSED Nd LASERS

The maximum energy characteristics of radiation of Nd lasers are the same as in the case of the Cr lasers, and are obtained as a result of optimisation of the parameters of the resonators and the temperature of the active medium (Fig. 2.29 and 2.30). At a constant pumping energy, an increase of the resonator length (Fig. 2.29a) and of the temperature of the active medium (Fig. 2.29b) reduces the radiation energy of all

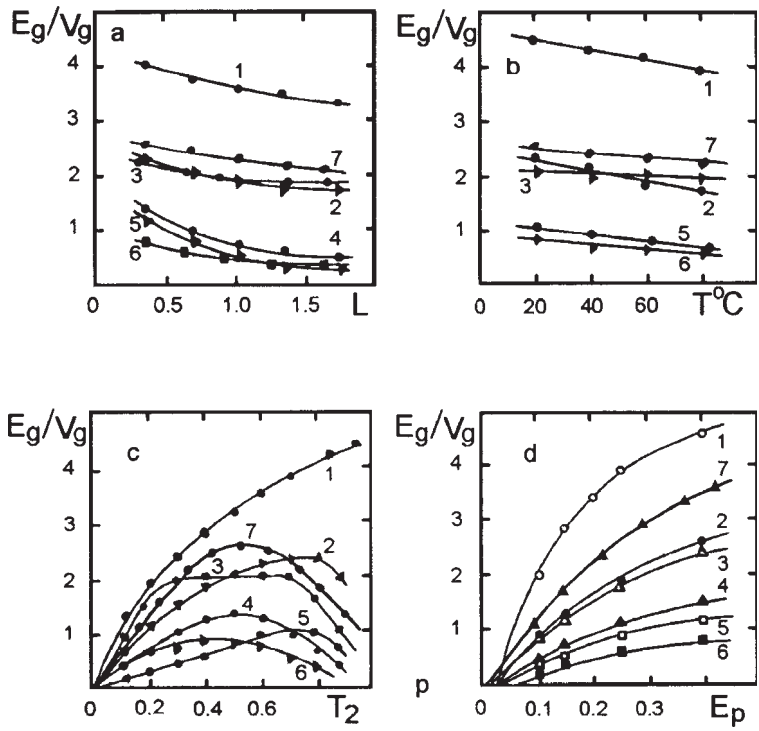

Fig.2.29 Dependence of the densities of lasing energy E_g/V_g (J/cm^3) on the length of the resonator L (m) (a), the temperature of active media T (b), the coefficients of transmission of the output mirror of the resonator T_2 (c) at a constant pumping energy E_p = 0.3 kJ (a,b,c) and pumping energy E_p (kJ) (d) for lasers: Nd:Cr:GSGG (1), Nd:BLN (2), Nd:YAG (3), Nd:KNFS (4), Nd:LNA (5), Nd:GLS-22 (6) and Nd:KGW (7). Generated volumes of the active media V_g = 0.5 (Cr:GSGG), 0.56 (BLN), 2.5 (YAG, GLS-22), 2 (KNFS), 0.28 (LNA) and 1.57 cm^3 (KGW).

Nd lasers, with the exception of the Nd:YAG laser. The values of the optimum transmission factors of the output mirror of the laser resonator characterised by the highest lasing energy reach saturation at pumping levels of $E_p \geq 0.4$ kJ (Fig. 2.30a).

At low pumping levels, the radiation energy of the Nd lasers was usually characterised by a linear dependence on pumping energy (Fig. 2.29d). Increasing pumping energy resulted in the saturation of the radiation energy of the lasers as a result of a decrease of the efficiency of pumping due to the increase of the fraction of short-wave radiation in the pumping spectrum which was cut off by a liquid filter.

The smallest divergence of radiation was recorded in the case of the Nd:KGW laser (2.30b) as a result of the high homogeneity of the crystal and good heat conductivity. Therefore, the highest luminosity of radiation from the unit volume of the active medium was obtained in the case of the Nd:KGW laser regardless of the fact that the Nd:Cr:GSGG laser was characterised by higher efficiency and specific energy of lasing.

2.10 PROBLEM OF NON-ATTENUATING PULSATIONS OF RADIATION IN SOLID-STATE LASERS

The experimental results presented above indicate that the free lasing of the Cr lasers with flat mirrors always takes place in the regime of non-attenuating pulsations of radiation intensity, in contrast to the Nd lasers. The reasons for the formation of non-attenuating pulsations of radiation in solid-state lasers have been discussed for more than 30 years in a large number of studies and dissertations. In the majority of investigations lasing was presented in a quasi-classic description characterised by the classic examination of the electromagnetic field and the quantum-mechanics analysis of the active medium. The balance equations, describing

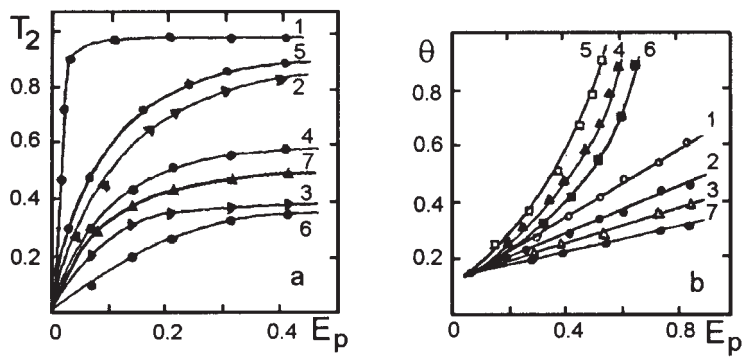

Fig.2.30 Dependence of the optimum coefficient of transmission of the output mirror T_2 (a) and the angle of divergence of laser radiation Θ (mrad) (b) of the pumping energy E_p (kJ) for lasers: Nd:Cr:GSGG (1), Nd:BLN (2), Nd:YAG (3), Nd:KNFS (4), Nd:LNA (5), Nd:GLS-22 (6) and Nd:KGW (7).

the lasing and linking together the energy of the field in the resonator and the difference of the populations of the working levels, were obtained in the conditions of a large number of simplifying assumptions and in a limited range of the variation of the laser parameters.

The formation of automodulation and non-attenuating pulsations of radiation intensity in solid-state lasers have been explained by a large number of reasons in many investigations: 1) the process of establishment of the stationary lasing regime [57]; 2) the anisotropy of the gain curve [58]; 3) the effect of different non-linear effects of interaction of the radiation field with the active medium [59–61]; 4) the multimode lasing regime [62); 5) the heterogeneity of pumping [63]; 6) the effect of spontaneous noise [64]; 7) the effect of saturated absorption in the active medium above the critical level [65]; 8) the effect of instabilities of the resonator parameters [66]; 9) the effect of fluctuations of intensity with respect to the amplitude above the attenuation decrement [67]; 7) the non-uniform nature of broadening of the gain line [68]; 11) the effect of focusing of radiation [69]; 12) the effect of the periodic structure of inverse population [70]; 13) the effect of the thermal drift of the gain line [71].

All the proposed mechanisms, causing the non-attenuating pulsations of the radiation intensity of solid-state lasers, can be divided into physical, determined by internal physical processes and not associated with the specific equipment, and technical, determined by external factors (instability of the parameters of the resonator and pumping). The effect of the technical factors on the free lasing dynamics is eliminated by a relatively simple means, as shown previously, even in the conditions of the pulsed lasing regime. Analysis of the experimental results, presented in the study, indicates that none of the previously described physical mechanisms explains the reasons for the formation of the non-attenuating pulsations of the radiation intensity in Cr lasers. The experiments with a ruby laser showed clearly the effect of the physical mechanisms causing such pulsations.

Comparison of the lasing characteristics of radiation of the TEM_{ooq} modes of the lasers on the chromium and Nd ions in the crystal of the gadolinium–scandium–gallium garnet, having the same matrix of the active medium and, consequently, identical non-linearities, excludes the physical mechanisms associated with the spatial interaction of the modes in the active medium. Under the same experimental conditions, the Cr:GSGG laser generates in the regime of non-attenuating pulsations of radiation, and the Nd:GSGG laser in the quasistationary regime.

This quantitative difference in the dynamics of free lasing of these lasers is determined by large differences in the structures of their working levels. If irradiation of the chromium ions is determined by the elec-

trons of the outer 3*d*-shell, the irradiation of the Nd ions is determined by the electrons of the 4*f*-shell, which is highly screened. Consequently, the generated electric field of laser radiation in the active medium affects only the chromium ions, leading to additional splitting of its working levels as a result of the dynamic Stark effect.

In the conditions of the spatially non-uniform field in the active medium, generated by the standing wave whose spatial structure changes during the lasing process (Fig. 1.4), the dynamic Stark effect leads to the modulation of the gain factor of the active media with time and the non-attenuating pulsations of radiation intensity. The forced smoothing of the spatial heterogeneity of the field in the active media eliminates the induced modulation of the gain factor with time and leads to quasistationary lasing (Fig. 1.6).

Chapter 3

Generation of powerful single-frequency giant radiation pulses in solid-state lasers

The large number of investigations using powerful solid-state lasers in superhigh resolution spectroscopy in the selective ionisation and excitation of atoms and molecules, plasma diagnostics and beams of atoms and ions, etc., imposes more and more stringent requirements on the laser radiation parameters: power, the width of the spectrum and its tuning, the time and spatial distribution of intensity, the stability of the spectrum and the time of appearance of the pulse. The solid-state lasers with Q-factor modulation (active and passive) in the giant pulse regime are used widely in various areas of science, investigations and technology.

3.1 METHODS OF PRODUCING SINGLE-FREQUENCY LASING IN LASERS WITH Q-FACTOR MODULATION

In lasers with the passive Q-factor modulation of the resonator (Q-modulation), the efficiency of selection of longitudinal modes is considerably higher than in lasers with active Q-modulation. This is determined by the fact that in the lasers with passive Q-modulation, the duration of the linear development of the giant pulse is approximately 1 microsecond, whereas in the lasers with active Q-modulation, it is an order of magnitude shorter.

During linear development, various modes increase from the level of spontaneous noise independently of each other, and the ratio of the amplitude of the modes at the moment of non-linear development of the giant pulse determines the modes that are included in lasing. In the case of passive Q-modulation, the number of passages of photons through the resonator is of the order of 1000. Consequently, the necessary difference in the losses for the two modes, after which the intensities of these modes at the end of linear development will differ by an order of magnitude, is approximately 10^{-3} (1.4). In a laser with passive Q-modulation, single-frequency lasing is achieved in the conditions of slight discrimination

of the longitudinal modes. In the lasers with active *Q*-modulation, the number of passages through the resonator is reduced to several tens. Consequently, it is not possible to carry out sufficiently strong discrimination of the longitudinal modes when using the conventional selection methods, in order to obtain lasing on a single longitudinal mode.

1. Dispersion prisms, diffraction gratings and interference-polarisation filters are used as the dispersion elements, characterised by not too high frequency selectivity for the separation of individual modes. However, because of a wide dispersion range, these elements are used in the lasers with a wide gain band of the active medium. In the laser on Nd in glass with passive *Q*-modulation and the prism dispersion resonator, the radiation wavelength of the giant pulse is modified in the range 5.6 nm, with the spectrum 0.1 nm wide [1].

When using the complex dispersion resonator, consisting of a holographic diffraction grating and a non-sprayed resonance reflector, it is possible to achieve single-frequency lasing of the giant pulse with the retuning of the radiation wavelength in the regime of passive *Q*-modulation in the ruby lasers [3], in the Nd:YAG lasers [4], and in lasers on Nd glass [5]. The retuning of the radiation wavelength is carried out by the smooth change of the total thickness of the crystal wedges, and its range in the laser on the Nd glass is 13.4 nm, and the spectral width 4.5 pm [5].

2. The higher efficiency of the selection of longitudinal modes in the lasers with passive *Q*-modulation is obtained when using a resonance reflector, consisting of two or more plane-parallel sheets, separated by air gaps. Using the resonance reflector as the output mirror the resonator, it is quite easy to achieve single-frequency lasing in a ruby laser [6,7] and in the vicinity of the threshold in a Nd glass laser [8,9]. The retuning of the radiation wavelength of the giant pulse is carried out by changing the pressure of the air gap. However, the resonance reflector without mirror coatings is characterised by reduced selectivity and does not make it possible to obtain single-frequency lasing in lasers with active *Q*-modulation even in the vicinity of the threshold.

3. The duration of the linear development of the giant pulse can be artificially increased in lasers with active *Q*-modulation as a result of slow [10, 11] or two-stage [12,13] application of the *Q*-factor. In this case, as in the regime with passive *Q*-modulation, single-frequency lasing of the giant pulse is achieved in the conditions of slight discrimination of the longitudinal waves in the ruby laser [11,12] and in the Nd laser on potassium tungstate [30]. However, with slow activation of the *Q*-factor of the resonator, intra-resonator losses rapidly increase and the power of the giant pulse decreases. In addition, with slow activation of the *Q*-factor, it is necessary to work only the vicinity of the threshold, otherwise lasing will involve several pulses with different spectral char-

acteristics, and this also restricts the power of the giant pulse. These restrictions are eliminated when activating the *Q*-factor of the resonator in two stages. In the first stage of activation of the *Q*-factor, the gate is partially opened and a weak single-frequency radiation pulse forms during the period of linear development. At the moment corresponding to the maximum volume of the pulse intensity, the second voltage pulse is supplied to the gate and completely opens the latter, and a single-frequency giant pulse is irradiated without any loss of power.

4. Lasers with the electro-optical *Q*-modulation of the resonator are used when accurate synchronization of the time of appearance of the giant pulse with the examined process is required. The most efficient method of ensuring single-frequency lasing in these lasers is the method of injection of the external signal [14]. After activating the *Q*-factor, single-frequency radiation from a low-power master laser is injected into the resonator of the high-power laser. Since the duration of linear development of the giant pulse is inversely proportional to the logarithm of radiation intensity in the laser resonator, the radiation in the giant pulse will not form from the spontaneous noise with a wide spectrum but it will form from external single-frequency radiation whose intensity is an order of magnitude higher than that of spontaneous noise. In the case of capture of the wavelength, the spectrum of the giant pulse is identical to that of the external signal. The absence of selecting elements in the resonator of the high-power laser makes it possible to generate high power of the giant pulse of radiation in the single-frequency regime. The gain factor of a weak monochromatic signal may reach $\sim 10^{10}$. The method of injection of the external signal was used in ruby lasers with electro-optical *Q*-modulation [15] and in Nd glass lasers [16–18]. In addition to solid-state lasers, the method of injection of the external signal is used widely in liquid [19, 20] and gas [21, 22] lasers.

The lasing of Cr and Nd lasers in the regime with active and passive *Q*-modulation was examined by the authors of this book in Ref. 33–38,51,53.

3.2 POWERFUL SINGLE-FREQUENCY TUNABLE RUBY LASER WITH INJECTION OF THE EXTERNAL SIGNAL

The method of injection of the external signal was examined in detail by the authors of the book in a ruby laser with electro-optical *Q*-modulation of the resonator in [23–28, 34–38]. In a three-mirror variant of the injection system of the external signal, the output mirror of the master laser was represented by a dense mirror of a high-power laser (Fig. 3.1). The master laser was represented by a single-frequency ruby laser in the quasistationary regime with the parameters shown in Fig. 1.8. In this case, there was no need for additional synchronization of the operation of the two lasers,

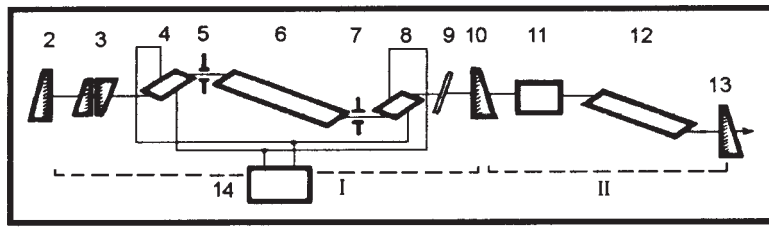

Fig.3.1 Diagram of a three-mirror single-frequency ruby laser with electro-optical modulation of the *Q*-factor: I – single-frequency master quasi-continuous laser (Fig. 1.1); II – powerful laser: 10, 13 – mirrors (T_{10} = 0.02 T_{10} = 0.02 T_{13} = 0.7); 11) electro-optical gate; 12) ruby.

in addition to the simultaneous activation of pumping lamps. The electro-optical gate of the master laser was opened when the maximum inversion was reached 0.3–0.5 ms after the start of lasing of the master laser.

At the edge of the retuning range, the width of the radiation spectrum of the master laser in the absence of capture of the radiation wavelength of the master laser was 15 pm (Fig. 3.2a). In the spectral range 180 pm wide the wavelength of external single-frequency radiation was captured, and the lasing spectrum of the giant pulse completely coincided with the spectrum of the external signal (Fig. 3.2b). However, in this case, the powerful laser generated a split radiation pulse (Fig. 3.2c). This is associated with a decrease of the reflection factor of the general mirror 10 (Fig. 3.1) as a result of the increase of the energy stored in the resonator of the master laser in the process of increase of the intensity of the giant pulse. This increases the losses and the self-excitation threshold in the powerful laser. The power of the giant radiation pulse of the executive laser on a level of approximately 1 MW in this circuit was restricted by the failure of the mirror coatings of the Fabry–Perot selector-etalon in the master laser.

The power of the giant radiation pulse was increased as a result of the application of a four-mirror system for the injection of the external signal (Fig. 3.3). The master laser 1 remained unchanged, and the resonator of the powerful laser was formed by one of the ends of the ruby rod 5 and by the dense mirror 8. The lasers were separated by the electro-optical gate, consisting of two Archard–Taylor prisms 2 a 4 and the Pockels cell 3 which was activated for the passage of radiation of the master laser for a period of approximately 50 ns several nanoseconds prior to opening the electro-optical gate of the powerful laser. The radiation of the giant pulse with a power of ≥ 10 MW was transferred through the side face of the polarisation prism 2 which was often damaged at very high powers of the giant pulse.

To eliminate this shortcoming, investigations were carried out into

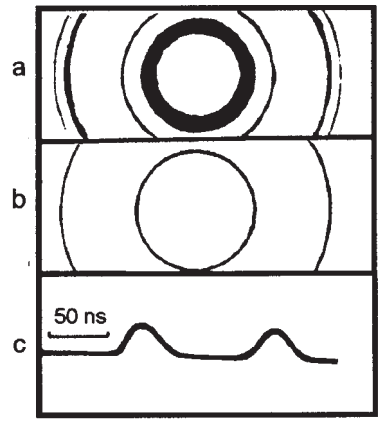

Fig.3.2 Interferograms of the lasing spectra of the master and high-power lasers in the absence (a) and in capture (b) of the radiation wavelength of the external signal, the range of dispersion of the interferometer is 0.4 nm (a) and 8 pm (b); c) oscillogram of the intensity of radiation of the giant pulse in capture of the wavelength of the external signal.

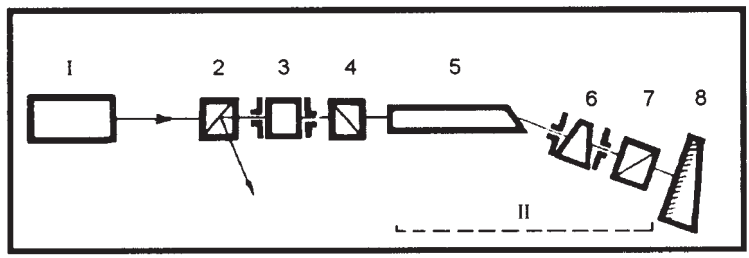

Fig.3.3 Diagram of a four-mirror powerful laser with electro-optical modulation of the *Q*-factor: I – master single-frequency quasi-continuous laser; II – powerful laser with electrical modulation of the *Q*-factor: 2–4) electro-optical decoupling of the lasers; 5) ruby; 6,7) electro-optical gate; 6) Pockels cell; 7) polarisation prisms.

the circuit of injection of the external signal with a ring-shaped resonator of a powerful laser (Fig. 3.4). In this circuit, the effect of the giant radiation pulse on the master laser was eliminated without using electro-optical decoupling owing to the fact that the capture of radiation of the external signal took place not only with respect to the spectrum but also direction. This greatly simplified the experimental system. In the ring-shaped laser, the input and output of radiation was ensured through the prism 4 with a disrupted total internal reflection. The length of the resonator of the ring-shaped laser was 1.5 m, and the longitudinal modes were separated by a diaphragm with a diameter of 1.7 mm. The *Q*-modulation of the resonator was carried out by the electro-optical gate (9) which

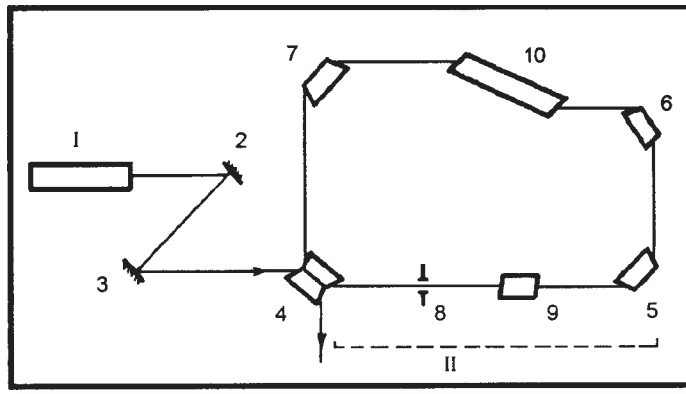

Fig.3.4 Diagram of a powerful single-frequency ruby laser with a ring resonator: I – master single-frequency quasi-continuous laser; II – powerful laser with electro-optical modulation of the Q-factor: 4–7) rotating prisms of the resonator; 9) electro-optical gate consisting of the Pockels cell and polarisation trace; 10) ruby.

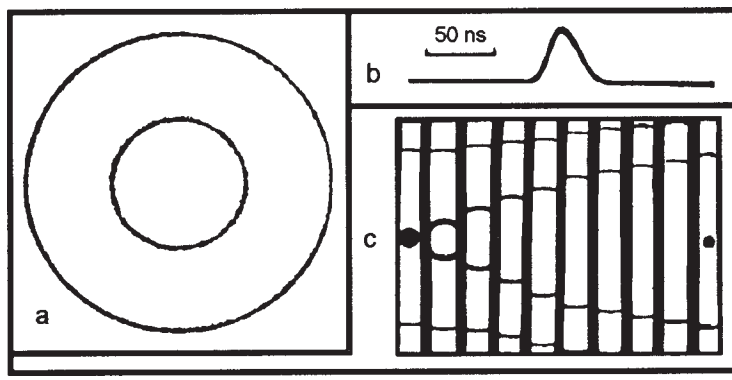

Fig.3.5 Parameters of lasing of a powerful single-frequency ruby laser with electro-optical modulation of the *Q*-factor of the resonator: a) interferrogram of the radiation spectrum of the giant pulse, the range of dispersion of the interferometer 1.6 pm; b) oscillogram of radiation intensity; c) sequence of interferograms of the radiation spectrum of the giant pulse, illustrating the range of rearrangement of the radiation wavelength, region of dispersion of the interferometer 240 pm.

consisted of a Pockels cell on a DKDP crystal with ends under the Brewster angle and of a polarisation trace.

In these experiments, the giant radiation pulse was generated on a single longitudinal mode (Fig. 3.5a) with a power of 50 MW and with smooth retuning of the radiation wavelength in the range 250 pm (Fig. 3.5c).

The application of a more powerful single-frequency, quasi-continuous master laser with spherical mirrors in the regime of inertia of the spectrum with the parameters, shown in Fig. 1.16, greatly simplified the circuit

of experimental equipment. In this case, experiments were carried out with a linear four-mirror variant of the injection circuit without electro-optical decoupling between the lasers. The higher radiation intensity of the master laser made it possible to inject its radiation into the resonator of the powerful laser through its dense mirror. In this case, the reverse effect of the giant pulse on the master laser was very small. The spherical front of the master laser was matched with the flat front of the powerful laser using a telescope. When using, in the powerful laser, a ruby crystal with sapphire tips with a length of 240/320 mm and a diameter of 40 mm, the single-frequency lasing of the giant pulse with a power of 200 MW was recorded. The retuning of the radiation wavelength was carried out by misaligning one of the mirrors of the master laser, and its range was 1.20 pm.

For the ruby laser, the experimentally measured minimum value of the intensity of the external signal resulting in the stable capture of its radiation wavelength in the centre of the gain line, was approximately 0.1 W/cm^2.

3.3 POWERFUL SINGLE-FREQUENCY TUNABLE Nd-DOPED LASERS WITH INJECTION OF THE EXTERNAL SIGNAL

The method of injection of the external signal in Nd lasers with electro-optical modulation of the *Q*-factor was investigated by the authors of this work in Ref. 28, 34–38. In the Nd lasers, the injection circuits for the external signal included relatively powerful single-frequency master lasers whose radiation was injected into the resonator of the powerful laser through a dense resonator mirror. In this case, it is not necessary to carry out optical decoupling of the lasers. To develop a powerful single-frequency Nd:YAG laser, the circuit for injection of the external signal included a master Nd:YAG laser in the regime of the single-frequency quasistationary lasing of the TEM_{mnq} modes, whose parameters are shown in Fig. 2.7. Using a garnet crystal 100 mm long and 6 mm in diameter in a powerful laser it is possible to obtain (in the regime of capture of the radiation wavelength of the external signal) single-frequency lasing of the giant pulse of the Nd:YAG laser with a power of 40 MW with retuning of the radiation wavelength in the range 0.35 nm.

In order to increase the width of the range of retuning of the radiation wavelength in the vicinity of 1.06 μm, tests are carried out with the circuit of injection of the external signal with a Nd laser in phosphate glass GLS-22 (Fig. 3.6). The master laser was represented by a single-frequency quasistationary laser on Nd in glass with the lasing parameters shown in Fig. 2.3. The increase of the energy of quasistationary lasing of the TEM_{ooq} modes in the master laser was achieved by increasing

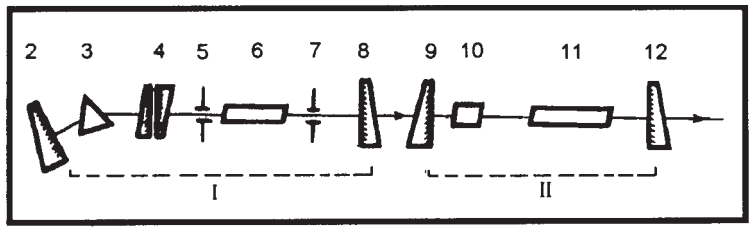

Fig.3.6 Diagram of a powerful single-frequency adjustable tuneable neodymium laser in glass with electronic modulation of the *Q*-factor: I – master single-frequency quasi-continuous neodymium laser in glass; II – powerful laser: 10) electro-optical gate; 11) neodymium rod GLS-22 diameter 15 mm, length 302 mm.

the length of the Nd rod to 300 mm and the diameter of the diaphragm to 3 mm, with the resonator length being increased at 230 cm. Consequently, the energy of single-frequency lasing of the master laser on glass was increased to 0.5 J.

In the region of capture of the radiation wavelength of the external signal, the radiation spectrum of the giant pulse was almost completely identical with the radiation spectrum of the external signal (Fig. 3.7a). The absence of 'beating' of the intensity of radiation of the giant pulse (Fig. 3.7b) shows that lasing in this case takes place on a single longitudinal mode. The power of the giant radiation pulse was 180 MW, the width of the range of retuning of the radiation wavelength was 5.6 nm (Fig. 3.7c).

The experimental measured intensity of the radiation of the external signal, required for stable capture of its radiation wavelength by the giant pulse of the Nd laser, was approximately 0.5 W/cm^2. With increase of the pumping energy, the width of the band of capture of the radiation wavelength slowly increased. The rapid increase of the radiation intensity of the external signal did not result in any significant broadening of the capture band of its length.

Evaluation of the band of capture of the frequency of radiation of the external signal ($\omega_s - \omega_0$) by the giant pulse was carried out assuming that the inverse population in the active medium during the period of linear development of the giant pulse ($t_d \sim 10^{-7}$ s) remained almost unchanged ($\partial n(\omega,t)/\partial t = 0$). Consequently, the spectral density of radiation $I(\omega, t)$ is governed by the equation

$$\frac{dI(\omega, t)}{dt} = \left[\sigma n(\omega) - \tau_p^{-1}\right] I(\omega, t) + S(\omega) + \tau_p^{-1} U(\omega_s). \qquad (3.1)$$

Here σ is the cross-section of induced transition; τ_p is the lifetime of

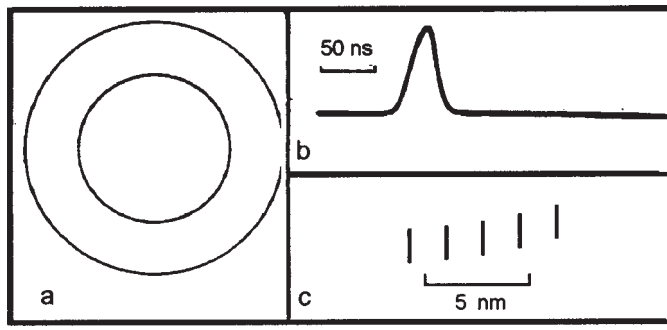

Fig.3.7 Parameters of lasing of a powerful single-frequency neodymium laser in glass with electro-optical modulation of the *Q*-factor of the resonator: a) interferogram of the radiation spectrum of the giant pulse, the rate of dispersion of the interferometer 8 pm; b) oscillogram of radiation intensity; c) sequence of spectrograms of radiation of the giant pulse, illustrating the tuning range of the radiation wavelength.

the photon in the resonator; $S(\omega)$ is the intensity of spontaneous radiation; $U(\omega_s)$ is the intensity of the external signal; $n(\omega)$ is the inverse population. Since the circuit of the non-uniformly broadened line has the Gaussian shape with the width Γ, we have the following equation for the inverse population and the intensity of spontaneous noise:

$$n(\omega, t) = n_0 \exp\left[-\left(\frac{\omega-\omega_0}{\Gamma}\right)^2\right],$$
$$S(\omega) = S_0 \exp\left[-\left(\frac{\omega-\omega_0}{\Gamma}\right)^2\right]. \qquad (3.2)$$

Assuming that $I(\omega, 0) = 0$, we obtain the solution of the equation (3.1) in the form:

$$I(\omega,t) = \frac{\left\{(\omega_s) + S_0\tau_p \exp\left[-\left(\frac{\omega-\omega_0}{\Gamma}\right)^2\right]\right\}}{\sigma n_0 \tau_p \exp\left[-\left(\frac{\omega-\omega_0}{\Gamma}\right)^2\right] - 1} \exp\left[\kappa(\omega)t - 1\right], \qquad (3.3)$$

where $\kappa(\omega) = \sigma n_0 \exp\left[-\left(\frac{\omega-\omega_0}{\Gamma}\right)^2\right] - \tau_p^{-1}$ is the gain factor. As regards the order of magnitude, for t_d we have:

$$t_d = \frac{1}{\kappa(\omega)} \ln\left[\kappa(\omega)\tau_p I_d / (U + S\tau_p) + 1\right], \tag{3.4}$$

where I_d is the spectral density of radiation at the end of the linear stage of development of the giant pulse.

The criterion of capture of the wavelength of external radiation may be the condition:

$$|\omega_s - \omega_0| < \Gamma\left[\ln\left(\frac{\sigma n_0 \tau_p}{1 + Q\tau_p t_d^{-1}}\right)\right]^{1/2}, \tag{3.5}$$

where

$$Q = \ln\left[1 + \frac{10S\kappa\tau_p}{U + S\tau_p}\right].$$

Equation (2.5) shows that the band of capture of the radiation wavelength of the external signal slowly increases with increasing intensity of the external signal $U(\omega_s)$. At same time, the duration of linear development of the giant pulse slowly decreases with increasing intensity of the external signal.

3.4 SINGLE-FREQUENCY TUNABLE Nd LASERS WITH PASSIVE Q-MODULATION

The energy and spectral characteristics of radiation of Nd lasers in crystals YAG, BLN, Cr:GSGG and LNA with passive *Q*-modulation with gates based on lithium fluoride crystals with F_2^- dye centres have been examined in detail by the authors of this book in Ref. 29–38.

Because of their simple and easy operation, phototropic gates are used widely for the passive modulation of the resonators of solid-state lasers. However, passive gates on dyes have high losses and are not stable. The crystals with the dye centres in strontium fluoride were used for

the first time for passive *Q*-modulation in a ruby laser [39], but because of low thermal and beam instability of the dye centres they were not efficient and have not been used widely. Only after developing F_2^- dye centres stable at room temperature in the crystals of lithium fluoride (F_2^-:LiF) [40] were they used as non-linear filters [49] and passive laser gates [42]. The availability of the crystals of lithium fluoride, the simple procedure used for radiation-induced colouring using γ–radiation ^{60}Co, high heat conductivity and beam strength have stimulated the extensive use of these crystals as phototropic gates for the production of giant radiation pulses in Nd lasers.

The absorption cross-section of the phototropic F_2^-:LiF gate at a wavelength of 106 nm is 1.7×10^{-17} cm^{-2}, the relaxation time is 90 ns [43]. The heat conductivity coefficient is 0.1 W/cm K and the thermal strains do not exceed several per cent of the strains in the Nd:YAG crystals [44]. The measured absorption factor at the concentration of the active centres of 2×10^{16} cm^{-3}, taking Frenel reflection into account, is 0.41 cm^{-1} [45]. The threshold of failure of the individual crystals is approximately 2 GW/cm^2 at a pulse time of 20 ns [45], but in the majority of crystals the thresholds of failure are usually 4–5 times lower. Consequently, it is necessary to select crystals on the basis of this parameter. In addition, the large scatter of the impurity composition of the initial crystals of lithium fluoride makes it more difficult to obtain reproducible results.

The high heat conductivity of the F_2^-:LiF crystals makes it possible to obtain stable energy characteristics of the emission of giant pulses of Nd lasers at a repetition frequency of up to 100 Hz [46]. When using the F_2^-:LiF gates, the linear polarisation of the giant pulses may be achieved in the absence of a polariser in the laser resonator [43]. A review of the earlier studies into the passive laser gates with dye centres was published in [47].

3.4.1 Energy and spectral characteristics of radiation

The maximum energy of lasing of the giant pulses of laser radiation was obtained when optimising the transmission factors of the output mirror T_2 (Fig. 3.8a) and the passive filter T_{pf} (Fig. 3.8a). The radiation energy in this case was measured for a single giant pulse up to the appearance of a second pulse whose lasing threshold was approximately 1.2 of the lasing threshold of the single pulse. Increasing pumping energy increased the number of giant pulses and the radiation energy increased in proportion to the radiation energy of the single pulse. At a high pumping energy, the total energy of the giant radiation pulses was of the order of the free lasing energy.

The dependences of the radiation energy of the giant pulses of the

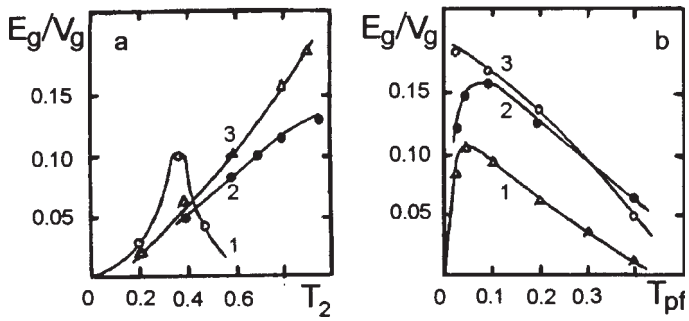

Fig. 3.8 Dependence of the density of lasing energy E_g/V_g (J/cm^3) on the coefficients of transmission on the output mirror of resonator T_2 (a) and transmission of the passive filter T_{pf} (b) at a constant pumping energy $E_p = 12E_t$ of giant radiation pulses for lasers: Nd:YAG (1), Nd:BLN (2) and Nd:Cr:GSGG (3). L = 40 cm. Generated volumes of active media V_g = 1.24 (YAG), 0.56 (BLN) and 0.5 cm^3 (Cr:GSGG).

transmission factors of the output mirror of the resonator and the passive filter had maxima. An exception was a Nd:Cr:GSGG laser in which maxima of this type were not detected even at the maximum possible experimental values of the coefficients T_2 = 0.96 and T_{pf} = 0.04. Because of the very low values of the lasing energy of radiation, the graphs do not give the energy dependences for the Nd:LNA lasers. At the optimum parameters of the resonator and the passive filter, the specific powers (P_g/V_g) of the giant radiation pulses in the lasers were: 80 (Nd:Cr:GSGG), 16 (Nd:BLN), 11 (Nd:YAG) and 0.5 MW/cm^3 (Nd:LNA).

With increase of the length of the flat resonator, the radiation energy of the giant pulses increased linearly (Fig. 3.9). In the entire range of the variation of the wavelength of the resonator, the duration of the giant pulses, with a smooth symmetric shape, varied from 10 to 15 ns (Fig. 3.10a). When there was no selection of longitudinal modes, several longitudinal modes were included in lasing.

When the output mirror of the resonator was represented by a resonance reflector consisting of two sapphire substrates, stable single-frequency lasing of the giant pulses of radiation (Fig. 3.30b) was obtained in all media. In a complex dispersion resonator single-frequency lasing of giant pulses (Fig. 3.10b) with smooth retuning of the radiation wavelength was observed in the ranges: 0.2 (Nd:YAG), 0.3 (Nd:GSGG), 0.4 (Nd:BLN) and 0.5 nm (Nd:LNA).

3.5 SINGLE-FREQUENCY TUNABLE ALEXANDRITE LASER WITH PASSIVE Q-MODULATION

In alexandrite lasers, giant radiation pulses were produced in the regimes of active [48,49] and passive *Q*-modulation of the resonator [50–53].

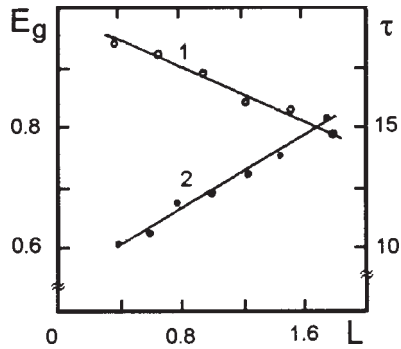

Fig. 3.9 Dependence of the relative radiation energy E_g (1) of the giant pulse on its duration τ (ns) (2) for neodymium lasers on resonator length L (m). $E_p = 1.2E_t$.

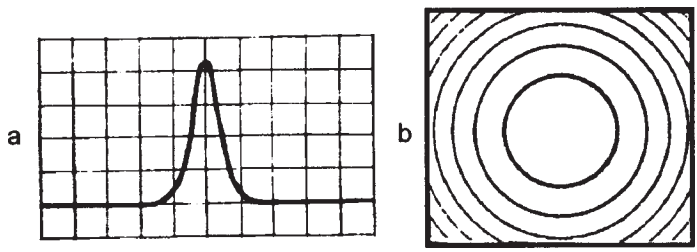

Fig. 3.10 Parameters of the lasing of powerful single frequency neodymium lasers with passive modulation of the *Q*-factor of the resonator by a gate on LiF:F_2^- crystal: a) oscillogram of the radiation intensity of the giant pulse, scale 20 ns/division; b) interferogram of the lasing spectrum, the range of dispersion of the interferometer 20 pm.

In the active *Q*-modulation regime, the efficiency of the selection of the longitudinal modes rapidly decreases and it is not possible to obtaine single-frequency lasing under the normal conditions. In Ref. 50, the passive *Q*-modulation of the resonator was carried out using a gate on Cr^{4+}:Y_2SiO_2 crystal whose maximum of the absorption bands coincides with the maximum of gain of the alexandrite crystals. In the regime of the giant pulse with a duration of 70 ns, an energy of 20 mJ was obtained. Without the selection of the longitudinal modes of the flat resonator with a length of 30 cm, the width of the lasing spectrum of the laser on alexandrite in the *Q*-modulation regime was 2 nm.

For the passive duration of the resonator of the alexandrite laser, the authors of Ref. 51 used a gate based on the crystal lithium fluoride with thermally transformed F_3^- dye centres (LiF:F_3^-). Narrow-band lasing with the spectrum 10 nm wide was obtained, the pulse time was 100 ns, retuning of the wavelength of lasing took place in the range 710–780 nm. The selection of the longitudinal modes and the retuning of the radiation wavelength in the laser with flat mirrors were carried

out using dispersion prisms and a Fabry–Perot selector-etalon. In Ref. 52, similar passive gates were used to produce giant radiation pulses in an alexandrite laser with a duration of 800 ns, energy 1.5 mJ, the width of the lasing spectrum 5×10^{-3} cm^{-1} . The selection of the modes in the laser with a hemispherical resonator was carried out in self-injection conditions using an additional passive resonator containing a diffraction grating and a Fabry–Perot etalon.

The F_3^- dye centres in the LiF crystals were generated at high doses of γ–radiation ^{60}Co (2×10^8 R) without special cooling. At room temperature, they have two wide absorption bands with maxima at 710 and 800 nm. The effect of powerful optical radiation on the short-wave absorption bands causes failure of the F_3^- dye centres. They remain stable when the wavelength of laser radiation coincides with their long-wave absorption band. The low thermal stability of the F_3^- centres complicates their use as modulators of the *Q*-factor of laser resonators.

In thermal annealing lithium fluoride crystals with F_3^- centres at a temperature 425 K new, thermally transformed (TT) F_3^- centres appear with a wide absorption band with the maximum at a wavelength of 780 nm and a different vibron structure [54] in comparison with the conventional F_3^- centres in cooling. The temperature of failure of the TT F_3^- centres is 100 degrees higher than the temperature of thermal transformation of the F_3^- centres (425 K), indicating the high thermal stability of the TT F_3^- centres. The contrast between the optical density in the initial and clarified conditions in the case of the TT F_3^- centres was almost an order of magnitude. Relatively high values of the concentration of TT F_3^- centres in the LiF crystal and the transverse the cross-section of absorption result in a high absorption factor of ~2.5 cm^{-1}. Consequently, it is possible to use passive gates because of their small thickness (3 ÷ 10 mm). The TT F_3^- centres are characterised by high photoresistance. In the radiation of a passive gate with the laser radiation with the power density of 100 MW/cm^2 at a wavelength of 800 nm, there were no significant changes in the concentration of the TT centres [54]. However, as in the case of conventional F_3^- centres, the TT centres failed under the effect of laser radiation of a ruby laser (λ = 694 nm), indicating the presence in the centres of a second absorption band in this spectral range, as in the case of th F_3^- centres.

3.5.1 Experimental equipment

The circuit of the alexandrite laser [53] is shown in Fig. 3.11. An alexandrite crystal (6) with a diameter of 5.5 and 85 mm long, with the ends cut under the Brewster angle, was used. The laser was pumped with a IFP–800 lamp, the pumping pulse time was 0.25 ms, the crystal temperature 70 °C; this temperature was maintained using a thermostat pumping

the solution of the KN-120 dye and cutting off the ultraviolet radiation of pumping below 300 nm. Part of this pumping radiation was converted by the dye into a rule absorption band of the alexandrite, increasing the efficiency of pumping [55].

The laser resonator was formed by flat dielectric mirrors: a non-transmitting mirror (2) (R = 99.5% at λ = 750 nm), and the output mirror (8) (T = 50%), sprayed on wedge-shaped substrates. The Q-modulation of the laser was carried out by the passive gate (3) of the lithium fluoride crystal with thermally transformed F_3^- centres. The longitudinal modes were separated by the diaphragm (7). The selection and smooth retuning of the lasing wavelength were carried out with an interference–polarisation filter (IPF) (4) with a thickness of 8 mm and a scanning Fabry–Perot interferometer (SFPI) (5), with a base of 3 mm, controlled in the automatic regime by the electronic unit (14).

The electronic unit (14) was controlled by a step motor, rotating the IPF around its axis with the accuracy to 1 angular minute, adjusted the mirror of the SFPI with respect to the angle using two piezoceramic columns with the accuracy to 1 angular second and maintained with the high accuracy with respect to time the base of the SFPI using a piezoceramic ring to which one of the mirrors of the interferometer of a He–Ne laser (1) and feedback circuits (9–13) were bonded. The parasitic selection of the longitudinal modes in the resonator was completely eliminated: all the optical elements in the resonator were slightly wedge-shaped, the elements (3,4) were positioned under the Brewster angle, and the optical axis of the SFPI (5) deviated from the axis of the resonator by

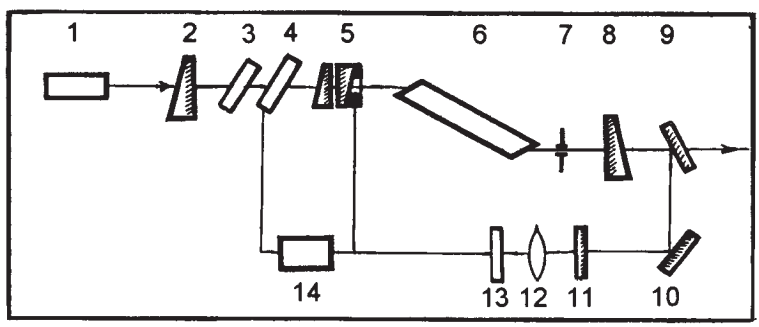

Fig. 3.11 Diagram of a single-frequency tuneable aleksandrite laser with passive modulation of the key factor: 1) He–Ne-laser; 2,8) the mirrors of the resonator, dense and output, respectively; 3) passive gate on LiF crystal with TT F_3^- dye centres; 4) interference–polarisation filter (IPF); 5) scanning Fabry–Perot interferometer (SFPI); 6) aleksandrite crystal, diameter 5.5 mm, length 80 mm; 7) diaphragm; 9,10) dense mirrors, λ = 6.33 nm; 11) interference filter, λ = 633 nm; 12) long focus lens; 13) photodiode with a crossed photocathode; 14) electronic unit of controlling SFPI and IPF.

an angle of the order of 1 degree.

The spectrum of the giant pulse of radiation was recorded with a Fabry–Perot interferometer with the dispersion range of 8 pm and with a photographic camera. The region of retuning of the lasing wavelength was controlled using a spectrograph. The time characteristics of the giant pulse were investigated using a coaxial photodiode and a high-speed oscilloscope.

3.5.2 Spectral–time and energy parameters of lasing

The lasing wavelength of the alexandrite laser and, consequently, the base of the SFPI were stabilised on the wavelength of the single-frequency He–Ne laser, whose radiation passed through the resonator of the laser, the SFPI and, using two mirrors (9,10), the interference pattern from the SFPI was projected with a long-focus lens (12) on the photodiode (13) with a cross-shaped photocathode. A small part of the arc of one of the interference rings was focused in the cross of the photocathode. Smooth retuning of the lasing wavelength within in the limits of the transmission band of the SFPI was carried out by supplying stabilised voltage to the piezoceramic ring of the SFPI from the electronic unit (14). The wide-band retuning of the lasing wavelength of the alexandrite laser (Fig. 3.12a) was carried out using the electronic unit (14) by synchronous rotation of the IPF by the step motor and the smooth change of the base of the SFPI when supplying high-stability voltage.

The single-frequency lasing of the alexandrite laser (Fig. 3.12c) was obtained as a result of numerical optimisation (in a computer) of the transmission band of the IPF and the region of dispersion of the SFPI taking into account the length of the laser resonator and the absorption band of the passive gate at a wavelength of 760 nm.

Laser radiation at this wavelength was used previously by the authors of this book [51] for the two-photon spectroscopy of the beam of helium atoms at the $2^3S \rightarrow 3^3D$ transition. Laser beam diagnostic makes it possible to take local measurements of the magnetic field and the spatial distribution of the field in high-temperature plasma utilising the Zeeman effect. The measurement accuracy is increased by eliminating the Doppler broadening of the spectral line of radiation of the beam atoms when using the method of two-photon spectroscopy [56].

The duration and energy of the giant pulse of the alexandrite laser depend greatly on the transmission factor of the passive gate and the resonator length. As shown previously (Fig. 1.33a) [55], at high pumping energy ($\geq$ 500 J) the increase of the length of the flat resonator of the alexandrite laser from 0.4 to 1.5 m decreases the lasing energy by a factor of 4 or more times with increasing pumping energy. Therefore, in the experiments, the length of the flat resonator was selected mini-

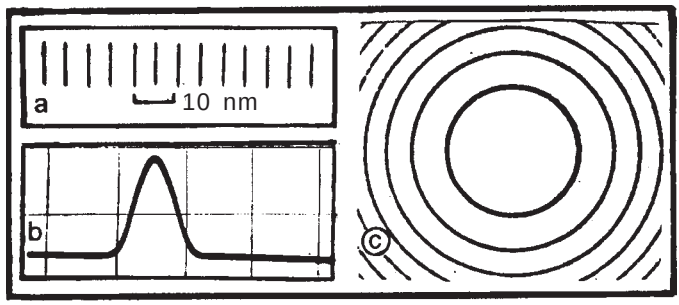

Fig. 3.12 Parameters of lasing of the single-frequency tunable alexandrite laser with passive modulation of the *Q*-factor of the resonator by the LiF:F_3^- crystal gate: a) sequence of spectrograms of the integration radiation spectrum, produced in STE-1 spectrograph, illustrating the tuning range of the lasing wavelength; b) oscillogram of the intensite of radiation of the giant radiation pulse, scale 150 ns/div; c) interferogram of the spectrum of the lasing pulse, the dispersion range of the Fabry–Perot interferometer 8 pm.

mum possible (0.5 m) so that it was possible to install all the necessary elements of the dispersion resonator.

In contrast to the case of F_2^- dye centres, used widely for the passive *Q*-modulation of the lasers on Nd ions (see previously), the passive gate on the F_3^- centres proved to be highly critical to the value of the transmission factor. The range of the transmission factors at which it was possible to generate a single giant pulse per pumping pulse was very narrow and this greatly complicated practical operation with these gates.

For every pumping level it is necessary to select very carefully the optimum transmission factor of the passive gate. For this purpose, it is necessary to have a relatively wide set of such passive gates or re-polish the existing passive gates. At a transmission factor of the passive gate of 65%, the duration of the giant pulse is of the order of 11 ns (Fig. 3.12b), the energy is 80 mJ.

Chapter 4

Lasing of stable supershort radiation pulses in solid-state lasers

The active synchronisation of longitudinal modes and the lasing of supershort radiation pulses were obtained for the first time in a helium–neon laser [1]. The passive synchronisation of the longitudinal modes was observed for the first time in a ruby laser [2] and in Nd-doped glass lasers [3,4]. In Ref. 55, the authors proposed a fluctuation model of the formation of supershort radiation pulses (SRP).

The model is based on the assumption that from a large number of fluctuation intensity transients, existing in the resonator at the start of the amplification process, as a result of the non-linear effect of the saturating absorber, the maximum transient is separated and amplified, and others are suppressed. The quantitative theory, describing the process of lasing of the laser with an antireflection filter, was developed in Ref. 6, in which it was shown that regular pulsations of radiation intensity can form in the laser with a saturating absorber without external regular effects. In Ref. 7 it was reported that in the Sixties the minimum duration of the SRP was reduced by an order of magnitude every two years, whereas in the Seventies, seven years was already required for reducing the duration of the SRP by an order of magnitude. The approximate duration of the light pulses to the fundamental limit in a single light period can be expected when using the lasers on active media with very wide gain lines.

The supershort radiation pulses are used widely in various areas of science and technology: non-linear optics, the development of superstrong fields, examination of high-rate processes, optical information processing, communications, location, etc. [8, 9]. At present, extensive investigations are being carried out into various types of SRP generators, directed to: 1) improvement of the energy characteristics and peak power of the generated light pulses; 2) retention of their duration; 3) increase of the reproducibility of the parameters of the produced pulses; 4) lasing of

SRP in a wide spectrum range; 5) improvement of the quality of pulses (absence of the time structure, photon emission and phase modulation); 6) operation with the repetition frequency of pulses in a wider frequency range; 7) improvement of the reliability and ease of operation of the SRP generators.

In comparison with other types of generators, the solid-state lasers have a number of important special features and advantages. They have good energy characteristics, wide gain bands, required for the formation of the SRP of picosecond and femtosecond duration, they are compact, reliable and easy to operate. In the solid-state lasers, it is possible to greatly amplify the produced SRP in the giant pulse regime. On the whole, the solid-state lasers represent a suitable basis for the development of advanced SRP generators. The examination of the lasing dynamics of solid-state lasers in the regime of passive synchronisation of the modes has been recently the subject of a large number of investigations (for example, [11–17]). A significant shortcoming of the solid-state lasers is the instability of the regime of passive synchronisation of the modes in which the shortest duration of the produced light pulses is obtained. The resultant instability is linked basically with the self-modulation of the *Q*-factor of the resonator, caused by the illumination of the saturating absorber.

The positive feedback, determined by clearing up, in addition to the formation of the SRP, leads to an avalanche-like increase of the intensity, averaged for the axial period of intensity, with the duration of approximately 10–100 ns. This results in the formation of a giant pulse and lasing is interrupted until the completion of the process of formation of the SRP. The duration and shape of the SRP depend greatly on the initial lasing conditions and can not be reproduced. The process of separation of the single pulse from the initial fluctuation field of the laser with a saturating absorber has been examined in Ref. 5.

In dye lasers, the instability of this type does not form because the positive feedback, determined by the illumination of the saturating absorber, is compensated by a negative feedback formed as a result of the saturation of the gain of the active medium. The negative feedback in this case operates efficiently because of the large cross-section of the working transition of the dyes.

The solid-state lasers have high energy characteristics of the generated pulses. The long lifetime of the inverse population of the upper working level of the solid-state active media and the possibility of operation in the giant pulse regime make it possible to enhance the formation of the SRP by a simpler method in comparison with that used in other types of lasers. The energy of the SRP of the solid-state lasers reaches the value of the order of a milliJoule, whereas in the dye lasers this energy

is slightly higher than nanoJoule. This is explained by the fact that the intensity of saturation of the gain of the active media of the solid-state lasers is three orders of magnitude higher than the intensity of saturation of the dye lasers. Consequently, the mechanism of synchronisation of the modes of the solid-state lasers greatly differs from the mechanism of the dye lasers.

In the solid-state lasers, the active medium has only a slightly effect on the formation of the SRP and the mechanism of compression of the produced pulse is completely determined by the saturating absorber. Consequently, the method of synchronisation of pumping, which is highly effective in the dye lasers, does not operate in the solid-state lasers.

4.1 METHODS OF PRODUCTION OF STABLE SUPERSHORT RADIATION PULSES

In most cases, the supershort radiation pulses in solid-state lasers are generated by the passive and active synchronisation of the modes and by the combination of these methods. The method of active synchronisation of the longitudinal modes of the laser is characterised by high reproducibility of the SRP but it is very difficult to obtain the duration of generated light pulses shorter than 50 picosecond because of the high inertia of the currently available modulators [18]. These lasers with stable SRP parameters are used widely for the pumping of dye lasers in order to produce the SRP of the femtosecond range of duration in the synchronous pumping regime.

In passive synchronisation of the modes, the compression of the produced pulse is carried out mainly as a result of undercutting of its leading and near edges during passage through the saturating absorber. The typical values of the relaxation time of the saturating absorbers are 10–50 picoseconds, so that the duration of the supershort pulses does not exceed several picoseconds.

Recently, work has been carried out with the passive synchronisation of the longitudinal modes with almost inertialess gates based on the Kerr effect [17] and the intra-resonator conversion to second harmonics [19, 20]. In this case, the duration of the generated light pulses is determined mainly by the width of the band of the amplifier of the active medium which in laser media such as alexandrite or sapphire with titanium is comparable or greater than the width of the band of the gain of the dye lasers. The removal of the non-reproducibility of the SRP of the light, associated with the fluctuation of the formation of pulses during the passive synchronisation of the modes in solid-state lasers, makes it possible to develop reliable and technologically efficient high-power sources of light picosecond and femtosecond pulses.

To improve the reproducibility of the SRP of the solid-state lasers and decrease their duration, a number of methods have been proposed:

1. The decrease of the number of generated modes [21];
2. Injection of an external signal [27];
3. The regime of the second threshold [22,23];
4. Self-stabilisation regime [24];
5. Introduction of additional losses [26].

The lasing of stable supershort radiation pulses in lasers on the ions of Cr and Nd has been examined by the authors of this book in Ref. 27–30.

4.1.1 The method of decreasing the number of lasing modes

The probability of the appearance of a transient whose intensity is considerably higher than that of other transients, is inversely proportional to the number and, consequently, the width of the lasing spectrum. The increase of the probability of realisation of the regime of the single pulse in the axial period is achieved by decreasing the number of lasing modes [21]. For this purpose, it is necessary to place a selecting element in the resonator of the laser with passive synchronisation of the modes. This element stabilizes and extends the length of the lasing pulses. In Ref. 21, it was proposed to 'thin out' the lasing spectrum. The width of the lasing spectrum and, consequently, the pulse time remained unchanged. In addition, the 'thinning out' of the lasing spectrum decreases the repetition period of the SRP.

4.1.2 The method of injection of the external signal

The authors of Ref. 27 proposed a method of injection of a short highly coherent light pulse into the laser resonator with the passive synchronisation of the modes in the initial moment of the linear development of lasing. This makes it possible to eliminate the effect of fluctuations of the intensity of initial noise emission. The power of the injected pulse is considerably higher than the level of the spontaneous radiation noise in the laser resonator. In this case, together with 100 percent realisation of the single pulse in the axial period, the reproducibility of the form of the SRP is improved.

4.1.3 The method of the regime of the second threshold

When the saturation of the absorber and the amplifier takes place simultaneously, the regime of the so-called second threshold is realised. In this case, if the noise field does not contain transients greatly higher than other transients, the small difference in their intensity causes that the pulses with lower intensity appear with higher probability below the gain threshold [22, 23]. Therefore, in order to ensure more efficient

synchronisation of the modes, it is necessary to operate in the vicinity of the lasing threshold. For example, to apply this approach in an Nd laser, it is necessary to ensure that the gain is approximately 0.03 higher than the threshold. This imposes very stringent requirements on the stability of the pumping source of the laser and the resonator parameters.

4.1.4 The method of the self-stabilisation regime

The reproducibility of the SRP in lasers with passive synchronisation of the longitudinal modes greatly increases in the self-stabilisation regime [24]. The expansion of the light beam in the saturating absorber using the intra-resonator telescope decreases the efficiency of the positive feedback, caused by clarification of the absorber. Thus, the mechanism of 'swinging' of inversion–field self-oscillations weakens. Free lasing starts to develop at the start of the transition process.

At the start of lasing, the spectrum of intra-resonator radiation is relatively wide and the number of transients with the intensity considerably higher than the general noise level is not large. The probability of appearance of a high-intensity transient increases with lasing when due to the dispersion of the gain line and the effect of the spatial heterogeneity of the inversion, formed in the field of the standing waves, the width of the spectrum decreases.

The dependence of the probability of appearance of a single pulse in the axial period on the width of the spectrum was confirmed by experiments. If no transient was detected in the noise initial field club with the intensity of the transient considerably higher than the general level, the peak of free lasing was observed. In the following peak of the same lasing transient, the process is repeated until an intensive noise transient forms in some of the peaks and is capable of causing saturation of the absorber and does not lead to the display of the sequence of the single light pulses in the axial period, with the envelope in the form of a giant pulse.

Thus, the increase of the reproducibility of lasing with single SRP in the axial period is obtained as a result of increasing the number of different realisations of the initial conditions of passive synchronisation of the modes and different peaks of the single laser pulse. Without taking special measures in the solid-state lasers during passive synchronisation of the modes in the regime of the giant pulse, the absorber is initially saturated and this is followed by saturation of the amplifier. On the other hand, in the self-stabilisation regime, the amplifier is the first to be saturated and this is followed by the absorber.

The problem of effective realisation of the method of self-stabilisation is manifested in the accurate correspondence of the levels of the density of intensity in the active medium and the saturating absorber, and

also the stabilisation of the pumping power and losses in the resonator.

4.1.5 The method of introducing additional losses

The passive synchronisation of the modes in solid-state lasers takes place in the regime of the giant pulse. Because of the short duration of the effective interaction of radiation with the saturating absorber, the process of the formation of the SRP from the initial noise field appears to be incomplete. To increase the duration of interaction of the field in the non-linear medium, it has been proposed to add additional losses to the laser resonator at the moment of lasing when the saturating absorber is being clarified. Consequently, it is possible to maintain the intensity of intra-resonator radiation on a constant level during the given period of time [26].

The SRP can also be stabilised by suppressing instabilities characteristic of solid-state lasers. Consequently, the passive synchronisation of the modes of the solid-state lasers becomes identical with the passive synchronisation of the modes of dye lasers. In this case, after the transition period, the lasing of a single stable stationary pulse on the axial period is set in the laser. The parameters of this pulse are determined by the properties of the laser system and are independent of the initial lasing conditions. This regime operates without changes up to the end of the pumping pulse.

As regards the reproducibility and duration of the resultant SRP, the solid-state lasers in this regime are similar to the dye lasers. To stabilise the passive synchronisation of the modes of solid-state lasers, it is initially necessary to suppress the instability associated with the oscillating of relaxation self-oscillations of intensity and inversion which in the case of sufficiently dense saturating absorbers is manifested as the clarification of the giant pulse. This type of instability is suppressed by the application of the electronic-optical negative feedback.

Another type of instability, formed at times of the order of 100 μs, is associated with the formation of a random transverse distribution of the generated radiation. In movement to the subpicosend range of duration, the instability associated with the phase modulation of the formed pulses starts to appear.

4.2 LASING OF STABLE SUPERSHORT PULSES OF RADIATION BY THE METHOD OF INJECTION OF THE EXTERNAL SIGNAL

In examination of the method of injection of the external signal in a ruby laser with a ring-shaped resonator (Fig. 3.4), we realised the regime of lasing of stable supershort radiation pulses [27–29] in cases in which the duration of the pulse of external radiation, injected into the resonator

of a powerful laser, was considerably shorter than the duration of passage through the resonator of the ring-shaped laser ($\tau_s \ll L/c$). The length of the resonator of the ring-shaped laser was 1.5 m, and longitudinal modes were separated by a diaphragm with a diameter of 1.7 mm.

The pulse of external radiation with a duration of approximately 1 ns was separated from the radiation of the single-frequency quasi-continuous master laser (Fig. 1.8d) using an electro-optical gate placed between the lasers. The external pulse was introduced into the resonator of the powerful laser after fulfilling the threshold conditions of lasing of the giant radiation pulse. To reduce the duration of the introduced pulse of external radiation, a passive gate was placed in the resonator of the powerful laser. The gate contained a solution of cryptocyanine in methyl alcohol with an initial transmittance of 40%.

Figure 4.1 shows the fragments of time evolution of the spatial distribution of the radiation intensity of the powerful laser with a passive gate with injection of the external pulse (a, b) and without injection (c, d). In the conditions of absence of the external pulse of radiation in passive synchronisation of the modes with the passive gate, in 10% of cases we observed the lasing of a single pulse in the axial period with a duration of the order of 300 ps, with strong background illumination (Fig. 4.1c). The width of the integral spectrum of radiation was 2 pm and the product of the duration of the supershort pulse τ_p by the width of the spectrum $\Delta\nu$ was $\tau_p \cdot \Delta\nu = 4.5$. In the majority of cases (~90%), lasing took place in the regime of several pulses on the period (Fig. 4.1d).

When an external radiation pulse with the duration $\tau_s \ll L/c$ was introduced into the resonator of the powerful laser, a single radiation pulse was detected in the period with a high contrast and 100% reproducibility (Fig. 4.1a, b). The width of the integral radiation spectrum was 2.9 pm and the relationship $\tau_p \cdot \Delta\nu = 1.8$ indicates the high coherence of supershort radiation pulses. The density graph of the time evolution

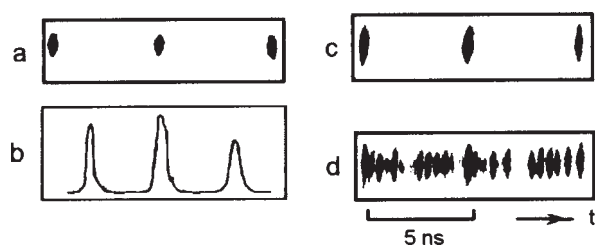

Fig. 4.1 Parameters of the lasing of a ruby laser with a ring resonator in the regime of passive synchronisation of modes in injection of the external signal with $\tau_s < L/c$ (a,b) and in its absence (c,d): a,cd) fragments of time evolution of the spatial distribution of radiation, obtained using a photochronograph; b) density pattern of the fragment of time evolution (a).

(Fig. 4.1b) shows that the duration of the SRP remained almost constant in lasing. This is caused by a large difference of the shape of the envelope of the introduced light pulse from the Gaussian shape, and this is associated with the flattening of the tip of the external light pulse as a result of the small curvature of the modulated function of the electro-optical gate.

In injection of the external radiation pulse into the ring resonator of a powerful laser, the reversed radiation wave was completely suppressed (Fig. 4.2a). In this case, the laser resonator did not contain any non-mutual elements. In the absence of the external radiation pulse, lasing included both waves with almost identical amplitudes, Fig. 4.2b.

For the pulse with the Gaussian shape, the estimates indicate a decrease of the duration of the SRP by a factor of 5 for the same experimental conditions. The parameters of the ultra-short radiation pulses in the injection regime are determined by the parameters of the external light pulse. The high coherence of the introduced light pulse, formed from the monochromatic radiation of the master laser, results in complete synchronisation of the phases of the generated modes. When fulfilling the corresponding conditions, it is possible to obtain reproducible SRP with a very short duration.

The addition of losses to the resonator of the powerful laser with a ring-shaped resonator (Fig. 3.4) in the stage of non-linear development of the giant radiation pulse made it possible to reduce 50 times the width of the introduced external pulse in the ruby laser (Fig. 4.3a). The additional losses in the resonator of the powerful laser were generated using the two-stage supply of the voltage pulse, opening the electro-optical gate. The duration of the pulses, measured on the basis of two-photon fluorescence, was approximately 30 ps (Fig. 4.3b).

The method of injection of the external nanosecond pulse without the application of the negative feedback was used in Ref. 31, 32. In Ref.

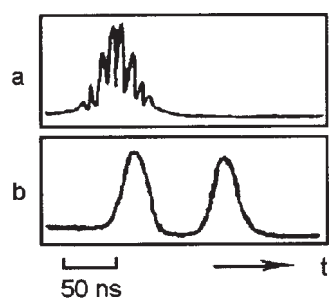

Fig. 4.2 Oscillograms of the radiation intensity of direct and reversed waves of the ruby laser in injection of the external signals with $\tau_s < L/c$ (a) and without the external signal (b).

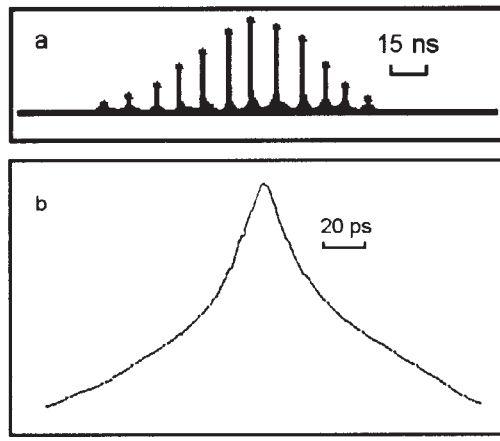

Fig. 4.3 Parameters of supershort radiation pulses of a ruby laser in the regime of a giant pulse with passive synchronisation of modes in injection of the external signal and introduction of a negative feedback: a) oscillogram of supershort radiation pulses; b) density of the track of a pulse in two-photon fluoresence.

31, the width of the injected external pulse in the Nd:YAG laser was reduced 8 times.

4.3 LASING OF STABLE SUPERSHORT RADIATION PULSES BY THE METHOD OF INTRODUCING INTRA-RESONATOR LOSSES

The regime of stable stationary supershort radiation pulses in the solid-state lasers with the passive synchronisation of the modes in the stationary regime is realised when suppressing the instability associated with the illumination of the saturating absorber, by means of a negative feedback [26]. The regime of the negative feedback was used for producing stable supershort radiation pulses in ruby lasers [30,33–35], in Nd-doped lasers in phosphate glass [16,30,33,36–39,44], yttrium-aluminium garnet [13,30,33,40–42], potassium–gadolinium tungstate [33, 43], yttrium aluminate [11,40] and other active media.

Experimental investigations of the stabilisation of the passive synchronisation of the modes of solid-state lasers indicate new possibilities of developing stable sources of SRP with unique parameters as regards the pulse time, their reproducibility and radiation power. Consecutive suppression of the instabilities, formed during passive synchronisation of the modes for solid-state lasers, makes it possible to realise long-term non-linear self-effect of radiation in these systems, determine the fine details of the self-organisation of radiation in the self-effect, and examine the physical mechanisms of the formation of instabilities and special features of their suppression.

To obtain the maximum power of the supershort radiation pulses, a number of authors [11,37,38,40] selected the configuration of the laser resonator for which the application of negative feedback resulted in a small increase of the duration of the giant pulse, sufficient for the formation of a single pulse on the axial period. In this circuit, the radiation inside the resonator is not focused in a cuvette with the saturating absorber and the strength of the field in the active medium is relatively high. In this case, there is no equilibrium between 'dumping' of inversion in the active medium and pumping. This leads to a rapid removal of the inversion resulting in a reduction of the duration of lasing to several microseconds, and the formation of SRP takes place in the conditions of the non-equilibrium process. In this case, the value of the inverse population in the active medium continuously changes and this results in a change of the equilibrium duration of the SRP. Consequently, the SRP parameters change in the lasing process.

To accelerate the process of formation of the single pulse in the axial period, additional activation of synchronisation of the modes was carried out [12,13,39,45]. In Ref. 14,41,44, the inertia negative feedback was represented by a non-linearly absorbing semiconductors sheet made of gallium arsenide placed in the laser resonator. SIB with a duration of 4.5 picosecond were obtained in a Nd doped laser yttrium aluminate [41].

4.3.1 Experimental equipment

Investigations were carried out into the lasing of stationary supershort radiation pulses with a relatively long time of formation of the SRP with interaction with the saturating absorber. In this case, the lasing time was determined by the duration of the pumping pulse which is considerably longer than the transition process, and the main intensity of radiation in the active media was close to the free lasing level. This was achieved by focusing radiation in a cuvette with a solution of the saturating absorber; in this case, the requirements on the parameters of the negative feedback system were greatly reduced.

The diagram of experimental equipment is shown in Fig. 4.4 [30]. A hemispherical resonator with a solid spherical mirror with a radius of curvature of 30 cm (1) and a flat output wedge-shaped mirror (8) were used; the transmittance factor of the mirror was selected by experiments in relation to the active medium. The length of the laser resonator of the ruby laser was 1.5 m, and that of the Nd-doped laser 2.0 m. The cuvette with the saturating absorber with a thickness of 0.2 mm (2) was placed at the focus of the spherical mirror and the spherical lens (3), with a focusing distance of 10 cm. The lasing conditions were optimised by changing the density of radiation power in the saturating absorber.

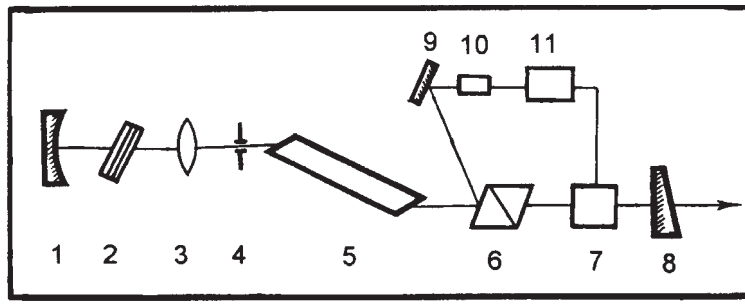

Fig. 4.4 Diagram of a solid state laser with stable supershort radiation pulses: 1) convex lense resonator mirror with $R = 30$ cm, $T = 99.7\%$; 2) cuvettr with a saturating absorbent; 3) spherical lens ($f = 10$ cm); 4) diaphragm, separating longitudinal modes; 5) active medium; 6) Archard–Taylor polarisation prism with ends under the Brewster angle; 7) electro-optical gate; 8) flat output mirror of the resonator; 9) high-reflection mirror; 10) high-current photomultiplier 14ELU-FK; 11) electronic unit.

This was achieved by moving the cuvette with the dye solution along the resonator axis. The dye cryptocyanine was used for the passive synchronisation of the modes of the resonator of the ruby laser, and N3247y polymethine dye was used for the Nd-doped laser. The longitudinal modes of the resonator were separated by the diaphragms (4) with a diameter of 1.5 mm in the ruby laser and 2.0 mm in the laser on Nd ions. The lasing of stable supershort radiation pulses was examined in active media (5): a ruby crystal with a diameter of 7 mm, length 120/180 mm with the ends cut under the Brewster angle; Nd:YAG, diameter 5 mm, length 100 mm, and Nd in phosphate glass of type GLS-22, diameter 6 mm, length 130 mm, with the bevelled and clarified ends. The pumping of the active rods was carried out with an IFP-800 lamp in a quartz single unit illuminator, pumping pulse time was 0.25 ms. The ruby crystal was cooled in distilled water, and the Nd rods were cooled with a liquid filter, cutting off the ultraviolet radiation of pumping.

The negative feedback was produced using an electro-optical amplitude modulator of the ML-102A type (7), operating on the basis of the transverse Pockels effect. To reduce the controlling voltage, the investigators used the quarter-wave circuit of modulation of the *Q*-factor of the laser resonator in which the modulator (7) was placed between the solid mirror of the resonator and the polariser (6). The part of intra-resonator radiation (~5%), reflected from the polariser (6), was transferred to the photoreceiver of the system of the inertia negative feedback. The voltage of complete closure of the ML-102A gate at a wavelength of 1.06 μm was approximately 170 V.

For the effective stabilisation of the regime of stationary SRP, the time to establishment of negative feedback was shorter than the characteristic

time of the variation of the radiation intensity averaged over the axial period (~10^{-6} s) and longer than the time required by the light beam to pass around the laser resonator (~10^{-8} s). The depth of the inertia feedback was sufficient to compensate the decrease of the losses in the laser resonator formed as a result of clarification of the saturating absorber and leading, in the normal conditions, to scintillation of the giant pulse. In the experiments, the time to establishment of the circuit of the inertia negative feedback was 20 ns. The circuit of the negative feedback consisted of a solid mirror (9) of ELU-FK high-current photomultiplier (7) and the electronic unit (11).

The time parameters of lasing were recorded with coaxial photographic elements with an S1-75 oscilloscope with a time resolution of ~1.5 ns and Agat-SF1 electronic-optical camera with a resolution of the order of 10^{-12} s. The lasing spectrum was controlled with a Fabry–Perot interferometer and a photographic camera with a long-focus lens. The energy of the lasing pulse was measured with an IMO-2 device.

4.3.2 Parameters of supershort radiation pulses

Ruby lasers

Free lasing in a ruby laser in the normal condition always takes place in the regime of non-attenuating pulsations of radiation intensity. In contrast to the Nd-doped lasers, in the ruby laser it is far more difficult to obtain stable supershort radiation pulses throughout the entire free lasing pulse. This requires a more careful selection of the parameters of the inertia negative feedback system.

At the start of the transition lasing process, radiation of the ruby laser consisted of a large number of intensity fluctuation transients in accordance with the static nature of formation of the SRP [6]. The lasing spectrum was approximately 0.008 nm wide and had a random structure. At the end of the transition process with a duration of approximately 0.1 ms, the structure of the lasing spectrum was ordered and became angular. Subsequently, in the stage of formation of stationary SRP (~0.1 ms) the process of selection of the most intensive fluctuation pulse was completed and the laser resonator contained one pulse with the duration, shape and power determined by the parameters of the laser system.

The width of the lasing spectrum in the regime of lasing of stationary supershort radiation pulses in a ruby laser (Fig. 4.5) was ~0.07 nm. This width of the spectrum corresponds to the duration of the supershort radiation pulses of approximately 8 ps. When evaluating the duration of the SRP, no account was made of phase modulation because its contribution to the width of the spectrum of the stationary SRP was very small [46], and it was assumed that the SRP pulses have the form

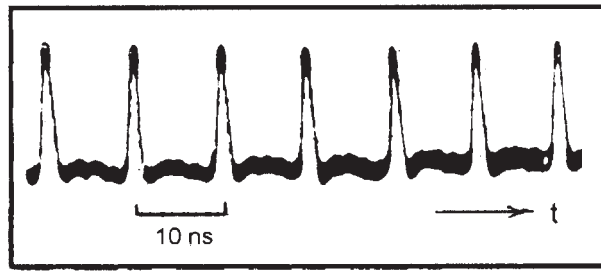

Fig. 4.5 Oscillograms of the intensity of supershort radiation pulses of a ruby laser in the regime of passive synchronisation of modes in introduction of intra-resonator losses.

of the square of the hyperbolic secant [47]. The duration of the produced SRP was an order magnitude shorter than the duration of the pulses produced in solid-state lasers with active synchronisation of the modes [7].

At the transverse size of the beam in the cuvette of approximately 0.3 mm and the mean radiation power in the resonator of approximately 500 W, the peak intensity in the saturating absorber was ~8×10^7 W/cm^2. This is an order magnitude higher than the saturation intensity of cryptocyanine (6×10^6 W/cm^2) and corresponds to the condition of the highest rate of compression of the SRP in the saturating absorber [48].

The lasing regime of the stationary SRP in the ruby laser was interrupted slightly earlier than the end of the pumping pulse. This interruption of lasing, according to additional investigations, is caused by the formation of a transverse instability of radiation inside the laser resonator.

Nd:YAG lasers

Like the ruby crystal, the Nd:YAG crystal is characterised by a uniformly broadened gain line with the half width slightly smaller than in the ruby crystal. However, the lifetime of the upper working level of Nd:YAG is an order of magnitude shorter. This results in the situation in which the time to establishment of the stationary lasing regime in the Nd:YAG laser is reduced by almost an order magnitude, in comparison with the ruby laser, and is ~10 μs (Fig. 4.6). In the stationary lasing regime of SRP, the radiation of the Nd:YAG laser was also represented by a continuous sequence of single pulses, followed by an axial period of 13 ns. The envelope of the lasing spectrum was bell-shaped without a fine structure. This indicated the absence of the time structure of the supershort radiation pulses. Throughout the entire lasing process, the structure of the spectrum was almost constant. This indicated that no

Fig. 4.6 Oscillograms of the intensity of radiation of an Nd:YAG laser in the regime of passive synchronisation of modes with addition of intra-resonator losses.

phase modulation took place. The duration of the SRP, calculated from the width of the generated spectrum, was 10 ps.

It should be noted that in the Nd:YAG laser, the transition to the regime of stable stationary supershort radiation pulses was obtained in a wider range of the radiation of the laser parameters (pumping, the extent of the feedback, technical perturbations) in comparison with the ruby laser.

Nd doped phosphate glass lasers

Nd glass is characterised by a wide gain band and can be used to produce light pulses of subpicosecond duration. Peak power may reach the values at which the non-linear-optical effects start to operate, such as the phase and self-modulation of the produced pulses associated with the non-linearity of the refractive indices of the resonator elements. At a high value of phase self-modulation, an instability forms in the process of passive synchronisation of the modes in the lasing regime of the stationary SRP.

In Nd doped lasers on phosphate glass GLS-22, the duration of the transition process was approximately 30–50 μs (Fig.4.7a). During this period, the carrier frequency radiation was shifted to the short-wave region of the spectrum by 0.6 nm. The width of the lasing spectrum of the laser with a passive gate on N 3274y dye, whose relaxation time is ~13 ps, in the steady stationary regime of lasing of SRP (Fig. 4.7b) was 2.3 nm, and the shape of the spectrum was described with sufficient accuracy by the square of the hyperbolic secant [47]. This width of the lasing spectrum corresponds to the duration of the supershort radiation pulse of 0.5 ps.

In passive synchronisation of the modes with a gate based on N 3955 dye, with a relaxation time of 22 ps, we obtained stationary SRP with the duration of the order of 2 ps. To obtain the same duration of the SRP in the giant pulse regime, investigations were carried out using a saturating absorber with a considerably shorter relaxation time of 4.6 ps [49] and 2.5 ps [50].

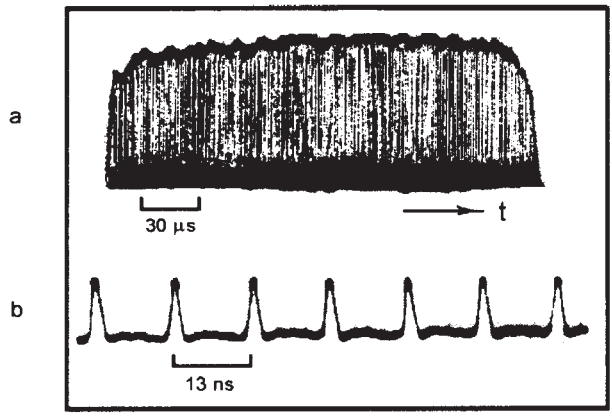

Fig. 4.7 Oscillograms of the intensity of radiation of an Nd doped laser in phosphate glass in the regime of passive synchronisation of modes with the addition of intra-resonator losses.

The larger shift of the carrier frequency of lasing was recorded in the Nd doped laser on silicate glass in which the width of the gain band was slightly larger than in the phosphate glass laser. In addition, in the case of silicate glass, the non-linearity of the refractive index is higher and silicate glass shows effects of phase modulation with a high degree of probability leading to the formation of an instability in the regime of stationary supershort radiation pulses.

The larger deviation of the carrier frequency from the maximum of the gain band leads to a decrease of the efficiency of amplification of the produced pulse, and the gain factor for the noise with no phase modulation, was higher than for the phase-modulated pulse. The starter with a more efficient gain displaces the produced pulse from the lasing and the increase of the lasing intensity results in the phase modulation and shift of the carrier frequency.

Chapter 5

Increasing the lasing efficiency of solid-state lasers

In the solid-state lasers on ions in the dielectrics (crystals and glasses) the matrix of the dielectrics plays a significant role in the lasing processes; it is therefore necessary to ensure that the active impurity ions are added uniformly to the matrix in a sufficiently high concentration, without disrupting its optical and mechanical properties.

The matrix should be optically homogeneous and transparent in the spectral range of pumping and lasing radiation and should have high heat conductivity, heat resistance, mechanical and optical stability. In addition, the matrix should satisfy the technological requirements on optical treatment. At present, there are hundreds of solid-state matrixes of active media used for lasing. In most cases, activators in the solid-state lasers are represented by the ions of elements of transition groups. The atoms of these groups are characterised by the presence of internal partially filled electron shells. The transitions in which these non-filled shells take part also determine the spectral-luminescence properties of the active medium. The activators are implanted in the matrix and exist there in the form of ions.

In the widely used solid-state lasers on active media with trivalent ions of the iron transition group, these ions lose the screening shell and their spectra in different matrixes differ from the spectra of the free ions and depend on the forces of the crystal field of the matrix. The ions of other transition elements of the group of rare earths change only slightly their spectral-luminescence properties with changes of the solid-state matrix, because of the presence of screening electron shells in these ions. The working electron shells of rare-earth ions are screened to such an extent that the crystal fields of the matrixes have only a slight effect on their state and configuration.

At present, the solid-state lasers are used most widely in practice, regardless of strong competition with other types of lasers. The solid-

state lasers are characterised by high lasing energy parameters combined with the capacity of working in the greatly differing conditions, from the regime of lasing of supershort radiation pulses to the regime of continuous high-power lasing. They are also exceptionally reliable, durable, and compact in comparison with other types of lasers.

One of the main problems facing the developers of solid-state lasers is how to increase the efficiency factor (EF) of solid-state lasers which in the measurement of lasers is on the level of several percent. It is also important to widen the spectral range of lasing of the solid-state lasers. The problems of increasing the efficiency of lasing of the solid-state lasers have been examined by the authors of this book in Ref. 1.

5.1 INCREASING PUMPING EFFICIENCY

The absorption factor of pumping radiation by the active medium is determined by the efficiency of the illumination system, the efficiency of radiation of the pumping pulse and the matching of the radiation spectrum of the pumping pulse with the spectral bands of absorption of the active media. The illumination system is improved by optimising the focusing of pumping radiation in the area of position of the active element and by increasing the efficiency of the illuminator.

To increase the pumping efficiency, it is necessary to minimise the possible losses of light energy in the elements of the pumping system and non-active absorption in the active medium. The presence of the narrow absorption bands of the solid-state active media in comparison with the radiation spectrum of the pumping lamps causes that a large part of the energy of the pumping lamps is not utilised by the active medium or is used with insufficient efficiency. In addition, the spectral components of the active medium with low absorption require multiple passes.

To improve pumping efficiency, it is important to ensure the spectral transformation of part of the pumping radiation not absorbed in the active medium, in the region of its active absorption. Under specific conditions, the plasma of the pumping lamps may be such an effective re-emitter. The return to the lamps of the light energy not absorbed in the active medium and its subsequent repeated radiation with the losses not exceeding 20% is efficient from the energy viewpoint (‘light boiler’) [2]. The ‘light boiler’ is realised with the highest efficiency when the active medium is situated between the reflector and the plasma layer, i.e. with the coaxial active element. Using such an element made of Nd glass, the authors of Ref. 3 obtained the efficiency factor in the regime of free lasing of 9% in relation to electric energy. In the pumping system of the ‘light boiler’ type, with the Nd:YAG active

elements positioned symmetrically around the pumping lamps with close packing in the quartz single unit, the efficiency factor of laser was ~3% in the giant pulsed regime [3].

The efficiency of transformation of the pumping energy may decrease using, as the material of the reflector in the illuminator, zirconium oxide (ZrO_2) or silicate ceramics (kersil), characterised by a high degree of diffusion reflection in the spectral range from 400 to 1000 nm and by the possibility of alloying with different materials for the conversion of the reflective light spectrum. The application of reflectors made of kersil in the optical pumping systems of the lasers increases the efficiency factor of lasers by 30%, improves the energy and spatial characteristics of radiation, increases endurance and durability of the laser systems. Reflectors have been produced from kersil for absorbing ultraviolet pumping radiation and converting this radiation in the region of the absorption bands of solid-state media [4]. The ultraviolet pumping radiation is also used for quartz glass lamps with a titanium silicate coating [5].

In Ref. 6 and 7, the ultraviolet radiation of pumping lamps was converted to the green range spectrum in one of the absorption bands of chromium ions in the alexandrite crystal using a solution of KN-120 dye.

5.1.1 Selective pumping of the active medium

The selective pumping of solid-state media is realised using both gas-discharge sources of narrow-band radiation and laser semiconductor emitters. The main contradiction, formed in the development of selective pulsed pumping lamps is based on the requirement for the high brightness of the plasma that can be achieved only at high plasma temperature and density. In this case, the plasma of the pumping lamps becomes almost completely non-transparent and its spectrum discontinuous. In continuous arc pumping lamps it is possible to produce a narrow-band radiation spectrum; this was also realised in krypton gas discharge lamps which have been used efficiently for the pumping of continuous solid-state lasers.

The sapphire lamps with the additions of alkali metals are an efficient means of the pumping of low-threshold solid-state media at low levels of pumping power. When pumping an Nd:YAG laser with a potassium-rubidium sapphire lamp, the pumping efficiency was twice that in the case of the krypton lamp [8], as a result of better matching of the radiation spectrum of the resonance lines of K and Rb with the absorption spectrum of the garnet crystal.

The application of hybrid conditions of supplying power to the gas-discharge lamps with a constant and pulsed component of the discharge

makes it possible to change the radiation spectrum of the pumping lamp and increased its efficiency [5].

5.1.2 Laser pumping

In comparison with lamp pumping, laser pumping increases the efficiency with respect to the energy contribution by almost two orders of magnitude. This greatly extends the possibilities of application of rare-earth active media. The increase of the energy contribution makes it possible to reduce greatly the requirements on the upper working level, its lifetime and the laser transition section. Consequently, the gain factor of the active media greatly increases, together with increase of lasing energy.

Laser pumping makes it possible to greatly reduce the level of technical perturbations of the active medium and the resonator, shorten the length of the active medium without any loss of its general gain, increase the threshold density of the laser radiation flux, and solve the problem of self-focusing of radiation in optical amplifiers

5.1.3 Laser diode pumping

Recently, the extent of application of semiconductor lasers for the laser pumping of solid state lasers has greatly increased [10,11]. This is caused by the relatively rapid development of the technology of production of powerful light-emitting diodes, matrixes and semiconductor lasers.

The main advantage of solid-state lasers with diode pumping in comparison with lamp pumping is the higher efficiency factor. In the group of the solid-state lasers, Nd lasers have been used most extensively. The efficiency factor of these lasers in lamp pumping does not exceed 1–3%. This is caused by poor matching of the absorption bands of the Nd ions with a wide radiation spectrum of the pumping lamps. In contrast to lamps, the laser diodes have a narrow spectral emission line enabling good matching of the radiation spectrum with the absorption bands of solid-state active media. The development of high efficiency laser diode gratings on GaAlAs emitting at a wavelength of 810 nm with a power higher than 0.2 W has resulted in the efficiency factor of 8% in the Nd:YAG laser in the lasing regime of the TEM_{oo} mode (a single zero transverse mode) [12]. Increase of the power of laser pumping to 1 W resulted in the development of continuous single-mode Nd:YAG lasers with the total efficiency higher than 10% [13,14]. When using yttrium vanadate with Nd ions as the active medium, it is possible to obtain the efficiency factor of a laser of 19% [15].

The solid-state lasers with diode pumping are characterised by higher stability of the frequency of laser radiation in comparison with lasers with lamp pumping. The extremely higher stability of the frequency

of solid-state lasers with lamp pumping is not better than 17 kHz because of the presence of technical noise, characteristic of the pumping pulse [16]. The application of diode pumping and a monolithic ring-shaped resonator with active stabilisation has improved the stability of the lasing frequency of Nd:GGG laser to 30 Hz [17].

Diode pumping has simplified the design of solid-state lasers, greatly reduced their weight and dimensions. Diode pumping sources have wider functional possibilities of controlling the pumping regime in comparison with the lamp sources. They make it possible to regulate in a wide range the duration and shape of the pumping pulse, stabilise the pumping energy and greatly improve the lasing parameters of the solid-state lasers. The application of diode pumping increases by more than an order of magnitude the service life of solid-state lasers operating in both the continuous and pulsed regimes.

In addition to the above mentioned advantages, it is also important to mention the current shortcomings of the solid-state lasers with diode pumping in comparison with lamp pumping: considerably lower energy and power of emitted radiation, and a considerably higher price of a diode pumping source in comparison with the lamps.

In the solid-state lasers with diode pumping there are two configurations of the pumping system: longitudinal and transverse. Longitudinal pumping (from the end of the active element) makes it possible to obtain better mode matching and a longer length of the absorption part of radiation which weakens the requirement on the pumping wavelength, i.e. the degree of control of the temperature of the laser diode. However, longitudinal pumping requires more powerful diodes with a low divergence of radiation.

The application of transverse pumping in the solid-state lasers enables a large number of diode gratings to be used. These gratings are positioned parallel to the axis of the active element and normal to the direction of propagation of laser radiation in the resonator. This greatly increases the pumping power.

In most cases, to obtain the maximum mode matching of pumping radiation, the diameter of the active element should be small. This restriction leads to a short length (~3 mm) of absorption of pumping radiation and lower efficiency in comparison with longitudinal pumping. Thus, to obtain the corresponding level of the output power in the solid-state laser with transverse pumping, it is necessary to use a considerably larger number of laser diodes in comparison with the laser with longitudinal pumping. Regardless of these shortcomings, transverse pumping makes it possible to increase almost without bounds the radiation power (to the kilowatt level) of the solid-state lasers with diode pumping.

5.2 INCREASING THE CONCENTRATION OF IMPURITY ACTIVE IONS

The concentration of active ions in the majority of solid-state media does not exceed 3×10^{20} cm^{-3}. An increase of the concentration of the impurity ions leads to both widening of the absorption bands and increase of the intensity, and also to the concentration quenching of luminescence for the majority of active media.

However, in trivalent Er ions in an yttrium–erbium crystal of the aluminium garnet the concentration decay of luminescence at the $^4I_{11/12} \rightarrow {}^4I_{12/2}$ transition is not present up to the Er ion concentration of 4×10^{21} cm^{-3} and the efficiency of lasing rapidly increases [18].

The effect of concentration decay of luminescence is quite strong in Nd^{3+} ions as a result of the multipole-resonance interaction of absorption ($^4I_{9/12} \rightarrow {}^4I_{13/2}$, $^4I_{15/2}$) and emission ($^4F_{3/2} \rightarrow {}^4I_{15/2}$, $^4I_{13/2}$) transitions of the adjacent ions. This results in a large decrease of the lifetime of the upper working level $^4F_{3/2}$ (Fig. 5.1).

The harmful effect of concentration decay of luminescence is prevented as a result of detuning these transitions by displacing the energy levels and by a corresponding relative shift of the frequency of the transitions, or as a result of increasing the width of the transitions by selecting the chemical composition of the active medium. The probability of the multipole-resonance interaction, which in dipole–dipole interaction changes as $1/r^6$, rapidly decreases when increasing the distance $r \geq 0.45$ nm between the interacting ions. When this condition is fulfilled, the interaction between the Nd ions, situated in the sites of the crystal

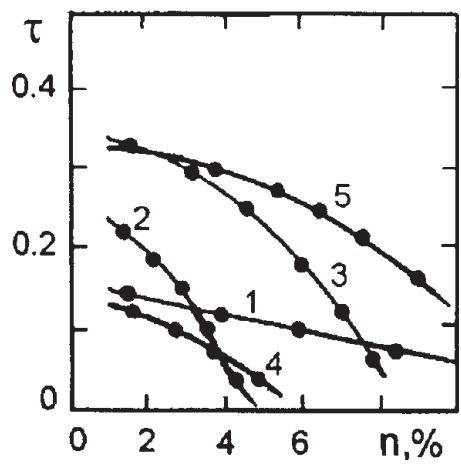

Fig. 5.1 Dependence of the lifetime τ (ms) of the upper working level $^4F_{3/2}$ of Nd^{3+} on the concentration n (%) in different active media: 1) Nd:KGW, 2) Nd:YAG; 3) Nd:CNPhS (KNFS), 4) Nd:BLN, 5) Nd:LNA.

lattice, is greatly weakened, irrespective of the high resonance of the electronic transitions.

The concentration of the active Nd ions of up to 4×10^{21} cm^{-3} without any significant luminescence decay was obtained in neodymium pentaphosphates NdP_5O_{14} [19] and neodymium tetraphosphates $LiNdP_4O_{12}$ [20]. However, these media are highly unstable and dissociate during heating. In addition, it is quite difficult to grow large single crystals. Therefore, these media are used mainly for the development of minilasers.

In Ref. 21 the authors reported lasing on Li–Nd–La phosphate glass (KNFS) with the Nd ion concentration of 3×10^{21} cm^{-3}, without any significant luminescence decay. KNFS glass is characterised by a small width of the lasing line, a lower threshold and higher lasing efficiency than silicate and phosphate glass. However, the KNFS glasses are not used widely because of the low heat conductivity coefficient, hardness and high hygroscopicity.

The crystals of potassium–gadolinium tungstate ($KGd(WO_4)_2$, KGW) with the Nd ion concentration more than 5×10^{20} cm^{-3} are also characterised by a low concentration luminescence decay and higher lasing efficiency [22]. The efficiency factor of the Nd:KGW laser in the free lasing regime is twice as high and the energy of the giant pulse is four times higher in comparison with the Nd:YAG laser.

The high concentration of active ions can be obtained using disordered crystals in the form of mixed compounds (solid solutions) [23]. In these crystals, the active ions are situated in different positions differing in the force and symmetry of the crystal field. These structural variants of the crystal field are of statistical nature and result in detuning of the resonance between the ions situated in different positions. Consequently, the resonance bond between the adjacent activator ions weakens. These crystals have wide and non-uniform luminescence bands which change slowly with temperature. The absorption bands in these crystals are also wider and more intensive, and concentration luminescence decay is less marked. Consequently, the efficiency of application of the radiation of pumping lamps increases several times and the lasers with these matrices have a lower threshold and higher efficiency than the lasers on simple crystals.

5.3 SENSITISING OF LASER SOLID-STATE MEDIA

Lasing efficiency can be increased by developing matrices with double or even triple activation. Consequently, the functions of absorption of pumping energy by a certain type of activator and the emission functions by another type are separated. This method is referred to as sensitising. A sensitizer should efficiently absorb the pumping energy and also transfer efficiently excitation to the lasing activator. This

condition is satisfied by fulfilling a large number of requirements [24] on the sensitizer: efficient widening of the excitation spectrum of the active medium; the presence of the metastable level above the upper working level of the activator; absence of other levels capable of trapping the excitation of the activator; the absence of the main or induced absorption on the lasing wavelength. Since it is difficult to satisfy all the requirements simultaneously, only a limited number of the effective sensitising active media have been produced so far.

The most efficient co-activator in crystals and glasses with trivalent rare-earth elements is the ion of trivalent chromium. The chromium ions Cr^{3+} prefer (because of special features of electron configuration) to occupy sites in the crystals with the octahedral co-ordination sphere.

The chromium ions have wide high-intensity absorption bands overlapping almost the entire visible spectral range. Gently absorbing pumping radiation, the ions of trivalent chromium transfer the excitation by the multipole-resonance mechanism to the upper working level of the activator. In addition, the energy of some levels of the chromium ions depends strongly on the force of the crystal field D_q [25] (Fig. 5.2). The main role in the process of exchange by interaction is played by the energy gap ΔE between the levels ^2E and $^4T_2$ of the chromium ions [26].

With increasing force of the crystal field the energy gap between the levels ^2E and $^4T_2$ increases. The force of the crystal field in the ruby crystal (Cr^{3+}:Al_2O_3) is such that the size of the energy gap is ΔE = 2300 cm^{-1}, in yttrium–aluminium garnet ($Y_3Al_5O_{12}$) it is 1300 cm^{-1}, consequently, the excitation relaxes from the long-life level ^2E to the ground level $^4A_2$, bypassing level $^4T_2$. The energy gap in the GSGG crystals ΔE is only 80 cm^{-1} [18] (Fig. 5.3).

At room temperature, the electrons with the energy of thermal excitation are transferred from the metastable level ^2E to the short-life level

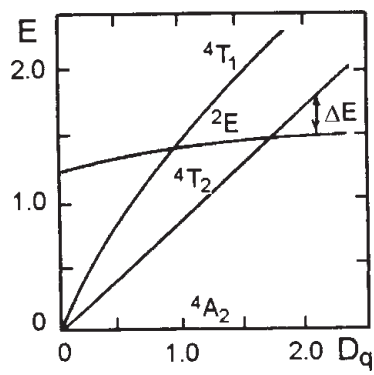

Fig. 5.2 Dependence of the energy $E \times 10^3$ (cm^{-1}) of several levels of Cr^{3+} ions on the strength of the crystal field $D_q \times 10^3$ (cm^{-1}).

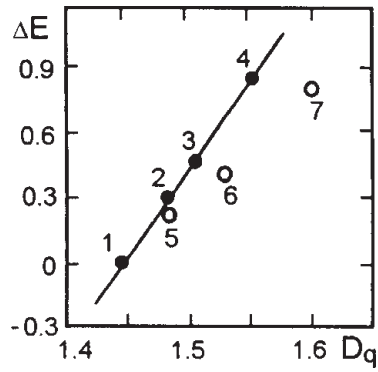

Fig. 5.3 Values of the energy $\Delta E \times 10^3$ (cm^{-1}) between the levels ^2E and $^4T_2$ of Cr^{3+} ions on the strength of the crystal field $D_q \times 10^3$ (cm^{-1})for different crystal with Cr^{3+} ions: 1) GSGG, 2) GGG, 3) YGG, 4) YAG, 5) YSGG, 6) emerald, 7) aleksandrite.

$^4T_2$ which relaxes through the $^4T_2 \rightarrow {}^4A_2$ strong transition in the form of a wide spectral luminescence band. This transition reaches resonance with absorption transitions of the ions of neodymium, erbium and ytterbium, and some other ions. If the chromium concentration and the concentration of the activator ions are correctly selected, the quantum yield of transfer is close to unity.

The transfer of excitation energy from Cr^{3+} to Nd^{3+} ions does not take place from the metastable state ^2E but from the $^4T_2$ state. The low value of the energy gap between them results in the rapid population of the $^4T_2$ level. The spectrum of the wide-band luminescence from this level is efficiently overlapped by the spectrum of absorption of the Nd ions. This results in a high rate of emissionless transport of energy. Fast transfer of excitation energy from Cr^{3+} to Nd^{3+} ions (in comparison with the rate of deactivation of the upper working level $^4T_2$ of the Nd ions) is possible on the condition when $\Delta E \leq kT$.

The crystal of yttrium–scandium–gallium garnet, activated with the Cr and Nd ions (Nd:Cr:YSGG) resulted in the efficiency of laser lasing of 7.8%, and in the Nd:Cr:GSGG laser the efficiency in the same conditions was 7.1% [26].

5.4 CROSS RELAXATION AND STEPPED SYSTEMS OF PUMPING LASER TRANSITIONS

An important role in three- and four-level lasing systems is played by emissionless transitions resulting in the conversion of energy to the upper working level and the scattering of the lower working level (in the four-level system). The same transitions represent the basis of heat generation and determine the efficiency of the medium. Heat generation produces a number of physical factors complicating lasing

[24]. This is especially important in the case of infra-red lasers with the lasing wavelength greater than or close to 2 μm in which the mean pumping quantum is 5–10 times higher than the lasing quantum. The development of excitation systems, increasing lasing efficiency as a result of decreasing heat generation in wide-band pumping, is one of the significant achievements of the physics of solid-state lasers [28].

The application of cascade excitation of laser transition between a pair of excited levels may result in the inversion of the populations on the underlying levels. Intermediate laser heating in the presence of the laser cascade to three, four or more steps improves the efficiency of operation of the previous lasing channel, lowering it to the lower working level.

Multistep emission extraction of energy, supplied to the medium, and the resultant suppression of emissionless relaxation of the levels of the laser cascade result in a large decrease of the extent of heat generation in the medium and increases total lasing efficiency. In addition, the systems make it possible to widen the range of lasing wavelength [29].

A large number of variants of the cascade systems with the application of fluoride- and oxygen-containing crystals, activated with rare-earth ions, have already been developed. The spectral range of lasing has been extended to 5.15 μm. Lasing on the ions of praseodymium, neodymium, holmium, erbium and thullium has been achieved [30,31].

There is another physical process capable of competing with emissionless transitions, i.e. the so-called cross relaxation which is the transfer of excitation energy in which the donor transfers to the acceptor only part of its excitation energy. This increases the intensity of excitation by a factor 2 or sometimes 3, and in some media the quantum efficiency of the process may exceed unity. In transport of a group of electronic excitations, formed during cross relaxation to the upper laser level with the quantum efficiency close to unity, these excitations are efficiently transformed to lasing [32]. Cross relaxation is activated with increasing concentration of the activators and, consequently, many highly concentrated systems contain cross relaxation stages in their working stages.

In a crystal of yttrium–erbium–aluminium garnet at the transition of the erbium ions $^4I_{11/2} \rightarrow {}^4I_{13/2}$ with the chromium concentration higher than 10^{21} cm^{-3}, lasing was obtained at the radiation wavelength of 2.9 μm, with a mean output power higher than 20 W. During cross relaxation, excitation is transferred from the long-life lower level (τ = 6 ms) to the relatively rapidly relaxing upper level (τ = 100 μs). This takes place at exciting pumping rates higher than some critical value. The probability of interaction of the excited ions depends on

the population of the upper laser level. In this case, the laser transition ceases to be self-restricted and stationary inversion may take place. In stationary lasing in absorption of a single quantum in the visible end of the spectrum three quanta can be emitted in the 3 μm range [28].

Examination of the mechanisms of cross relaxation in the crystals of potassium–niobium–gallium garnet with the ions of trivalent thullium resulted in continuous lasing of radiation with a wavelength of 2.02 μm in pumping with laser radiation on an Nd-doped aluminium–yttrium garnet [33].

The efficiency of pumping radiation is also increased by stepped sensitising or the processes of summation of excitation. The physical nature of these processes is similar to the cross relaxation processes and they represent the emissionless transfer of excitation from one active centre to another. Above all, being an additional relaxation channel of excitation, they are capable of improving the operation of laser transitions ending on the metastable levels. Secondly, the stepped processes may ensure efficient utilisation of the energy absorbed in the bands, associated with the levels situated below the upper working level of the laser transition which in the conventional systems is assumed to be irreversibly lost. Finally, the efficient inclusion of electronic excitations stored on the storage levels in the course of prior cross relaxation conversion of absorption energy is possible during the process of pumping of laser transition. The quantum efficiency of excitation of the storage levels in the pumping bands of the medium is automatically transferred to the working level of the lasing transition [24].

The direction of investigations in this area is associated with the detection of the mechanisms and special features of the population of the main and intermediate levels of transfer of pumping energy [34,35] in order to obtain effective radiation parameters and optimise the lasing conditions [36].

5.5 LOW-THRESHOLD SOLID-STATE MEDIA

In addition to efficiency, another important characteristic of the solid-state laser is the lasing threshold, i.e. the minimum value of the pumping energy at which lasing starts. The main criterion of the low-threshold medium is the high value of the cross-section of the laser transition.

The widely used Nd:YAG crystal has the laser transition cross-section of $\sigma = 3.3 \times 10^{-19}$ cm^2 at a radiation wavelength of 1064 nm [37]. Active solid-state media with a larger laser transition cross-section are known, i.e. germanates of rare-earths, the transition cross-section of the $NAYGeO_4$ crystal with Nd at a wavelength of 1.06 μm is $\sigma_{1.06} = 4.1 \times 10^{-19}$ cm^2 [38]. The same large laser transition cross-

section $\sigma_{1.06} = 6 \times 10^{-19}$ cm^2 and a low lasing threshold are shown by crystals of cadmium vanadate with Nd (Nd:$CdVO_4$) [39]. Recently, experiments were carried out with lasing on new low-threshold and efficient active media: lanthanum scandoborate, activated with ions of Nd and Cr (Nd^3:Cr^{3+}:$LaSc_3(BO_3)_4$) [40], Nd^{3+}: $LaBGeO_5$ [41] and lithium–yttrium tetrafluoride ($LiYF_4$) with praseodymium [22]. The high values of the laser transition cross-section and the low duration threshold are also typical of the crystal of potassium–gadolinium tungstenate with Nd (Nd:KGW) [22]. Investigations of these crystals make it possible to increase greatly the lasing efficiency of solid-state lasers.

5.6 EXPANDING THE SPECTRAL RANGE OF LASING

Expansion of the spectral range of lasing of the solid-state lasers is of considerable scientific and practical importance. Investigations in this direction can be divided conventionally into two large groups: the development of laser sources generating radiation in new areas of the spectrum; the development of solid-state active media with wide amplification bands. The first group includes the previously mentioned laser sources of the short-range infra-red lasing region (1.5–5 μm), based on emitting transitions in rare-earth ions. The application of the methods of non-linear optics also makes it possible to expand greatly the spectral range of coherent radiation by means of the lasing of harmonics, the displacement of frequencies and parametric frequency transformation. Recently, extensive investigations were carried out into the development of active media with wide gain bands. This type of active media is attractive because of two aspects: the fact that lasing is easily modified in a wide spectral range, and the lasing of extremely short light pulses by the methods of mode synchronisation.

Of the wide-band solid-state media it is important to mention the crystals activated by ions of the group of transition metals. One of these ion crystals is the alexandrite crystal which was used for the first time to produce lasing on the electronic–vibrational transition of chromium ions $^4T_2 \rightarrow {}^4A_2$ [43]. The authors of Ref. 6,7,44,45 examined in detail the energy and, for the first time, the spectral–time parameters of the free lasing of an alexandrite laser and obtained tunable lasing in the range 700–800 nm. This stimulated the development of new active media with chromium ions. The lasing of Cr^{3+} ions on the electronic-vibrational transition was realised and examined on crystals: emerald (Cr^{3+}:$Be_3Al_2Si_6O_{18}$) [45, 46], perovskite ($KZNF_3$), beryllium hexa-aluminate ($BeAl_6O_{10}$), $ZnWO_4$, $SrAlF_5$, $ScBO_3$, $Al_2(WO_4)_3$. $KSc(WO_4)_2$, and others. Quite detailed investigations have been carried out on the crystals of rare-earth–gallium garnet with chromium, lasing in the $^4T_2 \rightarrow {}^4A_2$ electronic–vibrational; transition, which showed tunable lasing in the

spectral ranges: 740–830 nm (Nd:GSGG), 710–790 nm (Nd:YSGG) and 760–810 nm (Nd:GSAG) [7,45].

A unique active medium in the group of the examined active media is the sapphire crystal with titanium ions (Ti^{3+}:Al_2O_3), characterised by the widest amplification line of all active media, i.e. 680–1100 nm. In a spectrometer based on a titanium–sapphire laser, it was possible to realise continuously tunable lasing in the range 202–3180 nm. This crystal was used for producing record light pulses with a duration of 10 fs.

5.7 INCREASING THE BEAM STRENGTH OF SOLID-STATE MEDIA

The problem of the beam strength of solid-state active media is associated with the problem of laser failure of transparent materials. The mechanisms of laser failure can be divided into two groups [48]: determined by heating of absorbing defects in the medium; associated with impact and instantaneous ionisation, leading to optical breakdown in the medium.

Of the greatest importance with respect to the threshold of failure of the medium are metallic and nonmetallic inclusions. In glasses, the volume beam strength after radiation pulses with a duration of 30 ns is: in the presence of metallic inclusions 15 J/cm^2, at a content of ceramic inclusions 150 J/cm^2, and in the absence of inclusions 400-500 J/cm^2 [49]. In this case, thermal breakdown or explosion takes place as a result of rapid local heating in the areas of inclusions absorbing radiation. The inclusions usually appear during the growth of crystals or boiling of glass taking place at high temperatures, as microparticles of the crucible material. The improvement or modification of the technology of growth of laser active media and the purification of initial materials may minimise the number of microinclusions and suppress this failure mechanism.

Breakdown is usually associated with the formation of a subthreshold avalanche or multiphoton ionisation of defects or natural states of the matrix under the effect of the field of the light wave increasing the efficiency of absorption as a result of the appearance of excited carriers and dye centres [49].

A significant role in the failure of the active medium may be played by non-linear processes accompanying the propagation of radiation in the medium (in particular, self-focusing). In this case, the failure threshold is determined by the self-focusing threshold and not by the natural beam resistance of the material [48].

The build-up effect also plays a significant role in the processes of laser failure. In this effect, the micro-failure of the optical material takes place as a result of the effect of a series of laser radiation

pulses with the intensity lower than the threshold of single-pulse failure. In the presence of absorbing inclusions in the medium, this may be caused by the build-up of irreversible changes in the medium. In the absence of inclusions, the build-up effect is also observed but the reasons for this have not as yet been determined [49].

All the previously mentioned mechanisms also operate on the surface of the active medium. However, because of a considerably higher concentration of defects (in comparison with the concentration in the volume of the medium) in the subsurface layer there is a large scatter of the values of the breakdown threshold from specimen to specimen; in most cases, the thresholds of laser failure of the surfaces are lower (by a factor of 2 or more) than the threshold of volume failure [49].

It has been confirmed reliably that when self-focusing of radiation in the medium is avoided and the energy of the light quanta is smaller than the half width of the forbidden band, and there are no spatial-time fluctuations of laser radiation (single-mode and single-frequency radiation), the threshold of natural breakdown is a constant of the medium that does not depend on the radiation parameters and for K8 glass its value is 10^{13} W/cm^2 [49].

5.8 NEW OPTICAL CIRCUITS OF SOLID-STATE LASERS

Recently, new circuits and design of solid-state lasers have been developed ensuring high power and energy of radiation to be obtained with a high degree of spatial and time coherence. In solid-state lasers, a large part of the pumping energy is not converted to lasing radiation and is transferred to thermal energy, including heating of the active element. Thermal energy is removed from the active element from its surface by liquid flows. Consequently, thermal gradients and thermo-optical strains form in the active medium and lead to the distortion of the radiation wavefront, passing through the active medium.

The application of a circuit with the mechanical removal of the heat from the excitation channel makes it possible to eliminate the thermo-optical strains of the active medium [50] and obtain a high mean lasing power ($\geq$ 1 kW) at the diffraction divergence of radiation ($\leq$ 1 mrad). The application of thin flat sheets instead of round bars [51] under the condition of the homogeneity of pumping has greatly increased the lasing energy parameters with a significant improvement of the spatial characteristics of radiation.

In Ref. 52, the authors proposed a laser circuit with a plate-shaped active element with the zigzag passage of radiation through the plates. Consequently, it was possible to compensate the thermal optical distortions, induced in the active rod, by pumping radiation. The pumping radiation is induced in a plate-shaped active elements by bifocal lens with

birefringence [49]. In circuits with the zigzag passage, these distortions are compensated and added up together during the passage of the beam from one plane to another with the opposite sign. Consequently, compensation results in high spatial and angular characteristics of radiation. The output radiation power in optimised, compact circuits is higher than 0.5 kW, with a high beam coherence [53].

Chapter 6

Principles of lasing of solid-state lasers

6.1 QUANTUM KINETIC EQUATION FOR THE DENSITY MATRIX

In a semiclassic approximation in which the quantum fluctuations of the radiation field are ignored, the resonance interaction of the atom (or molecule) with the electromagnetic wave $\mathbf{E}(\mathbf{r}, t)$ can be described by the Schrödinger equation

$$\hbar \frac{\partial \Psi}{\partial t} = H\Psi \tag{6.1}$$

for the wave function $\Psi(\mathbf{r}, \xi, t)$, where $\mathbf{r}$ is radius-vector of the centre of inertia of the particles; ξ is the population of its internal co-ordinates. The particle energy is determined by the eigenvalues of the Hamiltonian

$$H = H_0 + \hbar V(\mathbf{r}, \xi, t) \tag{6.2}$$

which is represented by the sum of the operator of the energy of the non-perturbed electron shell and the operator of interaction with external fields $\hbar V$ $(\mathbf{r}, \xi, t)$.

In the statistical examination of the effect of the environment on the examined system, it is efficient to transfer from the wave function to the density matrix

$$\rho = \Psi^*(\mathrm{r}', \xi')\Psi(\mathrm{r}, \xi), \tag{6.3}$$

which makes it possible to describe by a simple procedure the completely and partially defined quantum mechanics state.

The Neuman equation for the density matrix

$$i\hbar \frac{\partial \rho}{\partial t} = [H, \rho], \tag{6.4}$$

obtained from (6.1) is, as is well known, the most general form of the quantum mechanics description of the evolution of different systems [1, 2]. In accordance with the principles of quantum theory, the calculations of the mean quantum mechanics values of the physical quantities are carried out using the equation

$$A = Sp_{\xi} \int \hat{A}\rho(\mathrm{r}\xi|\mathrm{r}\xi)d\mathrm{r}, \tag{6.5}$$

where $\hat{A}$ is the operator corresponding to quantity A.

When describing the interaction by internal variables and after averaging with respect to the degrees of freedom of the environment, excluding the field with a resonance interaction with the emission particle $\mathbf{E}(\mathbf{r}, t)$, equation (6.4) is greatly simplified and assumes the following form

$$\frac{\partial \rho_{jl}}{\partial t} = -i[V, \rho]_{jl} + R_{jl}, \tag{6.6}$$

where j, l are the indices of the energy levels. The interaction of the electromagnetic wave $\mathbf{E}$ ($\mathbf{r}$, t) with the examined particle is described in this case by the operator $V_{jl}(\mathbf{r}, t)$, whereas the operator R_{jl} takes into account the averaged-out effect of the environment on the particle which is usually assumed to be a stationary random process.

In the model of the relaxation constants, the quantum kinetics equations (6.6) have the following form

$$\left(\frac{\partial}{\partial t} + \Gamma_{jl}\right)\rho_{jl} = q_j \delta_{jl} - i[V, \rho]_{jl}. \tag{6.7}$$

Here Γ_{jl} are the elements of the relaxation matrix in the case in which their correlation time is short in comparison with the characteristic time of variation of $\rho_{jl}(t)$. The diagonal elements of the density matrix determine the population of the energy levels of j; non-diagonal elements ρ_{jl} characterise the correlation of the states j and l; the quantities q_j take into account the excitation of levels j.

For the simplest two-level model of the active particles, the system of equations for the elements of the density matrix, corresponding to the *m–n* transition, has the following form

$$\begin{aligned}
&\left(\frac{\partial}{\partial t}+\Gamma_m\right)\rho_{mm} = q_m + 2\,\mathrm{Re}\left(iV^*_{mn}\rho_{mn}\right),\\
&\left(\frac{\partial}{\partial t}+\Gamma_n\right)\rho_{nn} = q_n - 2\,\mathrm{Re}\left(iV^*_{mn}\rho_{mn}\right) + A_{mn}\rho_{mm},\\
&\left(\frac{\partial}{\partial t}+\Gamma\right)\rho_{mn} = iV_{mn}\left(\rho_{mm}-\rho_{nn}\right),
\end{aligned} \tag{6.8}$$

here Γ_m, Γ_n are the total widths of the working levels *m*, *n*; Γ is the constant of polarisation relaxation, induced by the radiation resonant in respect of *m–n*; A_{mn} is the Einstein probability of spontaneous decay. Equations of this type were obtained for the first time by Bloch for describing the precession of the nucleus spin in the magnetic field. From the physics of nuclear magnetic resonance, investigators transferred to the quantum electronics of the concept of transverse and longitudinal relaxation $T_2 = \Gamma^{-1}$, $T_1 = \Gamma_m^{-1}$ (and $\Gamma_m = \Gamma_n$), respectively.

In the electric dipole approximation, the operator of interaction with the electromagnetic field can be described by the equation

$$V_{mn} = -\frac{\mathrm{d}_{mn}\mathrm{E}e^{i\omega_{mn}t}}{\hbar} \tag{6.9}$$

where $\mathbf{d}_{mn}$ is the matrix element of the operator of the electric dipole moment $\mathbf{d}$; ω_{mn} is the Bohr frequency of the *m–n* transition. The polarisation of the medium $\mathbf{P}$ is the total dipole moment of the unit volume, and can be calculated from the following equation:

$$\mathrm{P} = Sp\left(\mathrm{d}\rho\right) \tag{6.10}$$

where the spur is calculated from the variables of the entire ensemble of the particles in the unit volume. In particular, the following relationship for polarisation corresponds to the two-level approximation:

$$\mathrm{P} = 2\,\mathrm{Re}\left(\mathrm{d}_{mn}\rho_{mn}e^{i\omega_{mn}t}\right). \tag{6.11}$$

The formal solution of the last equation of the system (4.8) has the following

form

$$\rho_{mn} = -\frac{i\mathrm{d}_{mn}}{\hbar}\int_{-\infty}^{t} e^{-\Gamma(t-t')-i\omega_{mn}t'}\mathrm{E}(t')N(t')dt'. \tag{6.12}$$

$$N = \rho_{mm} - \rho_{nn}$$

is the difference of the populations of the working levels. Consequently

$$\mathrm{P} = i\frac{|\mathrm{d}_{mn}|^2}{\hbar}\int_{-\infty}^{t}\left[e^{=\Gamma(t-t')+i\omega_{mn}(t-t')} - e^{-\Gamma(t-t')-i\omega_{mn}(t-t')}\right]\mathrm{E}(t')N(t')dt' \tag{6.13}$$

After double differentiation of these equations with respect to time, we obtain the following equation for the polarisation vector:

$$\frac{d^2\mathrm{P}}{dt^2} + 2\Gamma\frac{d\mathrm{P}}{dt} + \left(\Gamma^2 + \omega_{mn}^2\right)\mathrm{P} = -\frac{2\omega_{mn}}{\hbar}\mathrm{d}_{mn}^{*}\left(\mathrm{d}_{mn}\mathrm{E}(t)\right). \tag{6.14}$$

This equation, together with the equation for the difference of the populations $N(t)$ and the Maxwell equations for the electromagnetic field E, can be used for describing the laser generation process in a self-consistent manner.

6.2 EQUATIONS FOR THE ELECTROMAGNETIC FIELD

The electromagnetic field in a laser resonator can usually be represented in the form of two running waves:

$$\mathbf{E}(z, t) = \frac{e^{-i\omega t}}{2}\sum_{s\pm1}\mathbf{E}_s(t)e^{iskz} + k.s., \tag{6.15}$$

where $\mathbf{E}_s(t)$ are the slowly changing functions of time; the index s indicates the direction of propagation of the running wave with the frequency ω and the wave vector $k = \omega/c$. In a laser with a ring resonator, the lasing conditions form when $\mathbf{E}_s \neq \mathbf{E}_{-s}$. For a laser with a Fabry–Perot resonator we have: $\mathbf{E}_s = \mathbf{E}_{-s}$.

The field $\mathbf{E}(z, t)$ is governed by the Maxwell equations which can be written in the following convenient form:

$$\varepsilon_{\alpha\beta}\frac{\partial^2 E_\beta}{\partial t^2} - c^2\frac{\partial^2 E_\alpha}{\partial z^2} + \sigma_{\alpha\beta}\frac{\partial E_\beta}{\partial t} + 4\pi\frac{\partial^2 P_\alpha}{\partial t^2} = 0,$$
$$\alpha, \beta = x, y, z. \tag{6.16}$$

Here $\varepsilon_{\alpha\beta}$ is the tensor of dielectric permittivity; for the medium with no optical activity $\varepsilon_{\alpha\beta} = \delta_{\alpha\beta}$. All losses in the resonator are taken into account by introducing the tensor of effective conductivity $\sigma_{\alpha\beta}$. Consequently, it is the necessary to solve the boundary problem because the description of the losses by ohmic conductivity gives the same results.

The vector of polarisation of the active medium **P** is expressed by the density matrix using equation (6.7), which makes it possible to represent it in the form identical to (6.15):

$$\mathrm{P}(z, t) = \frac{e^{-i\omega t}}{2} \sum_{s=\pm 1} \mathrm{P}_s e^{iskz}. \tag{6.17}$$

Substituting (6.15) and (6.70) into (6.16), and carrying out averaging with respect to high-frequency oscillations, we obtain an equation for slow amplitudes of the field:

$$\left[\varepsilon_{\alpha\beta} \frac{\partial}{\partial t} + \frac{i}{2\omega} \left(\sigma_{\alpha\beta} c^2 k^2 - \varepsilon_{a\beta} \omega^2 \right) + \frac{\sigma_{\alpha\beta}}{2} \right] E_{s\beta} = 2\pi i \omega P_{s\beta}. \tag{6.18}$$

Subsequently, we examine the case of linearly polarised radiation and $\sigma_{\alpha\beta} = \sigma\delta_{\alpha\beta}$. Consequently, the equations can be greatly simplified.

6.3 MODELLING OF LASER SYSTEMS

The effect of an illuminating filter or some other non-linear medium under the effect of coherent radiation is modelled quite easily in the two-level approximation. The main equations, describing the behaviour of the two-level system in the field of the running wave, taking into account equation (6.18), have the following form

$$\frac{\partial P_s}{\partial t} - (\omega - \omega_{mn}) i P_s + \Gamma P_s = \frac{|d|^2}{3\hbar} i N E_s, \tag{6.19}$$

$$\frac{\partial N}{\partial t} = \gamma (N_0 - N) + \frac{1}{2\hbar} \left(E_s^* P_s - E_s P_s^* \right), \tag{6.20}$$

$$\begin{gathered} s \frac{\partial E_s}{\partial z} + \frac{1}{c} \frac{\partial E_s}{\partial t} + \frac{\sigma}{2c} E_s i \frac{\omega - \omega_r}{c} E_s = \frac{2\pi i \omega}{c} P_s, \\ \gamma = \Gamma_m = \Gamma_n \quad N_0 = \frac{q_m - q_n}{\gamma}. \end{gathered} \tag{6.21}$$

Here ω_r denotes the eigen frequency of the resonator which can differ both from the frequency of resonance transition ω_{mn} and from the frequency of the electromagnetic field ω; d is the reduced matrix element of the dipole moment.

The spatial heterogeneity of the inversion of populations might become evident in the field of coherent counter waves. At not too high intensities it is accompanied by the oscillator spatial modulation of the inversion of the populations of the type

$$N(z,t)N_1(z,t)+\left[N_2(z,t)e^{2ikz}+k.s.\right], \tag{6.22}$$

where $N_1(z, t)$ is the component of the inversion of the populations, slowly changing along the z axis; $N_2(z, t)$ is the amplitude of the rapidly changing part of the inversion of the populations, reflecting the presence of its spatial modulation. The system of self-consistent equations in this case has the form

$$\begin{gathered}\left[\partial_t+\Gamma-i(\omega-\omega_{mn})\right]P_s=i\frac{|d|^2}{3\hbar}(E_sN_1+E_{-s}N_{2s}),\quad s=\pm1;\\ N_{2s}=N_2\quad s=+1;\quad N_{2s}=N_2^*,\quad s=-1;\end{gathered} \tag{6.23}$$

$$(\partial_t+\gamma)N_1=N_0\gamma+\frac{i}{2\hbar}\sum_{s=\pm1}\left(E_s^*P_s-E_sP_s^*\right); \tag{6.24}$$

$$(\partial_t+\gamma)N_{2s}=\frac{i}{2\hbar}\left(E_s^*P_{-s}-E_{-s}P_s^*\right); \tag{6.25}$$

$$\left[\partial_t+\frac{\sigma}{2}-i(\omega-\omega_r)\right]E_s+cs\partial_zE_s=2\pi iwP_s. \tag{6.26}$$

The systems of equations (6.90)–(6.21) and (6.23)–(6.26) are analysed taking into account the boundary conditions, determined by laser geometry, and the initial conditions.

We examine a ring-shaped running wave laser on the condition that the rate of polarisation relaxation is high:

$$\partial_tP_s<<\Gamma P_s. \tag{6.27}$$

In this case, it may be assumed that the polarisation of the medium tracks the changes of the field:

$$P_s = \frac{|d|^2}{3\hbar}\frac{iNE_s}{\Gamma - i\Omega'}, \quad \Omega = \omega - \omega_{mn}. \tag{6.28}$$

In this case, the ring-shaped running wave laser can be described by the balance equations:

$$(\partial_t + \gamma)N = N_0\gamma - BU_sN; \tag{6.29}$$

$$(\partial_t + \sigma)U_s + sc\partial_z U_s = \beta NU_s; \tag{6.30}$$

$$U_s = \frac{|E_s|^2}{4\pi}, \quad B = 2B_{mn}(\omega), \quad \beta = \frac{B_{mn}\hbar\omega}{c},$$

where U_s is the density of radiation equal to the amount of energy of the electromagnetic field in the unit volume of matter;

$$B_{mn}(\omega) = \frac{4\pi|d|^2\Gamma}{3\hbar^2\left[\Gamma^2 + (\omega - \omega_{mn})^2\right]} \tag{6.31}$$

is the spectral Einstein coefficient characterising the probability of forced transition; BU_s is the quantity proportional to the probability of forced transition; BN describes the resonance amplification ($N > 0$) or absorption ($N < 0$) in the medium.

The density of radiation U_s in J/cm^3 is linked with the intensity of radiation I_s (W/cm^2) and with the number of photons in the unit volume n_s in cm^{-3} by the following equation:

$$U_s = \frac{I_s}{c} = n_s\hbar\omega. \tag{6.32}$$

In a laser with counter waves, if the periodic population grating does not form, it may be assumed that $N_2 = 0$, $N = N_1$, and the lasing behaviour at $\omega = \omega_r = \omega_{mn}$ in the balance approximation can be described by the equation:

$$(\partial_t + \gamma)N = N_0\gamma - BNU, \quad U = U_{+1} + U_{-1} \tag{6.33}$$

and by two equations of type (6.30) at $s = \pm 1$. For the processes that

are slow in comparison with the duration of double passage of radiation along the resonator T, these equations transform into a single equation for the total density of radiation U:

$$\partial_t U = \mu(\beta N - \sigma_0)U. \tag{6.34}$$

Here σ_0 is the coefficient of laser radiation losses; μ is the degree of filling of the resonator by the active medium. The system of equations (6.33), (6.34) corresponds to the simplest model of the solid-state laser and makes it possible to examine important relationships governing generation.

The systems of the energy levels of the active media enable the inversion of populations to be developed between two levels in the generation channel using external energy sources. For controlling lasing, in addition to the active medium, it is necessary to introduce laser media with the non-linear dependence of the difference of the populations of two levels of the intensity of laser radiation. Figure 6.1 shows the schema of the energy levels in cases of laser media that are of greatest interest for practice.

For the displayed two-, three- and four-level systems with the working m–n transition on the condition that polarisation tracks the resonance field of radiation, the behaviour of laser lasing is described by the balance equations (6.33), (6.34). However, in these schemes, the relaxation constant of the inversion of populations γ, the initial value of the inversion N_0 and coefficient B show different dependences of the probability of spontaneous decay A_{jl}, the probabilities of non-optical transition ν_{jl} and the probability of forced transitions.

1. For the two-level system (Fig. 6.1a), we have

$$\gamma = A_{mn} + \nu_{mn}, \quad N_0 = -q_n, \quad B = 2B_{mn}(\omega), \tag{6.35}$$

where the coefficient is described by equation (6.31).

2. A ruby laser operates on the basis of the three-level schema (6.1b). Taking into account the probability of forced absorption $B_p U_p$ in the pumping channel $n \to l$, the parameters of equation (6.33) have the following form:

$$\gamma = \eta B_p U_p + \gamma_{mn}, \quad \eta = \gamma_{lm}(\gamma_{\ln} + \gamma_{lm})^{-1}, \quad \gamma_{ji} = \alpha_{ji} + \nu_{ji}; \tag{6.36}$$

$$N_0 - q_n(\eta B U_p - \gamma_{mn})(\eta B_p U_p + \gamma_{mn})^{-1}. \tag{6.37}$$

Quantity η denotes the fraction of particles falling from the level l on

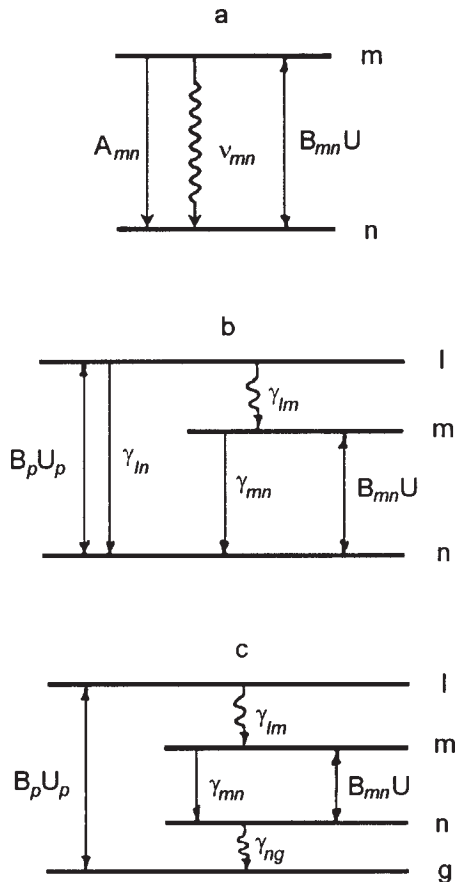

Fig. 6.1 Diagrams of energy levels and probability of transition between them in two-level (a), three-level (b) and four-level (c) laser systems.

the upper working level *m*.

3. The 4-level schema (6.1c), is described by the relationships:

$$N_0 = \eta B_p U_p \left(\eta B_p U_p + \gamma_{mg} + \gamma_{ng}\right)^{-1}, \quad \eta = \gamma_{lm}\left(\gamma_{lm} + \gamma_{\lg}\right)^{-1}. \tag{6.38}$$

In the initial stage of initiation of lasing when the radiation density U is not high and the level n can be regarded as not populated, the constants γ and B are expressed by the equations:

$$\gamma = \eta B_p U_p + \gamma_{mn} + \gamma_{mg}, \quad B = B_{mn}(\omega). \tag{6.39}$$

In the lasing regime, radiation density increases and together with it

the populations n, and in this case

$$\gamma = 2\left(\eta B_p U_p + \gamma_{mn} + \gamma_{mg}\right), \quad B = 2B_{mn}(\omega). \tag{6.40}$$

The four-level schema is used in the majority of lasers in which the media are activated by the ions of rare-earth elements (in particular, aluminium–yttrium garnet and glasses activated by Nd ions).

6.4 FREE LASING

In the previous section, it was shown that the simplest model of the solid-state laser is defined by the system of equations (6.33), (6.34) for the inversion of the populations N and radiation density U. The system permits the following stationary solutions:

$$U = 0, \quad N = N_0; \tag{6.41}$$

$$N_c = \frac{\sigma_0}{\beta}; \quad U_c = \frac{\gamma}{B}\left(\frac{N_0}{N_c} - 1\right). \tag{6.42}$$

The trivial solution of (6.40) corresponds to the case of the maximum attainable excitation of the medium in the absence of lasing. The solution of (6.41) describes the usual stationary lasing in which the gain in the system is equal to the losses.

Analysis of the stability of the stationary state of relatively small perturbations ΔU, ΔN is carried out by means of linearisation with respect to these perturbations. In this case, the solution of the linearised system of equations is found in the form

$$\Delta U \sim e^{\lambda t}, \quad \Delta N \sim e^{\lambda t}. \tag{6.43}$$

The roots of the quadratic characteristic equation in the case of the trivial solution

$$\lambda_1 = -\gamma, \quad \lambda_2 = \mu\left(BN_0 - \sigma_0\right) \tag{6.44}$$

show that it is stable at $\beta N_0 < \sigma_0$. In the reversed situation at $\beta N_0 > \sigma_0$, condition (6.40) is unstable and becomes a saddle-type singular point.

The stationary state (6.41) with non-zero intensity exists if $N_0 > N_c$. The characteristic equation for this case

$$\lambda^2 + \lambda \frac{\gamma N_0}{N_c} + \mu\sigma_0 B U_c = 0 \tag{6.45}$$

and its roots are

$$\lambda_{1,2} = -\frac{\gamma N_0}{N_c} \pm \sqrt{\frac{\gamma^2 N_0^2}{4 N_c 2} - \mu\sigma_0 B U_c}. \tag{6.46}$$

both roots are real and negative and

$$\left(\frac{\gamma N_0}{2 N_c}\right)^2 \geq \mu\sigma_0 B U_c. \tag{6.47}$$

In this case, small deviations from the stationary state are accompanied by a smooth return to this state, and the inversion tracks the field almost completely. The transition process of this type is characteristic of gas lasers and, in some cases, of solid-state lasers.

At a high density of radiation in stationary regime U_c, when the equality

$$\gamma < \frac{4\mu\sigma_0 N_c}{N_c}\left(1 - \frac{N_c}{N_0}\right), \tag{6.48}$$

is fulfilled, the roots of equation (6.44) are complex-conjugate

$$\lambda_{1,2} = -\tilde{\gamma} \pm i\nu; \tag{6.49}$$

$$\tilde{\gamma} = \frac{\gamma N_0}{2 N_c}; \tag{6.50}$$

$$\nu = \left[\mu\sigma_0 B U_c - \left(\frac{\gamma N_0}{2 N_c}\right)^2\right]^{1/2}. \tag{6.51}$$

Here ν is the frequency of damping pulsations of radiation density U and the inversion of populations N. The damping of the pulsations is characterised by the real part of the roots of the characteristic equation $\tilde{\gamma}$. The solution of the system of equations (6.33), (6.34) in this situation can be written in the following approximate form:

$$U(t) = U_c + \alpha e^{-\tilde{\gamma}t} \cos \nu t, \quad \alpha = \text{const}; \tag{6.52}$$

$$N(t) = U_c + \alpha\sqrt{\frac{4N_c}{\mu B U_c}}e^{-\gamma t}\cos(\phi); \tag{6.53}$$

$$\phi = \arctan\left(\frac{\mu}{\tilde{\gamma}}\right). \tag{6.54}$$

Equation (6.51) for the frequency of pulsations indicates that they are determined by the dynamic Stark effect with the resonance effect of strong radiation on the working levels of the active medium. In fact, in the limiting case of high radiation density

$$U_c >> \frac{(\gamma N_0 / 2N_c)^2}{\mu\sigma_0 B} \tag{6.55}$$

the frequency of slightly damping pulsations

$$\nu = \sqrt{\mu\sigma_0 B U_c}, \tag{6.56}$$

is, as indicated by equation (6.31) for the Einstein coefficient $B_{mn} = B/2$, proportional to the Raby frequency

$$G = \frac{|d \| E_c|}{\hbar}, \tag{6.57}$$

chatacterising the light splitting of the working levels by the resonance field.

The realisation of the condition of existence of pulsations (6.48) depends on the ratio of the constants characterising the main relaxation processes in the system (the losses of radiation in the resonator $\mu\sigma_0$, the relaxation of the inversion of populations γ), and also the pumping determining the degree of excitation of the active system N_0. In particular, a ruby laser is characterised by the following values of the parameters of the active medium [3]: $\gamma = \gamma_{mn} \sim 300$ s^{-1}; $B \sim 600$ erg^{-1} cm^{3}s^{-1}; $\sigma_0 \sim 5 \times 10^9$ s^{-1}; $\mu \sim N_c/N_0 \sim 10^{-1}$; $\mu B U_c \sim \gamma$. The value of radiation density in the stationary regime U_c corresponds in this case to intensity $I_c = cU_c \sim 10^4$ W/cm^2, and the conditions of existence of the pulsations (6.47), determined by the dynamic Stark effect, are fulfilled. The frequency of pulsations and the damping constant of the pulsations in accordance with equations (6.50), (6.51) are evaluated as follows: $\nu \sim 1.2 \times 10^6$ s^{-1};

$\tilde{\gamma} \sim 1500\ s^{-1}$. Consequently, the period of pulsations is $T = 2\pi/\gamma \sim 5 \times 10^{-6}$ s, and approximately 10^2 oscillations take place during the characteristic time of damping of the pulsations $\tilde{\gamma}^{-1}$. This is in complete agreement with the experimental results.

For a laser on aluminium–yttrium garnet, activated by Nd ions, we have $\gamma = \gamma_{mn} + \gamma_{mg} \sim 4400\ s^{-1} \sim \mu BU_s$; $\sigma_0 \sim 3 \times 10^8\ s^{-1}$; $\mu \sim N_c/N_0 \sim 10^{-1}$. In this laser, inequality (6.48) is not fulfilled as efficiently as in the ruby laser, and the value of the damping constant $\tilde{\gamma}$ of the pulsations rapidly increases ($\tilde{\gamma} \sim 2 \times 10^4\ s^{-1}$) if the frequency of pulsations is unchanged. Therefore, in the laser with the active medium of this type, the pulsations regime changes very rapidly to the stationary generation regime. This weakening of the effect of the dynamic Stark effect on the generation process is associated with the screening of the working levels by external electron shells.

6.5 THE GIANT PULSE REGIME

Single powerful lasing pulses can be induced by means of a sharp change of the gain or losses in the laser resonator. For rapid active changes of the losses in the laser resonators, it is recommended to use mechanical or electro- and magneto-optical *Q*-factor modulators with the switching time of the losses from microseconds to fractions of microseconds.

The lasing behaviour of a laser with active disconnection of the losses can be described by the system of equations (6.33) and (6.34). The initial inversion of the populations $N(t)$ at the moment of disconnection of the initial losses $\tilde{\sigma}_0$ at $t = 0$ is restricted by their value:

$$N(0) \le \tilde{\sigma}_0 / \beta. \tag{6.58}$$

After a rapid decrease of the losses to the value $\sigma_0 < \tilde{\sigma}_0$ which can be carried out using sufficiently powerful and long-term pumping at the moment when the inversion reaches the value $\tilde{\sigma}_0 / \beta$, when the gain becomes equal to the initial losses, the radiation of the inversion in lasing of the giant pulse is almost completely independent of the pumping and spontaneous transitions. Therefore, in equation (6.33) only the term *BNU*, describing the forced transitions, will remain for the inversion of the populations, and the development of lasing in the giant pulse regime is described by the following system of equations

$$dN/dt = -BUN, \tag{6.59}$$

$$dU/dt = \mu(\beta N - \sigma_0 U.) \tag{6.60}$$

This system is reduced to the following differential equation

$$dU = -\frac{\mu}{B}\left(\beta - \frac{\sigma_0}{N}\right)dN, \tag{6.61}$$

whose integration at the initial conditions

$$U\Big|_{t=0} = 0, \quad N\Big|_{t=0} = N(0) = \frac{\tilde{\sigma}_0}{\beta} = N_0 \tag{6.62}$$

results in a relationship linking radiation density U_c with the inversion of the populations N:

$$U(t) = \frac{\mu\beta}{B}\left(N_0 - N - \frac{\sigma_0}{\beta}\ln\frac{N_0}{N}\right) \tag{6.63}$$

The maximum of the giant pulse corresponds to the values $U = 0$, $N = \sigma_0/\beta$, and radiation density is

$$U_{\max} = \frac{\mu\beta}{B}\left(N_0 - \frac{\sigma_0}{\beta}\right) - \frac{\mu\sigma_0}{B}\ln\frac{N_0\beta}{\sigma_0}. \tag{6.64}$$

Taking into account the coefficient of inactive losses σ, the power of the radiation passing outside the limits of the resonator is

$$A = SLU(t)(\sigma_0 - \sigma), \tag{6.65}$$

where S is the cross-sectional area of the active medium, l is its length. Substituting (6.64) into (6.65) makes it possible to determine the maximum power of radiation passing outside the limits of the resonator.

The lasing of the giant pulse is accompanied by the release of the energy

$$W_g = SL\beta\int_0^t N(t)U(t)dt = \frac{Sl\beta}{B}(N_0 - N_{\min}). \tag{6.66}$$

inside the active medium.

The value of the minimum inversion of populations N_{min} remaining after the lasing of a giant single pulse, can be determined from equation (6.61) taking into account the fact that at the minimum $N(t)$ we have $dN/dt = 0$ and $U \gg 0$ in accordance with (6.56):

$$N_0 - N_{\min} \approx \frac{\sigma_0}{\beta} \ln \frac{N_0}{N_{\min}}. \tag{6.67}$$

The energy of the single pulse, leaving the resonator, E_g is determined in this situation by the equation:

$$E_g = W_g \left(1 - \frac{\sigma}{\sigma_0}\right) = \frac{SlB}{B} \left(N_0 - N_{\min}\right) \left(1 - \frac{\sigma}{\sigma_0}\right). \tag{6.68}$$

This energy is lower than the total energy stored in the active medium

$$W_g^{(0)} = Sl\beta N_0 / B, \tag{6.69}$$

since the fraction $W_g^{(0)}$ is used as a result of the inactive losses in the resonator, and the other part, expressed by the equation

$$\Delta W_g^{(0)} = Sl\beta N_{\min} / B, \tag{6.70}$$

remains in the medium because of incomplete scintillation.

The mean duration of the giant single pulse Δt is evaluated by the following equation, taking equations (6.62), (6.65) into account:

$$\Delta t = \frac{E_g}{A_{\max}} = \frac{N_0 - N_{\min}}{\mu\sigma_0} \left[N_0 - \frac{\sigma_0}{\beta} \ln \left(\frac{\beta N_0}{\sigma_0} \right) \right]^{-1.} \tag{6.71}$$

The estimates for ruby and Nd glass lasers with active media with the length $l \sim 10$ cm, cross-section $S \sim 1$ cm^2 and the resonators with the length $l \sim 10^2$ cm show that the maximum value of the power of the giant pulse are $A_{\max} \sim 10^8$ W, its energy $E_g \sim 1 \div 10$ J, and the duration $\Delta t \sim 10 \div 10^2$ ns.

Chapter 7

Stochastic and transition processes in solid-state lasers

7.1 STATISTICAL MODELLING OF LASING

The lasing properties of solid-state lasers are determined to a large degree by stochastic processes which have been the subject of special attention in recent years [1, 2]. In this chapter, we examine the statistical model of the transition processes in lasing. The initial and non-linear stages of lasing are analysed in detail. A dependence is found between the lasing conditions and the fluctuations of the time of realisation of the transition process. In the approximation of weak saturation, the stochastic behaviour of lasing can be stimulated using the Langevin equation for the total number of lasing photons in the unit volume n, having the form [3,4]:

$$\frac{dn}{dt} = \alpha n - \gamma n^2 + G + f(t). \tag{7.1}$$

Here G is the mean value of the lasing rate; $f(t)$ is the part of the rate of lasing fluctuating in a random manner. In the stochastic non-linear differential equation (7.1), the function $f(t)$ describes the δ-correlated random process, determining the properties of the latter in a Langevin source of fluctuations [3–5]:

$$\langle f(t) \rangle = 0, \quad \langle f(t) f(t') \rangle = Gn\delta(t - t'). \tag{7.2}$$

The origin of these fluctuations is determined by the fact that the photons can be excited by non-equilibrium radiation, and also in the absorption of the quanta of vibrations of the lattice (phonons) and of the photons of thermal radiation which are in thermal equilibrium with the active medium. The region of applicability of the balance equation (7.1) for the concentration of the photons is restricted by the limits of taking into

account only the linear and quadratic [with respect to n] terms, corresponding to taking into account the process of amplification of radiation and the saturation effect. Term αn describes the lasing of photons as a result of optical pumping. α denotes the effective coefficient of amplification of radiation. The dependence of coefficient α on radiation frequency ω reflects the specific features of the heterogeneous medium, including solid-state nanostructures with quantum wells. The term $-\gamma n^2$ determines the first correction non-linear with respect to the amplitude of the light field in the polarisation of the active medium taking saturation into account. The fluctuations of the number of seed photons and different random processes determine, during the multiplication period, the stochastic behaviour of the dynamics of increase of the photon concentration. This behaviour is reflected in the fact that in multiple and rapid lasings ($\alpha > 0$), in comparison with the time

$$\tau_0 = \alpha^{-1} \tag{7.3}$$

the increase of the photon concentration to some level below the asymptotic value

$$n_s = \frac{\alpha}{\gamma} \tag{7.4}$$

takes place in different periods of time.

We shall note several special features of the increase of lasing intensity resulting directly from (7.1). The point $n = 0.5n_s$, being the inflection point of the curve $n = n(t)$, and the first derivative of the function $n(t)$ at this point is equal to

$$\left.\frac{dn}{dt}\right|_{n=0.5n_s} = \frac{\alpha^2}{\gamma}. \tag{7.5}$$

In multiple realisation of the transition process this quantity does not change. Consequently, the slope of the curves of increase of the photons concentration $n(t)$ in the vicinity of the value $0.5\ n_s$ should be the same; the fluctuations of the number of seed photons result in the random parallel displacement of the curves $n(t)$ in the vicinity of the level $n = 0.5\ n_s$. For the statistical analysis of the transition processes it is convenient [6,7] to transfer from the stochastic differential equation (7.1) to the corresponding Focker–Planck equation for the photon distribu-

tion function $W(n, t)$:

$$\frac{\partial W}{\partial t} + \frac{\partial}{\partial n}\left[(\alpha - \gamma n)n + G\right]W = \frac{\partial^2}{\partial^2}(GnW). \tag{7.6}$$

This transition and the criteria of applicability of the non-linear Focker-Planck equation have been examined in detail in [3–5]. Equation (7.6) is valid for not too high concentrations n because it was derived using only the first and second moments of this random quantity. It should be noted that equations of the same type were used previously when describing the gas-discharge plasma [8] and quantum fluctuations of lasing [9, 10].

The probability of finding the value of the photon concentration in the range from n to $n + dn$ at the moment of time t is $W(n, t)dt$. Equation (7.6) describes the evolution of the initial distribution of the 'seed' number of the photons $W(n_0, 0)$ at a sudden variation of the lasing parameter α from the value $\alpha = -\alpha_1 < 0$ (below the threshold $\alpha = 0$) to the value $\alpha = \alpha_2 \Rightarrow 0$ (above the threshold).

Function $W(n, 0)$ can be easily found by assuming that the stationary state is established below the threshold. The solution of equation (7.6) in the form

$$W(n, 0) = C\exp\left[\frac{-(\alpha_1 + \gamma n/2)n}{G_1}\right], \tag{7.7}$$

corresponds to the case $\partial W/\partial t = 0$, where G_1 is the value of parameter G below the lasing threshold. Since the number of photons prior to excitation is small, the role of saturation below the lasing threshold is also negligible. From (7.7) we have the exponential dependence of the normalised distribution function on n:

$$W(n, 0) = \frac{1}{n_1}\exp\left(-\frac{n}{n_1}\right); \quad n_1 = \frac{G_1}{\alpha_1}. \tag{7.8}$$

After supplying a right-angled excitation pulse, the asymptotic state of stationary lasing with the Gaussian distribution of the photons

$$W(n) = W_0 \exp\left[-\frac{(n-N)^2}{2\sigma^2}\right], \tag{7.9}$$

is established. This distribution was obtained from (7.6) at $\partial W/\partial t = 0$. Here W_0 is the normalisation multiplier; $N = \alpha_2/\gamma$ is the mean number of the photons in the stationary lasing regime; the parameter characterises the dispersion of photon distribution. The switching off of the pumping is accompanied by the attenuation of lasing and a smooth transition of the distribution (7.9) to the exponential distribution (7.8) at relatively long times.

7.2 INITIAL AND NON-LINEAR STAGES OF THE LASING PROCESS

We shall examine the process of increase of the photon concentration at $\alpha > 0$. The exact solution of equation (7.6), describing this process, is not possible. Therefore, we shall use a number of simplifications which, as shown later, are fully acceptable in the examined case. In the initial stage of lasing, where the photon concentration is low, it is possible to ignore the saturation effect, assuming that

$$\alpha_2 >> \gamma n. \tag{7.10}$$

Consequently, equation (7.6) is written in the following form

$$\frac{\partial W}{\partial t} + \frac{\partial}{\partial n}(\alpha n W) = G_2 \frac{\partial}{\partial n}\left(\frac{\partial W}{\partial n}\right). \tag{7.11}$$

Its general solution can be expressed on the basis of the Green function $\tilde{G}(n, t|n_0, t_0)$:

$$W(n, t) = \int_0^\infty \tilde{G}(n, t|n_0, t_0)\, dn_0; \quad t_0 = 0. \tag{7.12}$$

To find the solution, in accordance with Feller [11], we use the Laplace transform:

$$w(s, t) = \int_0^\infty W(n, t)\left|e^{-sn}\right. dn, \tag{7.13}$$

the equation (7.11) in the Laplace variables is transformed to the form:

$$\frac{\partial w}{\partial t} + s\left(G_2 s + \alpha_2\right)\frac{\partial w}{\partial s} = -G_2 w s + \varphi(t). \tag{7.14}$$

in this case, the function $\varphi(t) = 0$ because of the general properties of $W(n, t)$, and to determine the Green function, we use the solution

$$w\left(s, t|n_0, t_0\right) = \frac{1}{as+1}\exp\left(-\frac{bs}{as+1}\right); \tag{7.15}$$

Carrying out the reversed Laplace transform, we obtain

$$a = n_2\left\{\exp\left[\alpha_2\left(t-t_0\right)\right]-1\right\},\ \ b - n_0\exp\left[\alpha_2\left(t-t_0\right)\right]; \tag{7.16}$$

where $I_0(u)$ is the Bessel function of the apparent argument.

Consequently, the solution of equation (7.11) is the initial function (7.8) at $t_0 = 0$ can be written in the following form

$$W(n, t) = \left[n_1\exp\left(\alpha_1 t\right) + a\right]^{-1}\exp\left\{-n\left[n_1\exp\left(a_2 t\right) + a\right]^{-1}\right\}. \tag{7.17}$$

At $t > \alpha_2^{-1}$, we obtain

$$W(n, t) = \left[\overline{n}_0\exp\left(\alpha_2 t\right)\right]^{-1}\exp\left\{-n\left[\overline{n}_0\exp\left(a_2 t\right)\right]^{-1}\right\};$$
$$\overline{n}_0 = n_1 - n_2. \tag{7.18}$$

This equation is derived from equation (7.6) at $\gamma = 0$ without the diffusion term, if we re-determine the initial distribution (7.8), replacing n_1 by $\overline{n}_0$. At $t > \alpha_2^{-1}$, the term with G_2 in equation (7.6) can be ignored, and the effect of the noise at $t > 0$ is reduced to the effective increase of the initial seed by the value n_2.

Equation (7.18) describes the process of transition from the stationary state below the lasing threshold, characterised by the photon distribution function (7.8), to the state of the initial stage of excitation of lasing with the linear increase of the photon concentration, accompanied by a decrease of the fluctuations of this concentration. As indicated by (7.18), this corresponds to decrease at $t \to \infty$ of the probability $W(n, t)\Delta n$ of obtaining, as a result of excitation, a photon concentration differing from

Δn by no more than n. With the development of the transition process and the approach to the stage of the stationary state, the behaviour of the photon concentration becomes less and less stochastic.

We now examine the non-linear period of the increase of the electron concentration in which it is necessary to take into account the saturation effect. The subsequent effect of noise can be ignored. In this situation, we can use equation (7.6) without the diffusion term

$$\frac{\partial W}{\partial t} + \frac{\partial}{\partial n}\left[(\alpha_2 - \gamma n) n W\right] = 0 \tag{7.19}$$

with the initial condition (7.17).

The solution of the problem (7.17)–(7.19) can be written in the form of (7.12), where now $\tilde{G}(n, t|n_0, t_0)$ is the Green function of equation (7.15) having the following form:

$$\tilde{G}(n, t|n_0, t_0) = \frac{\partial \tilde{n}}{\partial n}\delta(\tilde{n} - n_0);$$
$$\tilde{n} = n_s\left[\left(\frac{n_s}{n} - 1\right)e^{\alpha_2(t-t_0)} + 1\right]^{-1}; \quad n_s = \frac{\alpha_2}{\gamma}. \tag{7.20}$$

From equations (7.12), (7.70) and (7.19) at $t > \alpha_2^{-1}$ we obtain:

$$W(n, t) = \frac{1}{\tilde{n}_0}\left(\frac{n_s}{n}\right)\exp\left\{-\alpha_2 t - \frac{n_s}{\tilde{n}_0}\eta\exp(\alpha_1, t)\right\};$$
$$\eta = \left[\frac{n_s}{(n-1)}\right]^{-1}. \tag{7.21}$$

Multiple activation of pumping, being the source of lasing, formally corresponds to the 'switching on' of parameter α_2. The value determines the density of the tracks of the increase of lasing, corresponding to multiple 'switching on' of parameter α_2 and the concentration of the photons in the range from n to $n + \Delta n$ at the moment of time t.

7.3 ANALYSIS OF THE RELATIONSHIP BETWEEN THE LASING CONDITIONS AND FLUCTUATIONS OF THE DURATION OF THE TRANSITION PROCESS

From the viewpoint of practical applications, of greatest interest are

the fluctuations of the time of increase of the photon concentration to some selected level η, which are characterised by the density of the probability of appearance of the given number of photons $\tilde{W}(t)$ in the time period from t to $t + \Delta t$. The distribution functions $W(n, t)$ and $\tilde{W}(t)$ are linked by the relationship

$$W(n, t) = \left|\frac{dn}{dt}\right| = \tilde{W}(t), \tag{7.22}$$

where

$$\frac{dn}{dt} = (\alpha_2 - \gamma n)n \tag{7.23}$$

is the equation of balance for the electron concentration, describing the non-linear stage of lasing.

Using the relationship (7.16), we obtain the expression for the distribution function $\tilde{W}(t)$, corresponding to the arbitrary initial distributions of the electron concentration $W(n_0)$:

$$\tilde{W}(t) = \alpha_2 \theta e^{-\theta} \int_0^\infty e^{-n_0/n} I_0\left(\eta\sqrt{\frac{n_0}{n_2}\theta}\right) W(n_0)dn_0;$$
$$\theta = \frac{n_s}{n_2}\eta e^{-\alpha_2 t}. \tag{7.24}$$

Using the representation of the modified Bessel function $I_0(u)$ in the form of a series, the time dependence can be expressed in the explicit manner:

$$\tilde{W}(t) = \alpha_2 e^{-\theta} \sum_{k=0}^{\infty} \frac{\theta^{k+1}}{(k!)^2} L_k; \tag{7.25}$$

$$L_k = \int_0^\infty e^{-n_0/n_2} \left(\frac{n_0}{n_2}\right)^k W(n_0)dn_0. \tag{7.26}$$

From equations (7.19)–(7.21) we obtain the following expression for the function $\tilde{W}(t)$:

$$\tilde{W}(t) = \alpha_2 e^{-\theta} \sum_{k=0}^{\infty} \frac{\theta^{k+1}}{(k!)^2} L_k. \tag{7.27}$$

The mean time $\tilde{t}$ to the appearance of the given concentration of the photons n, determined by level η and dispersion σ_t^2 of this time, calculated using (7.27) are equal to respectively:

$$\tilde{t} = t_m + \frac{C}{\alpha_2}; \tag{7.28}$$

$$\sigma_t^2 = \left\langle \left(t - \tilde{t}\right) \right\rangle = \frac{\pi^2}{6\alpha_2^2}. \tag{7.29}$$

Here C = 0.577 is the Euler constant

$$t_m = \frac{1}{\alpha_2} \ln\left(\eta \frac{n_S}{\bar{n}_0}\right) \tag{7.30}$$

is the time when the distribution function $\tilde{W}(t)$ reaches its maximum value

$$W_m = \frac{\alpha_2}{e} \cong \frac{\alpha_2}{2.718}. \tag{7.31}$$

the equation for $\tilde{W}(t)$, expressed through the parameters W_n and t_m has a simpler form:

$$\tilde{W}(t) = W_m \exp\left\{-\alpha_2\left(t - t_m\right) + 1 - \exp\left[\alpha_2\left(t - t_m\right)\right]\right\}. \tag{7.32}$$

it is not possible to define more accurately the condition of rapid activation of the source of excitation taking into account the fluctuations of the time to establishment of the stationary regime. It is evident that for this purpose it must be that the duration of radiation of the parameter should be considerably less than $\tilde{t} \sim \alpha_2^{-1}$.

The relative fluctuations of the time to establishment of the given concentration of the photons, determined in accordance with (7.28), (7.29) by the relationship

$$\frac{\sigma_t}{\bar{t}} = -\frac{\pi}{\sqrt{6\left[C + \ln\left(\eta n_s / \bar{n}_0\right)\right]}}, \tag{7.33}$$

at the fixed values of $\bar{n}_0$ and η decrease logarithmically with increasing stationary concentration n_2.

Thus, in the proposed physical model of the transition processes of laser lasing it is shown that to eliminate the fluctuations of the photon concentration, it is necessary to stabilise the number of seed particles to the excitation of lasing, and also in the initial stage of excitation with the duration of the order of $-\alpha^{-1}$.

7.4 THE STATISTICAL MODEL OF THE EXCITATION OF LASING IN THE ABSENCE OF INITIAL THERMODYNAMIC EQUILIBRIUM

We shall examine a statistical model of the excitation of a photoflux in the absence of the initial thermodynamic equilibrium. At the arbitrary initial distribution $W(n_0)$, the mean time of establishment of $\bar{t}$ and the dispersion σ_t^2 will be calculated using the expansion of (7.25). As a result, we obtain:

$$\bar{t} = \frac{1}{2}\sum_{k=0}^{\infty}\frac{L_k}{k!}\left[\chi - \psi(k+1)\right]; \quad \chi = \ln\left(n\frac{n_s}{n_2}\right); \tag{7.34}$$

$$\sigma_t^2 = \frac{1}{\alpha_2^2}\sum_{k=0}^{\infty}\frac{L_k}{k!}\left\{\left[\chi - \psi(k+1)\right]^2 + \zeta(2, k)\right\} - t^2, \tag{7.35}$$

where $\psi(k + 1)$ is the Euler psi function; $\zeta(2, k)$ is the Rieman ζ-function. It may be seen that the main dependence of $\bar{t}$ and σ^2_t on the excess above the lasing threshold α_2 is the same for the functions can $W(n_0)$ is differing in the arbitrary manner, whereas at the given values of the parameters α_2 and n_2, the quantities $\bar{t}$ and σ^2_t depend on the coefficients L_k, i.e. determined by the form of the initial distribution $W(n_0)$.

The relationships (7.34) and (7.35) can be used for analysis of the statistical phenomena determined by the effect of the pumping pulses, separated in time, on the active medium. It is assumed that a right-angled initial excitation pulse is applied to the active medium in such a manner as to establish the asymptotics value of stationary lasing with the Gaussian distribution of the photons (7.9). After switching off this pulse, lasing attenuates and the distribution (7.9) changes smoothly over a relatively long period of time to the exponential distribution (7.8), chatacterising the thermodynamically equilibrium state of the system. The second pulse is applied after time T after the completion of the first excitation pulse, and the distribution (7.9), transformed to the moment $t = T$ is a result

of the relaxation system, will represent the seed distribution for the subsequent increase of lasing. Consequently, the quantities $\bar{t}$ and σ^2_t, corresponding to this increase, depend in the given situation on the delay time T between the excitation pulses.

We shall explain the variation of the distribution (7.9) at the moment of time $t = T$, after rapid switching of the parameter of lasing to the position below the threshold of appearance of the lasing photons. We examine the case in which the role of noise is not large because the distribution of the photon concentration at the moment of collapse of lasing may be approximated by the delta function

$$W(n_0) = \delta(n(t) - n_0). \tag{7.36}$$

This condition is realised at high values of the lasing parameters α_1 below the threshold.

The function $n(t)$ can be easily determined from the balance equation describing the attenuation of lasing without taking the fluctuations into account

$$\frac{dn}{dt} = -(\alpha_1 + \gamma n)n. \tag{7.37}$$

Consequently, for the initial condition, we obtain

$$n(t) = Ne^{-\alpha_1 t}\left[\frac{1+(1-e^{-\alpha_1 t})\alpha_2^0}{\alpha_1}\right]^{-1}; \quad N = \frac{\alpha_2^0}{\gamma}, \tag{7.38}$$

where α^0_2 is the lasing parameter corresponding to the first excitation pulse; N is the mean concentration of the photons in the stationary lasing conditions. Consequently, the dependence of the quantities $\bar{t}$ and σ^2 on the delay time T can be determined by means of the relationships (7.34) and (7.35) in which now

$$L_k = \left[\frac{n(T)}{n_2}\right]\exp\left[-\frac{n(T)}{n_2}\right], \tag{7.39}$$

and $n(T)$ is defined by equation (7.37) at $t = T$.

As a result of the summation of the series (7.34), term-by-term differentiation and subsequent integration, the expression for the meantime to establishment of the given photon concentration, generated by the second excitation pulse, can be reduced to the following form:

$$\bar{t} = \frac{1}{\alpha_2}\left\{\ln\left[\frac{n_s}{n(T)}\eta\right] + Ei\left[\frac{n(T)}{n_2}\right]\right\}; \tag{7.40}$$

here $Ei(x)$ is the integral exponential function.

As previously, the dispersion σ_t^2 is expressed by means of a series. This complicates the analysis of the dependence of σ_t^2 on T. However, it may be shown that the function $\sigma_t^2(T)$ is, like the dependence of $\bar{t}$ on T, a monotonically increasing dependence. From (7.40) in the limiting case $T \to \infty$, we obtain

$$\bar{t} \approx \frac{1}{\alpha_2}\left[C + \ln\left(\eta\frac{n_s}{n_2}\right)\right]. \tag{7.41}$$

In this case, the equation for σ_t^2 coincides accurately with the expression (7.29), and the equation (7.41) for $\bar{t}$ corresponds to the expression (7.28) at $n_1 \to 0$. This is in agreement with the approximation of the initial distribution by the δ-function.

At $T \to 0$, the mean time $\bar{t}$ and the dispersion σ_t^2 rapidly decrease. We determine the asymptotic expressions for them at $N \gg n_2$:

$$\bar{t} \cong \frac{1}{\alpha_2}\ln\left(\eta\frac{n_s}{n_2}\right); \tag{7.41}$$

$$\sigma_t^2 \cong \frac{8}{\alpha_2^2}\left[\ln\left(\eta\frac{n_s}{n_2}\right)\right]^2 e^{-N/n_2}. \tag{7.43}$$

To calculate σ_t^2 in this case, we can use directly equation (7.24) where we use the first and second terms of the expansion of the modified Bessel function $I_0(u)$ into a series, and also the asymptotics of these functions at low and high values of the argument. As indicated by (7.42), (7.43), the values of $\bar{t}$ and σ_t^2 decrease with increase of the mean concentration of the seed photons.

7.5 TRANSITION PROCESSES AT SLOW CHANGES OF THE LASING PARAMETERS

The excitation of lasing by pulses with a flat leading edge (in particular, trapezoidal pulses) corresponds to slow changes of the lasing parameter. The change of the lasing parameter with time in the vicinity of the threshold is assumed to be approximately linear. The process of passage of the lasing threshold in the given situation is described by the equation:

$$\frac{dn}{dt} = (\beta t - \alpha - \gamma n)n, \tag{7.44}$$

where β is the rate of variation of the lasing parameters $\alpha = -\alpha_1 + \beta t$; α_1 is the value of the lasing parameter below the threshold as the moment of the start of examination $t = 0$.

With the variation of t, the parameters α converts to 0 at the moment $t = \alpha_1/\beta$. According to (7.28), at this moment $\bar{t} \to \infty$. Consequently, in the vicinity of the threshold at any suitable slow change of the value of α, the transition process in the conventional meaning of the word takes place, i.e. lasing 'does not manage to follow' the variation of external perturbation. However, at $t > \alpha_1/\beta$, the lasing parameter α differs from 0 and continues to increase. The time to establishment of the given photon concentration $\bar{t}$ decreases, and the lasing 'tracks' perturbation in a quasistationary manner:

$$n(t) = \frac{\beta t - \alpha_1}{\gamma}. \tag{7.45}$$

Using the solution of equation (7.44) at $(\beta t - \alpha_1) \gg \gamma n$, it may be shown that the linear period of the development of lasing is determined by the time $\tau > 2/\gamma n$. This time is approximately equal to the mean time of increase of lasing in the presence of fluctuations and determines the range in which the transition process takes place.

At $t \gg \alpha_1/\beta$, after the moment of time there is a steady regime of lasing with the Gaussian distribution of the photon concentration (7.9) where n is now determined by equation (7.45). The physical pattern is such that the lasing at every successive moment of time is developed on the basis of lasing in the previous moment with the approximately delta-shaped initial distribution. Naturally, the intensity of fluctuations rapidly decreases in this case. At the same time, the fluctuations of the time of decrease of lasing are considerably smaller than the fluctuations of the time of increase of lasing.

References

1 A.M. Prokhorov, UFN, **148**, No.7 (1986).
2 A. Einstein, Verhandl. Deutsch. Phys. Ges., **18**, No.318 (1916), Collection of studies, Vol.3, Nauka, Moscow (1956), p.386.
3 I.I. Rabi, Phys. Rev., **15**, No.652 (1937).
4 L.D. Landau and E.M. Lifshits, Quantum mechanics, Nauka, Moscow (1974).
5 S.H. Autler and S.H. Townes, Phys. Rev., **100**, No.703 (1995).
6 S.G. Rautian, et al, Nonlinear resonance in the spectra of atoms and molecules, Nauka, Novosibirsk (1979).
7 N.G. Basov and A.M. Prokhorov, ZhETF, **27**, No.431 (1954) and **28**, No.249 (1955).
8 N. Bloembergen, Phys. Rev., **104**, No.324 (1956).
9 V.M. Kantorovich and A.M. Prokhorov, ZhETF, **33**, No.1428 (1957).
10 A. Javan, Phys. Rev., **107**, No.1579 (1957).
11 H.T. Maiman, Brit. Commun. Electr., **1**, No.674 (1960).
12 J.E. Geusic, et al, Appl. Phys. Lett., **4**, No.182 (1964).
13 A.I. Burshtein, UFN, **143**, No.533 (1984).
14 V.V. Antsiferov, et al, ZhETF, **55**, No.122 (1968).
15 V.V. Antsiferov, et al, Optics. Comm., **14**, No.388 (1975).
16 V.V. Antsiferov, et al, Kvant. Elektronika, **2**, No.57 (1975).
17 V.V. Antsiferov and Yu.D. Golyaev, Optika i Spektr., **52**, No.706 (1982).
18 K.P. Komarov and V.D. Ugozhaev, Pism'a ZhTF, **8**, No.1237 (1982).
19 K.P. Komarov, et al, Optics. Communs., **57**, No.279 (1986).
20 V.V. Antsiferov, et al, ZhTF, **62**, No.7 (1992).
21 V.V. Antsiferov, et al, Optika i Spektr., **72**, No.191 (1992).
22 V.V. Antsiferov, ZhTF, **63**, No.8, 89 (1993).
23 J.S. Uppal, et al, Phys. Rev. A., **36**, No.4823 (1987).
24 R.G. Harrison, Contemp. Phys., **28**, No.341 (1988).
25 W. Forysiak, et al, Phys. Rev. A., **39**, No.421 (1989).
26 D.A. Cardimona, et al, Phys. Rev. A., **47**, No.1227 (1993).
27 M.K. Olsen, et al, Phys. Rev. A., **50**, No.5289 (1994).
28 V.E. Zhakharov and A.B. Shabat, ZhETF, **61**, No.118 (1971).
29 V.K. Mezentsev and G.I. Smirnov, ZhETF, **94**, No.336 (1988).
30 E.A. Kuznetsov and J.J. Rasmussen, Phys. Rev. E., **51**, No.4479 (1995).
31 L. Kramer, et al, Pism'a ZhETF, **61**, No.887 (1995).

Chapter 1

1 V.V. Antsiferov and G.V. Krivoshchekov, Symposium on Nonlinear Optics,, Nauka, Novosibirsk (1968), Izv. VUZov, Radiofizika, **10**, No.879 (1967).
2 V.V. Antsiferov and G.V. Krivoshchekov, Optika i Spektr., **24**, No.454 (1968).
3 V.V. Antsiferov and G.V. Krivoshchekov, ZhEFT, **56**, No.526 (1969).
4 V.V. Antsiferov and G.V. Krivoshchekov, ZhTF, **39**, No.931 (1969).
5 V.V. Antsiferov and V.S. Pivtsov, ZhTF, **41**, No.2594 (1971).
6 V.V. Antsiferov, et al, Optika i Spektr., **32**, No.1159 (1972).
7 V.V. Antsiferov, et al, Avtometriya, No.5, 98 (1972).

8 V.V. Antsiferov, et al, Kvant. Elektronika, No.3(15), 57 (1973).
9 V.V. Antsiferov, Avt. Kand. Dissert., IFP SO AN SSSR, Novosibirsk (1973).
10 V.V. Antsiferov, Avtometriya, No.6, 103 (1974).
11 V.V. Antsiferov, et al, Kvant. Elektronika, **2**, No.591 (1975).
12 V.V. Antsiferov, et al, Optika i Spektr., **38**, No.599 (1975).
13 V.V. Antsiferov, et al, ZhPS, **24**, No.18 (1976).
14 V.V. Antsiferov and V.I. Kravchenko, Prep. IF AN No.4, USSSR, Kiev (1988).
15 V.V. Antsiferov, et al, Prep. SFTI, No.89-1, TsNIIatom, Moscow (1989).
16 V.V. Antsiferov and A.F. Solokha, in: Physical interactions in chemical reacting media, MFTI, Moscow (1991), p.119.
17 V.V. Antsiferov, A.F. Solokha, in: Physical interactions in chemical reacting media MFTI, Moscow (1991), p.124.
18 V.V. Antsiferov, et al, ZhTF, **62**, No.3, 7 (1992).
19 V.V. Antsiferov, et al, Prep. IYaFSO RAN, No.93-112, Novosibirsk (1993).
20 V.V. Antsiferov, et al, Prep. IYaFSO RAN, No.93-107, Novosibirsk (1993).
21 V.V. Antsiferov, et al, Prep. IYaF SO RAN, No.93-50, Novosibirsk (1993).
22 V.V. Antsiferov, ZhTF, **63**, No.8, 89 (1993).
23 V.V. Antsiferov, Laser. Tekhnika i Optoelektronika, No.3-4, 27 (1993).
24 V.V. Antsiferov, Avt. Dokt. Diss., IAeE SO RAN, Novosibirsk (1993).
25 V.V. Antsiferov and A.F. Solokha, Izv. S.-Peterburg., Univers., No.480 (1995), p.89.
26 V.V. Antsiferov, Nauch. Vest., NGTU, No.1, 11 (1995).
27 V.V. Antsiferov and G.I. Smirnov, Preprint INP SB RAS, No.97-46 (1997).
28 V.V. Antsiferov and G.I. Smirnov, Solid state lasers, SGUPS, Novosibirsk (1997).
29 V.V. Antsiferov, et al, Proc. of SPIE, **3485**, No.410 (1998).
30 V.V. Antsiferov and G.I. Smirnov, Preprint IYaF So RAN, No.98-87, Novosibirsk (1998).
31 D. Ross, Laser Lichtverstarker und Oszillatoren. Akad. Verlag., Frankfurt (1966).
32 T.H. Maiman, et al, Phys. Rev., **123**, No.1151 (1961).
33 G.V. Bukin, et al, Kvant. Elektronika, **5**, No.1168 (1978).
34 J.C. Walling, et al, IEEE J. Quant. Electron., **16**, 1302 (1980).
35 M.L. Shand and J.C. Walling, IEEE J. Quant. Electron., **18**, No.1829 (1982).
36 B. Struve, et al, Appl. Phys., **30**, No.117 (1983).
37 E.V. Zharikov, et al, Kvant. Elektronika, **10**, No.1916 (1983).
38 U. Brauch and U. Durr, Optics Communs., **49**, No.61 (1984).
39 S.T. Lai, et al, IEEE J. Quant. Electron., **24**, No.1922 (1988).
40 A.A. Kaminskii, et al, Izv. AN SSSR, Ser. Neorg. Ater., **23**, No.1931 (1987).
41 V. Petricevic, et al, Appl. Phys. Lett., **52**, No.1040 (1988).
42 F.R. Marshall and O.L. Roberts, Proc. IRE, Vol.50 (1962), p.2108.
43 R.H. Pantell and J. Warszawski, Appl. Phys. Lett., **11**, No.213 (1967).
44 T.I. Kuznetzova and S.G. Rautian, FTT, **5**, No.2105 (1963).
45 J. Free and A. Korpel, Proc. IRE, **52**, No.90 (1964).
46 B.L. Livshits, et al, Pism'a ZhETF, **1**, No.23 (1965).
47 E.A. Gerber and E.R. Ahlstrom, J. Appl. Phys., **35**, No.2546 (1964).
48 G.A. Askar'yan, ZhETF, **42**, No.1672 (1962).
49 C.L. Tang, et al, Appl. Phys. Lett., **2**, No.222 (1963).
50 R.V. Ambartsumyan, et al, ZhETF, **51**, No.724 (1966).
51 V. Evtuhov and A.E. Siegman, Appl. Optics, **4**, No.142 (1965).
52 J. Buchert and R.R. Alfano, Laser Focus, No.9, 117 (1983).
53 M.L. Shand and S.T. Lai, IEEE, J. Quant. Electron., **20**, No.105 (1984).
54 J. Buchert, et al, IEEE, J. Quant. Electron., **19**, No.1477 (1983).
55 Z. Hasan, et al, Physic C: Solid State Physics, No.19, 6381 (1986).
56 V.S. Gulev, et al, Kvant. Elektron., **14**, No.1990 (1987).

57 W. Kolbe, et al, IEEE J. Quant. Electron., **21**, No.1596 (1985).
58 K. Peterman and P. Mitzcherligh, IEEE J. Quant. Electron., **23**, No.1122 (1987).
59 V.S. Gulev, et al, Avt. Svidetel., SU N 1364189 A1, H01S 3/16 (1985).

Chapter 2

1 V.V. Antsiferov and N.M. Derzhi, ZhPS, **21**, No.921 (1974).
2 V.V. Antsiferov, Avt. Kand. Dissert., IFP SO AN SSSR, Novosibirsk (1973).
3 V.V. Antsiferov, et al, Optics. Comm., **14**, No.388 (1975).
4 V.V. Antsiferov, Preprint SFTI, No.4, Sukhumi (1980).
5 V.V. Antsiferov and Yu.D. Golyaev, Optika i Spetkr., **52**, No.706 (1982).
6 V.V. Antsiferov, Preprint SFTI, No.88-1, TsNIIatominform, Moscow (1988).
7 V.V. Antsiferov, et al, in: Interactions in spontaneous waves, Donish, Dushanbe (1988).
8 V.V. Antsiferov, et al, Preprint SFTI, No.90-15, TsNIIatom, Moscow (1990).
9 V.V. Antsiferov and G.V. Khaburzaniya, Lazer. Tekhnika i Optoeletronika, No..2(58), 3 (1991).
10 V.V. Antsiferov, et al, Tekhnika i Optoelektronika, No.2(58), 6 (1991).
11 V.V. Antsiferov, et al, Preprint, No.1820, IKI RAN, Moscow (1992).
12 V.V. Antsiferov and G.V. Khaburzaniya, Optika i Spektr., **72**, No.1, 191 (1992).
13 V.V. Antsiferov and A.F. Solokha, Prikl. Zadachi aeromekh. i Geokosm. Fiz., MFTI, Moscow (1992), p.134.
14 V.V. Antsiferov and A.F. Solokha, Prikl. Zadachi aeromekh. i Geokosm. Fiz., MFTI, Moscow (1992), p.138.
15 V.V. Antsiferov and A.F. Solokha, Prikl. Zadachi. Aeromekh. i Geokosm. Fiz., MFTI, Moscow (1992), p.149.
16 V.V. Antsiferov and A.F. Solokha, Prikl. Zadachi aeromekh. i Geokosm. Fiz., MFTI, Moscow (1992), p.152.
17 V.V. Antsiferov and A.F. Solokha, Fiz. Vzaimod. Khim. Reagir. Sist., MFTI, Moscow (1993), p.67.
18 V.V. Antsiferov, ZhTF, **63**, No.5, 41 (1993).
19 V.V. Antsiferov, Preprint No .93-50, IYaF SO RAN, Novosibirsk (1993).
20 V.V. Antsiferov, et al, Preprint No.93-105, IYaF SO RAN,(1993).
21 V.V. Antsiferov, et al, Preprint. No.93-106, IYaF SO RAN, Novosibirsk (1993).
22 V.V. Antsiferov, et al, Preprint No.93-112, IYaF SO RAN, Novosibirsk (1993).
23 V.V. Antsiferov, Laser. Tekhn. Optoelektronika, No.3-4(70-71), 20 (1993).
24 V.V. Antsiferov, Avt. Dokt. Disser., IAiE SO RAN, Novosibirsk (1993).
25 V.V. Antsiferov, Nauch. Vest. NGTU, No.1, 11 (1995).
26 V.V. Antsiferov and G.I. Smirnov, Preprint No.97-46, INP SB RAS,
27 V.V. Antsiferov and G.I. Smirnov, Solid state lasers, SGUPS, Novosibirsk (1997).
28 V.V. Antsiferov, et al, Proc. of SPIE, **3485**, No.410 (1998).
29 V.V. Antsiferov and G.I. Smirnov, Preprint No.98-99, IYaF SO RAN, Novosibirsk (1998).
30 A.M. Prokhorov, et al, Kvant. Elektronika, **5**, No.725 (1978).
31 A.M. Prokhorov, UFN, **148** (1986).
32 A.A. Kaminskii, Physics and spectroscopy of laser crystals, Nauka, Moscow (1986).
33 A.A. Kaminskii and B.M. Antinenko, Multilevel functional circuits of crystal lasers, Nauka, Moscow (1989).
34 G.M. Zverev and Yu.D. Golyaev, Crystal lasers and their applications, Radio i Svyaz', Moscow (1994).
35 R.C. Morris, et al, Appl. Phys. Lett., **27**, No.444 (1975).
36 Kh.S. Bagdasarov, et al, Kvant. Elektron., **10**, No.1645 (1983).

37 A.A. Kaminskii, et al, Kvant. Elektronika, No.4, 113 (1971).
38 E. Snitzer, Phys. Rev. Lett., **7**, No.444 (1961).
39 W.H. Keene and J.A. Weiss, Appl. Optics., **3**, No.345 (1964).
40 N.S. Belokrunitskii and A.D. Manuil'skii, UFZh, **12**, No.1720 (1967).
41 E. Snitzer and R. Woodcock, IEEE J. Quant. Electr., **2**, No.627 (1966).
42 V.I. Malyashev, et al, ZhPS, **7**, No.662 (1967).
43 B.L. Livshits and V.N. Tsykunov, ZhETF, **49**, No.1843 (1965).
44 V.A. Schugov and G.P. Shupulo, FTT, **10**, No.2821 (1968).
45 W. Koechner, Appl. Optics., **9**, No.1429 (1970).
46 D.S. Sumida, et al, IEEE J. Quant. Electron., **24**, No.985 (1988).
47 U. Brauch, et al, Optics Communs., **73**, No.62 (1989).
48 E.V. Zharikov, et al, Kvant. Elektronika, **10**, No.140 (1983).
49 V.G. Ostroumov and I.A. Shcherbakov, Kvant. Elektronika, **12**, No.2413 (1989).
50 P.G. Golubev, et al, Kvant. Elektronika., **12**, No.1834 (1985).
51 R. Scheps, et al, Optics Eng., **27**, 830 (1988).
52 Kh.S. Bagdasarov, et al, Kvant. Elektronika, **10**, No.1014 (1983).
53 Kh.S. Bagdasarov, et al, Kvant. Elektronika, **10,** No.1645 (1983).
54 A.I. Alimpiev, et al, Tez. Dokl. XIV Mezhd. Konf. KiNO'91, Leningrad, **3**, No.60 (1991).
55 A.I. Alimpiev, et al, Cryst. Resear. Technol., **30**, No.295 (1995).
56 T.Y. Fan and M.R. Konta, Rev. Phys. Appl., **24**, No.827 (1989).
57 R.J. Dunsmuir, Electron. Control., **10**, No.453 (1961).
58 R.W. Hellwarth, Phys. Rev. Lett., **6**, No.9 (1961).
59 J.R. Singer and S. Wang, Phys. Rev. Lett., **6**, No.351 (1961).
60 N.G. Basov, et al, ZhETF, **49**, No.895 (1965).
61 A.V. Fainer and K.P. Komarov, Optika i Spektr., **44**, No.766 (1978).
62 H. Statz and C.L. Tang, J. Appl. Phys., **35**, No.1377 (1964).
63 J.A. Fleck and R.E. Kidder, J. Appl. Phys., **35**, No.2825 (1964).
64 V.I. Bespalov and A.V. Gaponov, Izv. VUZov, Radiofizika, **8**, No.70 (1965).
65 V.I. Bespalov and E.I. Yakubovich, Izv. VUZov, Radiofizika, **8**, No.909 (1965).
66 B.L. Livshits, DAN SSSR, **194**, No.1298 (1970).
67 A.P. Kazantsev, et al, Kvant. Elektronika, **2**, No.165 (1975).
68 Ya.I. Khanin, Izv. VUZov, Radiofiz., **9**, No.697 (1966).
69 B.L. Zhelnov and V.S. Smirnov, ZhETF, **55**, No.1332 (1966).
70 V.P. Byakov, DAN SSSR, **206**, No.1078 (1972).
71 B.P. Kursanov, et al, Kvant. Elektronika, **1**, No.2211 (1974).
72 A.A. Pavlyuk and L.P. Kozeeva, Izv. SO AN SSSR, Ser. Khim. Nauk., **2**, No.91 (1976).
73 A.A. Pavlyuk, et al, Izv. AN SSSR, Ser. Neorg. Mater., **19**, No.847 (1983).

Chapter 3

1 V.B. Markov, et al, ZhETF, **64**, No.1538 (1973).
2 O.N. Pogorelyi, et al, Pis'ma ZhTF, **2**, No.49 (1976).
3 L. Girkovic, et al, Appl. Optics, **7**, No.981 (1968).
4 H.G. Danielmeyer, J. Quant. Electron., **6**, No.101 (1970).
5 Yu.N. Belyaev, et al, Izv. VUZov, Radiofizika, **13**, No.1405 (1970).
6 M. Hercher, Appl. Phys. Lett., **7**, No.32 (1965).
7 E.I. Nikonova, et al, Optika i Spektr., **22**, No.984 (1967).
8 A.L. Egorov, et al, Kvant. Elektronika., **2**, No.513 (1975).
9 J. Morellec, et al, Appl. Optics, **18**, No.141 (1979).
10 J.M. McMahon, IEEE J. Quant. Electr., **5**, No.489 (1969).
11 A.L. Mikaelyan, et al, Kvant. Elektronika, No.2, 96 (1971).

12 E.D. Isyanova, et al, ZhPS, **12**, No.834 (1970).
13 D.C. Hanna, et al, Optoelectronics, **3**, No.163 (1971).
14 A.N. Bondarenko, et al, Pis'ma, ZhETF, **6**, No.692 (1967).
15 Yu.V. Vinogin, et al, Optika i Spektr., **28**, No.168 (1970).
16 A.N. Bondarenko, et al, Izv. VUZov. Radiofizika, **12**, No.1895 (1969).
17 A.M. Dukhovnyi, et al, Optika i Spektr., **33**, No.733 (1972).
18 I.G. Zubarev and S.I. Mukhailov, Kvant. Elektronika, **1**, No.625 (1974).
19 L.E. Erikson and A. Szabo, Appl. Phys. Lett., **18**, No.433 (1971).
20 V.V. Kulikov, et al, Kvant. Elektronika, **7**, No.432 (1980).
21 R.F. Boikova and E.E. Fradkin, Optika i Spektr., **22**, No.834 (1967).
22 L.N. Derzhgin, et al, Radiotech. i Elektron., **16**, No.141 (1971).
23 V.V. Antsiferov, et al, Avtometriya, No.5, 94 (1972).
24 V.V. Antsiferov, et al, ZhPS, **18**, No.38 (1973).
25 V.V. Antsiferov, Avt. Kand. Dissert., IFP SO AN SSSR, Novosibirsk (1973).
26 V.V. Antsiferov, et al, Avtometriya, No.6, 97 (1974).
27 V.V. Antsiferov, et al, Kvant. Elektronika, **2**, No.57 (1975).
28 V.V. Antsiferov, et al, Preprint No.987, IKI AN SSSR, Moscow (1985).
29 V.V. Antsiferov, et al, Lazer. Tekhn. Optoelektr., No.2(58), 3 (1991).
30 V.V. Antsiferov, et al, Preprint No.93-105, IYaF SO RAN, Novosibirsk (1993).
31 V.V. Antsiferov, et al, Preprint No.93-106, IYaF SO RAN, Novosibirsk (1993).
32 V.V. Antsiferov, et al, Preprint No.93-112, IYaF SO RAN, Novosibirsk (1993).
33 V.V. Antsiferov and A.F. Solokha, Fiz. Vzaim. Khim. Reagir. Sistemakh, No.71 (1993).
34 V.V. Antsiferov, Avt. Dokt. Dissert., IA iE SO RAN, Novosibirsk (1993).
35 V.V. Antsiferov, Laser Technology and optoelectronics, No.3-4 (1995), p.3.
36 V.V. Antsiferov and G.I. Smirnov, Solid state lasers, SGUPS, Novosibirsk (1997).
37 V.V. Antsiferov, Preprint No.97-43, IYaF SO RAN, Novosibirsk (1997).
38 V.V. Antsiferov, ZhTF, **68**, No.10, 74 (1998).
39 R. Hultsch, Phys. Status Solidi (A), **47**, No.415 (1978).
40 Yu.L. Gusev, et al, Pis'ma ZhTF, **3**, No.305 (1977).
41 A.P. Maiorov, et al, Pis'ma, ZhTF, **6**, No.941 (1980).
42 A.P. Maiorov, et al, ZhTF, **51**, No.2391 (1981).
43 V.A. Buchenkov, et al, Kvant. Elektronika, **8**, No.2239 (1981).
44 V.A. Arkhangel'skaya, et al, Izv. AN SSSR, Ser. Fiz., **46**, No.2012 (1982).
45 V.S. Burakov, et al, ZhPS, **36**, No.494 (1982).
46 S.G. Vasil'ev, et al, Pis'ma, ZhTF, **7**, No.217 (1981).
47 N.A. Ivanov, et al, Izv. AN SSSR, Ser. Fiz., **10**, No.1985 (1982).
48 H. Samelson, et al, IEEE J. Quantum Electron., **24**, No.1141 (1988).
49 R.C. Sam, Proc. SPIE, Vol.1021 (1989), p.61.
50 Y.K. Kuo and M. Birnbaum, Appl. Phys. Lett., **67**, No.173 (1995).
51 V.V. Antsiferov and M.V. Astaf'ev, Preprint No.96-53, IYaF SO RAN, Novosibirsk (1996).
52 I.S. Tyryshkin, et al, Kvant. Elektronika, **25**, No.505 (1998).
53 V.V. Antsiferov and E.V. Ivanov, Preprint No.99-40, IYaF SO RAN, Novosibirsk (1999).
54 V.A. Arkhangel'skaya and A.E. Poletimov, Optika i Spektroskopiya, **57**, No.377 (1984).
55 V.V. Antsiferov, et al, ZhTF, **62**, No.3, 9 (1992).
56 L.S. Vasilenko, et al, Pis'ma ZhETF, **12**, No.161 (1970).

Chapter 4

1 L.E. Hargove, et al, Appl. Phys., **5**, No.4 (1964).

2 H. Mocker and R. Collins, Appl. Phys. Lett., **7**, No.270 (1965).
3 V.I. Malyshev and A.S. Markin, ZhETF, **50**, No.339 (1966).
4 A.I. de Maria and D.A. Stetse, Appl. Phys. Lett., **8**, No.174 (1966).
5 V.S. Letokhov, ZhETF, **55**, No.1077 (1968).
6 B.Ya. Zel'dovich and T.I. Kuznetsova, UFN, **106**, No.47 (1972).
7 G.H.S. New, Report of Progress of Physics, No.46, 877 (1983).
8 A.M. Prokhorov, UFN, **148**, No.7 (1986).
9 N. Herman and B. Wilhelmi, Lasers with supershort pulses, Mir, Moscow (1986).
10 J.M. Halbat and D. Grischkowsky, Appl. Phys. Lett., **45**, No.1281 (1984).
11 A.M. Val'shin, et al, Kvant. Elektronika, **13**, No.1713 (1986).
12 P. Heinz and A.J. Laubereau, Opt. Soc. Amer., **6**, No.1574 (1989).
13 P. Heinz and A.J. Laubereau, Opt. Soc. Amer., **7**, No.182 (1990).
14 A. Agnesi and G.C. Reali, Opt. Commun., **81**, No.306 (1991).
15 M.P. Sorenson, et al, Opt. Comm., **90**, No.1289 (1992).
16 C.P. Huang, et al, Opt. Lett., **17**, No.1289 (1992).
17 C. Radsewicz, et al, Opt. Comm., k**102**, No.464 (1993).
18 D.J. Kuizenga, Optics Comm., **22**, No.156 (1977).
19 K.A. Stankov, Appl. Phys., **52**, No.158 (1991).
20 K.A. Stankov, Appl. Opt., **28**, No.942 (1989).
21 I.I. Peshko, et al, Preprint, IF AN USSR, Kiev (1984).
22 E.G. Lariontsev and V.N. Serkin, Kvant. Elektronika, **1**, No.2166 (1974).
23 W.H. Glenn, IEEE J. Quant. Electron., **11**, No.8 (1975).
24 A.V. Malinkevich, et al, Preprint No.82, Inst. Fiz. AN BSSR, Minsk (1975).
25 S. Shapiro (ed), Supershort light pulses, Mir, Moscow (1981).
26 A.S. Kul'yanov, et al, Kvant. Elektronika, **10**, No.1315 (1983).
27 V.V. Antsiferov, et al, Avtometriya, No.6, 97 (1974).
28 V.V. Antsiferov, et al, Kvant. Elektronika, **2**, No.57 (1975).
29 V.V. Antsiferov and G.I. Smirnov, Solid state lasers, SGUPS, Novosibirks (1997).
30 V.V. Antsiferov, Preprint No.99-41, IYaF SO RAN, Novosibirsk (1999).
31 J.E. Murray and D.J. Kuizenga, J. Appl. Phys. Lett., **37**, No.27 (1980).
32 C.H. Brito Cruz, et al, Opt. Comm., **40**, No.298 (1982).
33 A.S. Kuch'yanov, Avtoref. Kand. Diss., IAiE SO RAN, Novosibirsk (1994).
34 K.P. Komarov, et al, Pis'ma ZhTF, **11**, No.168 (1985).
35 A.S. Kuch'yanov, Pis'ma ZHTF, **14**, No.665 (1988).
36 K.P. Komarov, et al, Kvant. Elektronika., **13, No.802 (1986).**
37 K. Burneika, et al, Kvant. Elektronika, **15**, No.1658 (1988).
38 A. Varanavichus, et al, Izv. AN SSSR, Ser. Fiz., **54**, No.2433 (1990).
39 S.A. Ametov, et al, Opt. Comm., **96**, No.75 (1993).
40 I.M. Bayanov, et al, Kvant. Elektronika, **16**, No.1545 (1989).
41 S.G. Rozuvan and E.A. Tikhonov, Kvant. Elektronika., **20**, No.163 (1993).
42 A.I. Andreeva, et al, Kvant. Elektronika, **16**, No.1604 (1989).
43 V.S. Gulev, et al, Izv. AN SSSR, Ser. Fiz., **56**, No.135 (1992).
44 A.V. Babushkin, et al, Kvant. Elektronika, **16**, No.2036 (1989).
45 R. Heinz, et al, Appl. Phys. A., **43**, No.209 (1987).
46 K.P. Komarov, et al, Opt. Commun., **5**, No.279 (1986).
47 H.A. Haus, Appl. Phys., **64**, No.3049 (1975).
48 W. Rudolph, Opt. Commun., **34**, No.491 (1980).
49 Yu. Vishchakas, et al, Kvant. Elektronika, **11**, No.2232 (1984).
50 B.I. Denker, et al, Kvant. Elektronika, **9**, No.1840 (1982).

Chapter 5

1 V.V. Antsiferov and G.I. Smirnov, Preprint No.98-98, IYaF SO RAN, Novosibirsk

(1998).
2 A.A. Mak, et al, OMP, No.1, 58 (1983).
3 A.D. Gondra, et al, Kvant. Elektronika, **14**, No.2449 (1987).
4 I.A. Pavlova, et al, Elektron. Tekhn. Ser. Laser. Tekhn. Optoelektronika., No.3(55), 108 (1990).
5 I.V. Dreval' and S.S. Pivovarova, Elektron. Tekhn. Ser. Laser. Tekhn. Optoelektronika., No.3(55), 108 (1990).
6 V.V. Antsiferov, et al, ZhTF, **62**, No.3, 9 (1992).
7 V.V. Antsiferov, et al, Preprint No.93-107 (1993).
8 N.I. Antropov, et al, Elektron. Tekhn. Ser. Laser. Tekhn. Optoelektronika., No.3(55), 106 (1990).
9 A.A. Danilov, et al, Kvant. Elektronika, **17**, No.1258 (1990).
10 Yu.G. Dyakova, et al, ???, Ser.11, Laser. Tekhn. Optoelektronika, No.6 (1989). CHECK ???
11 I.I. Kuratev and Yu.V. Tsvetkov, Izv. AN SSSR, Ser. Fiz., **54**, No.1994 (1990).
12 D.L. Sipes, Appl. Phys. Lett., **47**, No.74 (1985).
13 I.I. Kuratev, Elektron. Promsh., No.9(167), 97 (1987).
14 J. Berger, et al, Appl. Phys. Lett., **51**, No.1212 (1987).
15 R.A. Fields, et al, Techn. Digest. Conf. on Tunable Solid State Lasers Opt. Soc. of America (1989).
16 I.B. Vitrushchak, et al, ZhTF, **15**, No.36 (1989).
17 T. Day, et al, Electron. Lett., **25**, No.810 (1989).
18 V.V. Osiko, Izv. AN SSSR, Ser. Fiz., **51**, No.1285 (1987).
19 H.G. Danielmeyer and H.P. Weber, IEEE J. Quant. Electron., **8**, No.805 (1972).
20 S.R. Chinn and W.K. Zwicker, Appl. Phys. Lett., **31**, No.178 (1977).
21 B.I. Batyigov, et al, Kvant. Elektron., **3**, No.2243 (1976).
22 V.S. Gulev, et al, ZhPS, **32**, No.241 (1980).
23 Yu.K. Voroi'ko, et al, Izv. AN SSSR, Neorg. Mater., **2**, No.1161 (1966).
24 B.M. Antinenko and A.A. Mak, Spectroscopy of crystals, Nauka, Leningrad (1985), p.5.
25 Y. Tanabe and R.L. Sugano, J. Phys. Soc. Japan, **9**, No.760 (1954).
26 E.V. Zharikov, et al, Izv. AN SSSR, **48**, No.1330 (1984).
27 A.A. Danilov, et al, Kvant. Elektronika, **14**, No.1651 (1987).
28 A.M. Prokhorov, UFN, **148**, No.1, 7-33 (1986).
29 A.A. Kaminskii, Izv. AN SSSR, **7**, No.904 (1971).
30 L. Esterovitz, et al, Appl. Phys. Lett., **35**, No.236 (1979).
31 B.M. Antipenko, et al, Optika i Spektr., **61**, No.659 (1986).
32 B.M. Antipenko, et al, Pis'ma ZhTF, **4**, No.80 (1978).
33 Yu.K. Voron'ko, et al, Kvant. Elektronika, **23**, No.229 (1996).
34 B.M. Antipenko, et al, Kvant. Elektronika, **13**, No.980 (1986).
35 V.I. Zhekov, et al, Kvant. Elektronika, **16**, No.1138 (1989).
36 C. Hangle-Hanssen and N. Djeu, IEEE J. Quant. Electron., **30**, No.275 (1994).
37 A.A. Kaminskii, Physics and spectroscopy of laser crystals, Nauka, Moscow (1986).
38 A.A. Kaminskii, et al, Kristallografiya, **27**, No.522 (1982).
39 A.I. Zagumennyi, et al, Kvant. Elektronika, **19**, No.1149 (1992).
40 S.A. Kutovoi, et al, Kvant. Elektronika, **18**, No.149 (1991).
41 A.A. Kaminskii, et al, Kvant. Elektonika, **17**, No.957 (1990).
42 A.A. Kaminskii and A.V. Pelevin, Kvant. Elektronika, **18**, No.905 (1991).
43 M.L. Shand and I.C. Walling, IEEE J. Quant. Electron., **18**, No.1152 (1982).
44 V.V. Antsiferov, et al, Preprint No.89-1, TsNIIatominform, SFTI, Moscow (1989).
45 V.V. Antsiferov, Laser. Tekhn. Optoelektronika, No.3-4, 30 (1993).

46 V.S. Gulev, et al, Kvant. Elektronika, **14**, No.1990 (1987).
47 V.V. Antsiferov and G.I. Smirnov, Preprint No.98-97, IYaF SO RAN, Novosibirsk (1998).
48 A.A. Manenkov and A.M. Prokhorov, UFN, **148**, No.179 (1986).
49 A.A. Mak, et al, Nd glass lasers, Nauka, Moscow (1990).
50 S. Basu, et al, IEEE J. Quant. Electron., **22**, No.2052 (1986).
51 J.C. Almasi and W.S. Martin, US Patent No.3.631.362, H01S 3/08 (1971).
52 W.S. Martin and I.P. Chernoch, US Patent No.3.633.126 H01S 3/08 (1972).
53 Q. Lu, et al, Opt. Comm., **99**, No.201 (1993).

Chapter 6

1 S.G. Rautian, et al, Nonlinear resonance in spectra of atoms and molecules, Nauka, Novosibirsk (1979).
2 V.V. Antsiferov and G.I. Smirnov, Physics of coherent radiation processes in plasma, NGTU, Novosibirsk (1995).
3 A.M. Samson, et al, Self-oscillations in lasers, Nauka i Tekhnika, Minsk (1990).

Chapter 7

1 V.V. Antsiferov, et al, Pis'ma ZhTF, **21**, No.43 (1995).
2 S.V. Kalinin, et al, FTT, **37**, No.2090 (1995).
3 Yu.L. Klimontovich, Statistical physics, Nauka, Moscow (1982).
4 G. Haken, Synergetics, Mir, Moscow (1985).
5 Yu.L. Klimontovich, UFN, **164**, No.811 (1994).
6 S.M. Rymov, Introduction into statistical radiophysics, Nauka, Moscow (1966).
7 B.B. Kadomtsev, UFN, **164**, No.449 (1994).
8 G.I. Smirnov and G.G. Telegin, Fiz. Plazmy, **17**, No.253 (1991).
9 A.P. Kazantsev and G.I. Surdutovich, ZhETF, **56**, No.245 (1970).
10 A.P. Kazantsev and G.I. Surdutovich, ZhETF, **61**, No.1801 (1971).
11 W. Feller, Ann. Math., **54**, No.103 (1951).